

Optimization of Radial Jets Mixing in Cross-flow of Combustion Chambers using Computational Fluid Dynamics

Dissertation

zur Erlangung des akademischen Grades

Doktoringenieur

(Dr.-Ing)

von: M.Sc. Aryoso Nirmolo
geb. am: 8. August 1970
in: Yogyakarta, Indonesia

genehmigt durch die Fakultät für Verfahrens- und Systemtechnik
der Otto-von-Guericke-Universität Magdeburg

Gutachter: Prof.Dr.-Ing. Eckehard Specht
Prof. Dr.-Ing. Dominique Thévenin

eingereicht am: 2. Juli 2007

Promotionskolloquium am: 10. September 2007

P R E F A C E

This dissertation is submitted for the degree of *Doktoringenieur* (Dr.-Ing.) at Otto-von-Guericke-University of Magdeburg, Germany. The research described herein was conducted under the supervision of Prof. Dr.-Ing. Eckehard Specht between January 2002 and June 2007. To the best of my knowledge, this work is original, except where suitable references are made to previous work. Neither this, nor any substantially similar dissertation has been submitted for any degree, diploma or qualification at any other university or institution.

Aryoso Nirmolo
Magdeburg, 2 July 2006

A C K N O W L E D G E M E N T S

First and foremost, I would like to express my sincere gratitude and appreciation to my *Doctorvater*, Prof. Dr.-Ing. Eckehard Specht, for his continual support, encouragement, and enthusiasm. His knowledge, experience, guidance, and patience have also benefited me immensely. I would also like to express my deepest gratefulness to Prof. Dr.-Ing. Dominique Thévenin for his repetitive support, for reviewing this dissertation, and for valuable comments and suggestions. And I would like to convey my genuine thankfulness to Dr.-Ing. Herman Woche for all his knowledge, caring input, and encouragement.

I hereby would like to acknowledge the financial support provided by the State of Saxony Anhalt and the University of Magdeburg, without which I may not be able to live and conduct my study here in Germany.

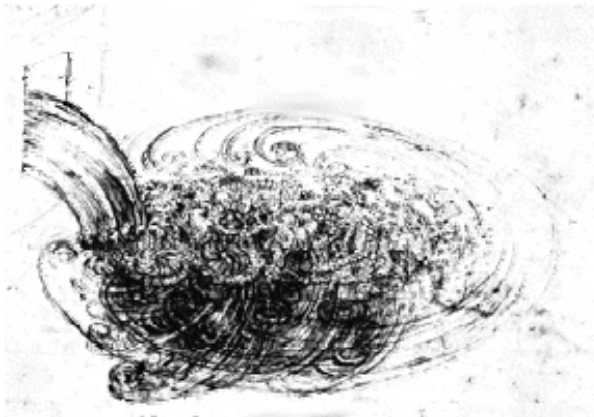
I would like to thank all colleagues of the Institute for Fluid Dynamics and Thermodynamics, University of Magdeburg for their assistances, friendships and many enjoyable times. Special thanks are given to Dr.-Ing. Frank Puschmann, Dipl.-Ing. Zbigniew Waniek, and Dr.-Ing. Agnieszka Bes. It was a pleasure to work with them. And I really appreciate Mr. Bhisma Pandit for the enormous helps during the writing of this dissertation.

I would like to thank all the Indonesian friends in Magdeburg for their endless sharing and companionship, and also to all my friends in Magdeburg and anywhere else in Germany.

Finally, I would like to take this opportunity to express my warm thankfulness to my wife, Savitri Nirmolo, to my son, Avanindra Rafi Nirmolo, to my brothers, sisters and to every member in my extended family for their unconditional love and support. Last but not least to both my parents, Humi Utami and Boma Wikan Tyoso, also to both my parents-in-law, Erna Soewarni and the late Bambang Sidharta, for their absolute love, care and lasting support, without which I won't be able to have any achievement.

DEDICATION

I would like to dedicate this piece of work to my parents and to my family which without their unconditional love and supports, it would not have been possible for me to learn many things all through my life.



"...the small eddies are almost numberless, and large things are rotated only by large eddies and not by small ones, and small things are turned by both small eddies and large."

Leonardo da Vinci (1452-1519)

A B S T R A C T

Multiple jets radially injected inwardly from a cylindrical chamber wall and outwardly from a chamber centerline into a cross-flow have been studied experimentally and numerically using FLUENT CFD code. The chamber diameter was varied from 0.3 m to 3 m and the number of nozzles from 4 to 32. The verification with other commercial CFD codes showed no significant differences in the determination of penetration depth. The validation with experimental values matched well with the CFD calculations. The maximum temperature difference over the chamber cross-sectional area was defined as the parameter to evaluate the mixing quality.

The optimum mixing condition of a single row of jets injected inwardly from the chamber wall into a cross-flow for both reactive and non-reactive flows were obtained at a penetration depth (h/R) of 0.6 which occurred at a normalized momentum flux ratio (J/n^2) of 0.3. This value is independent of the number of nozzles. However with an increasing number of nozzles, the mixing quality will be considerably improved. It is recommended that for operations with ever-changing conditions, which are typical in chemical process industries, to use a single row of jets with number of nozzles greater than 24 and J/n^2 greater than 0.3. Slightly different situations were found for jets injected outwardly from a small pipe in the chamber centerline into a cross-flow. Here the optimum mixing for ever-changing operating conditions can be obtained for J/n^2 greater than 0.4.

For multiple jets radially injected inwardly from a chamber wall, the single row of jets always provides much better mixing quality than the staggered nozzles arrangement of the double rows of jets. However, the inline nozzles arrangement of the double rows of jets will enhance the mixing quality if and only if the injected volumetric flowrates produce over and under-penetrated jets with a volumetric flowrate ratio of the first to second row of jets ($\dot{V}_{j01}/\dot{V}_{j02}$) of 3/1 or 1/3.

Z U S A M M E N F A S S U N G

Die mehrfachen Strahlen, die radial nach innen von einer zylinderförmigen Kammerwand und nach außen von einer Kammermittelachse in einem Querstrom eingedüst werden, wurden experimentell und numerisch mit dem CFD-Programmsystem FLUENT untersucht. Der Kammerdurchmesser wurde von 0.3 m bis 3 m und die Anzahl der Düsen von 4 bis 32 variiert. Der Vergleich mit anderen kommerziellen CFD-Programmen zeigte keine wesentlichen Unterschiede bei der Bestimmung der Eindringtiefe. Die experimentellen Daten stimmen gut mit den CFD Berechnungen überein. Der Maximaltemperaturunterschied in der Querschnittsfläche der Kammer wurde als Parameter eingesetzt, um die Mischensqualität einzuschätzen.

Das optimale Mischen einer einzelnen äußeren Reihe, wurde für die reaktiven sowie nichtreaktiven Strömungen bei einer Eindringtiefe (h/R) von 0.6 erhalten. Die trat bei einem normalisierten Impulsstrom (J/n^2) von 0.3 auf. Dieser Wert hängt nicht von der Anzahl der Düsen ab. Dennoch, bei einer zunehmenden Anzahl der Düsen, wird die Mischensqualität deutlich verbessert. Für sich ständig verändernde Betriebsbedingungen wird empfohlen, eine einzelne Reihe der Strahlen mit Düsenzahlen größer als 24 und J/n^2 größer als 0.3 zu verwenden. Für die nach außen aus einem kleinen Rohr aus der Kammermittelachse in einen Querstrom eingedürften Strahlen, wurde zu einer anderen Schlussfolgerung gekommen. Hier kann das optimale Mischen für sich ständig verändernde Betriebsbedingungen für J/n^2 größer als 0.4 erreicht werden.

Für die mehrfachen Strahlen, die nach innen von einer Kammerwand eingedüst werden, bietet eine einzelne Reihe der Strahlen immer eine bessere Mischensqualität an als eine versetzte Düsenanordnung für eine Doppelreihe der Strahlen. Jedoch kann eine inline Düsenanordnung für eine Doppelreihe der Strahlen die Mischensqualität verbessern, wenn die eingedüsten Volumenströme über- und unterdurchdringende Strahlen, für das Volumenstrom-verhältnis der ersten zu zweiten Reihe der Strahlen ($\dot{V}_{j01}/\dot{V}_{j02}$) von 3/1 oder von 1/3 erzeugen.

C O N T E N T S

PREFACE	iii
ACKNOWLEDGEMENTS	v
DEDICATION	vii
ABSTRACT	ix
ZUSAMMENFASSUNG	xi
CONTENTS	xiii
NOMENCLATURE	xv
CHAPTER 1	
INTRODUCTION	1
1.1 Background and Motivation	1
1.2 Overview of Past Researches	5
1.3 Overview of this Research	22
CHAPTER 2	
COMPUTATIONAL FLUID DYNAMICS SIMULATION	25
2.1 Phases of Modeling and Simulation	26
2.2 CFD Calculation	29
2.3 FLUENT Software Package	30
2.4 Combustion Modeling using FLUENT	35
2.5 Turbulence Modeling using FLUENT	38
2.6 CFD Simulation of this Work	42
CHAPTER 3	
EXTERNAL INJECTIONS WITH A SINGLE ROW OF JETS	45
3.1 Influencing Parameters	45
3.2 Penetration Depth	47
3.3 Verifications with other Commercial CFD Codes	53
3.4 Mixing Criterion	53
3.5 Mixing Conditions	55
3.6 Influence of Hot and Cold Injections	57
3.7 Influence of the Heating Value	58
3.8 Influence of the Number of Nozzles	59
CHAPTER 4	
EXTERNAL INJECTIONS WITH DOUBLE ROWS OF JETS	64

4.1	Influencing Parameters	66
4.2	Experimentation	67
4.3	CFD Calculations	71
4.4	Validation with Experiment	75
4.5	Influence of the Double Rows of Jets	80
4.6	Double Rows of Jets Simulation	85
CHAPTER 5		
	INTERNAL JETS INJECTIONS	87
5.1	Influencing Parameters	89
5.2	Penetration Depth	90
5.3	Influence of the Number of Nozzles	92
CONCLUSIONS		98
REFERENCES		100
APPENDIX		109
CURRICULUM VITAE		121

N O M E N C L A T U R E

d	[m]	nozzle diameter
f	[-]	mixture fraction
h	[m]	distance from chamber wall
h_u	[MJ/m ³]	heating value
z	[m]	distance from injection point, downstream distance
l	[m]	distance between two rows of jets
n	[m]	number of nozzles
p	[atm]	pressure
t	[s]	time
u, v	[m/s]	velocity
x, y, z, r	[m]	coordinates or directions
A	[m ²]	cross-sectional area
D	[m]	chamber diameter
J	[-]	momentum flux ratio jet-to-mainstream
R	[m]	chamber radius
R_{ij}	[-]	Reynolds stresses
T	[K]	temperature
\dot{V}	[m ³ /s]	volumetric flow rate
Z	[-]	elemental mass fraction
μ	[kg/m ³ s]	dynamic viscosity
ρ	[kg/m ³]	density
ϕ	[-]	quantity
θ	[-]	temperature difference ratio

Subscripts and Superscripts:

a	ambient
i	element
j	jets
m	mainstream
max	maximum

min	minimum
o	condition at standard temperature and pressure (STP) (STP: T=273 K; P=1 atm)
ox	oxygen

C H A P T E R 1

INTRODUCTION

1.1 Background and Motivation

The importance of research on jets in a cross-flow has been recognized as having a significant impact on a variety of practical applications. Jets in a cross-flow, also called transverse jets, are relevant to broad range of engineering practices and natural environments. In practical applications, jets in a cross-flow can be found both in unconfined and confined space.

One example of jets in an unconfined (semi-infinite) cross-flow includes the flow situation resulting from the action of crosswinds on effluents from cooling towers, chimney stacks, or flares from petrochemical plants. Another example includes the use of air curtains to prevent cold air from entering open spaces in industrial buildings. Similar flow situations may exist in the atmosphere when thermal plumes generated on the earth's surface rise to levels at which significant crosswinds exist, and also in the discharge of sewage or waste heat into rivers or oceans.

Practical examples of jets in a confined cross-flow are also numerous. One example exists in a Vertical/Short Take Off and Landing (V/STOL) aircraft in transition from hover to forward flight in which the jets from its engines impinge on the ground surfaces. Another example includes the cooling in gas-turbine engine where the transverse jets of air cool the turbine blades in order to protect them from the high exhaust temperatures. This air forms a thin insulating films cover over the blade surface and separates it from the hot gases. Another

example is found in the dilution of air jets in gas-turbine engines where the jets are injected radially into the combustion chamber through discrete holes along its circumference. The aims of these injections are to stabilize the combustion process near the head and to dilute the hot combustion products near the end.

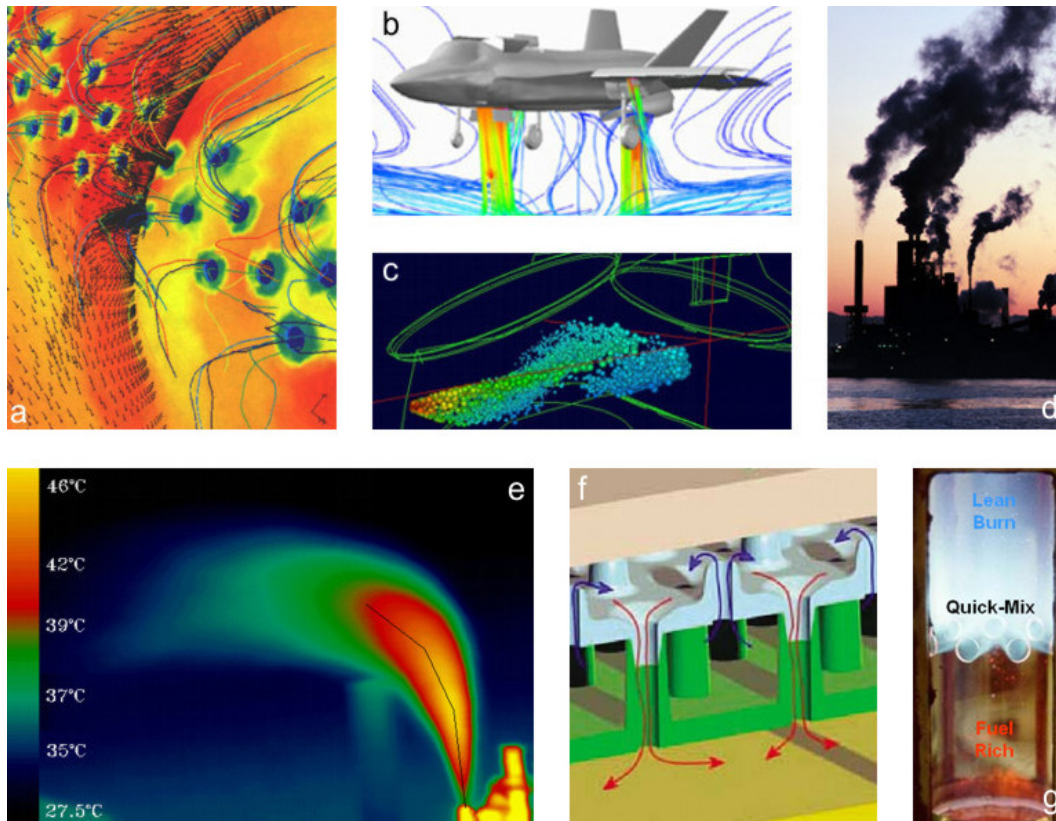


Figure 1-1: Wide range of practical applications of jets in cross-flow.

Figure 1-1 shows wide range of these practical examples such as: (a) the cooler air through holes of turbine blades as provided by CentaurSoft; (b) the jet wake from V/STOL aircraft as provided by CFD Research Corporation; (c) the injection of droplets fuel into the combustion chamber of an internal combustion engine as provided by FEV Motorentechnik GmbH; (d) the dispersion of waste disposal into atmosphere as provided by The Earth Institute at Columbia University; (e) radiant temperature of an industrial steam plume as provided by Proxemy Research Inc., Maryland; (f) the multiple jets impingement of a cooling liquid as discharged from micro-channels in microelectronics which is provided by Wang E, et al. (2004); and (g) the reacting Rich-Burn, Quick-Mix, Lean-Burn (RQL) Combustor as provided by Combustion Laboratory of University California, Irvine USA.

Similar flow situation of jets in a confined cross-flow also exists when two different streams in various chemical process industries have to be well-mixed. It is clear that the mixing quality improves as it moves further from the injection points, but one must note that for industrial purposes the chamber must be made as short as possible. Therefore mixing must be done rapidly and intensively in a minimum downstream distance. What is perceived as optimum depends both on the application and downstream distance, and for these industrial applications usually within twice the chamber diameter is perceived as practical downstream distance.

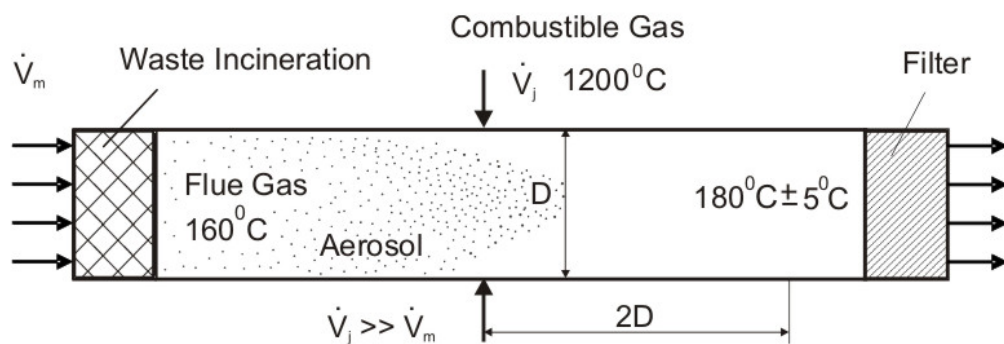


Figure 1-2: Example of chemical process industrial application for hot radial injections of combustible gas into a cold cross-flow of flue gas mixed with aerosol.

Example of chemical process industrial application to obtain rapid and intensive mixing within twice the chamber diameter can be found in some special processes of waste incineration as can be seen in Figure 1-2. The produced flue gas from a waste incineration is usually quite loaded with aerosol which has the potential to glue the tissue filters downstream. Therefore an aerosol with a temperature of about 160°C must be vaporised by lateral injections of hot combustion gases of about 1200°C . The volumetric flow rate of the combustible gas is smaller in comparison with the volumetric flow rate of aerosol and flue gas. If the mixing temperature at any streamline is too low, an incomplete vaporisation of the aerosol will occur, but if the temperature is too high, it could damage the coating of the inner walls and tissue filters. The desired mixing temperature is usually about $180^\circ\text{C} \pm 5^\circ\text{C}$ before reaching the filter.

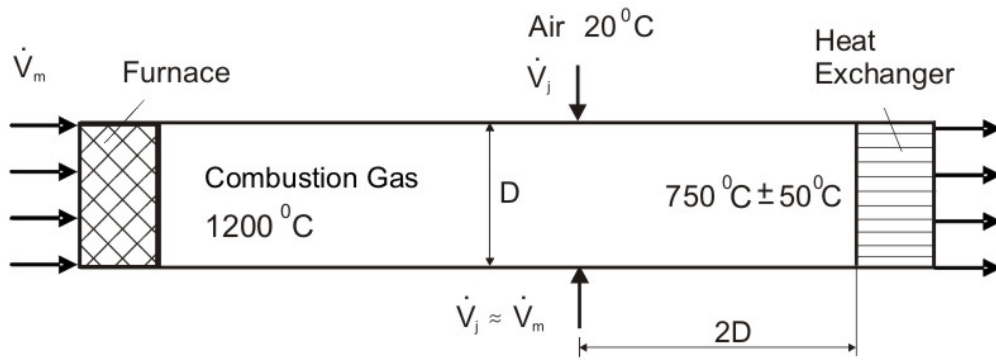


Figure 1-3: Example of chemical process industrial application for cold radial injections of air into a hot cross-flow of combustion gas.

Another example includes the cooling of hot combustion gas of about 1200°C by injecting cold ambient air to create a heating gas of about 800°C before going into a heat exchanger. The volumetric flow rate of both streams can be more or less the same. In doing so, intensive and rapid mixing must be performed within a distance of twice the chamber diameter. This is to prevent hot streams with a temperature higher than 800°C from damaging the heat exchanger downstream.

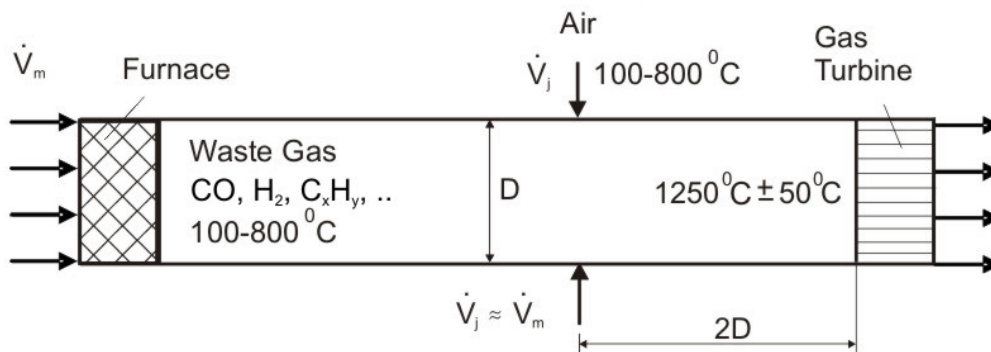


Figure 1-4: Example of chemical process industrial application for combustion of waste gas using single row of radial air injections.

Other applications include the combustion of waste and top gas containing combustible components such as: carbon monoxide, hydrogen, hydrocarbons, etc., using single or double rows of radial air injections as can be seen in Figure 1-4 and Figure 1-5 respectively. The volumetric flow

rate of for both mainstream and jet stream can be more or less the same. Here, the temperature downstream should not exceed $1300\text{ }^{\circ}\text{C}$ to avoid emissions of NO_x , and should not be less than $1200\text{ }^{\circ}\text{C}$ to completely destroy all the hydrocarbons, which is still an acceptable range of temperature for the turbine blade or boiler materials downstream.

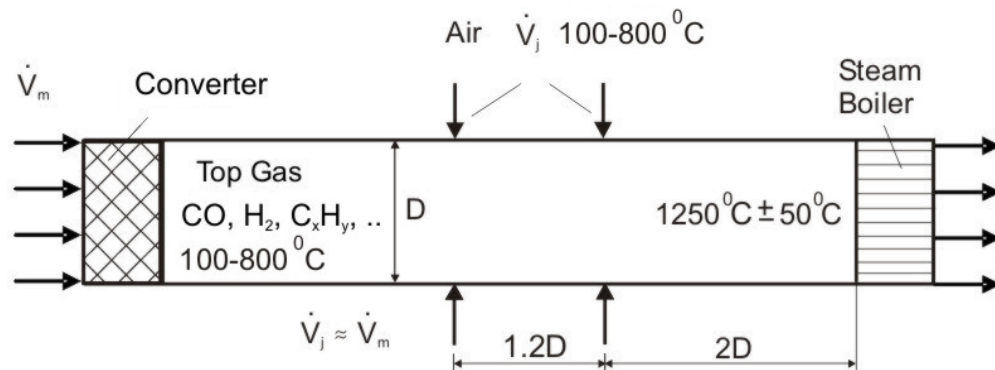


Figure 1-5: Example of chemical process industrial application for combustion of top gas using double rows radial air injections.

All of these practical industrial flows are actually quite complex, and for investigating these flows certain idealizations or simplifications are usually necessary. Although jets in a cross-flow have been extensively treated in the literature and many studies have been reported, one must always note that the information obtained in any given study is always determined by the special application. These special applications including the experimental configurations and the major conclusions of past researches will be discussed further in the next section.

1.2 Overview of Past Researches

A single jet or multiple of jets injected normally or at an angle into a cross-flow has motivated a number of studies over the past three decades. It is indeed difficult to predict accurately. Needless to say, the flow has such important engineering and environmental application that development of better and more accurate mathematical models are likely to continue for a long time. Over the

years, the modelling trend have moved from those based mainly on empirical findings to various numerical models which have been rapidly developed due to the availability of larger and faster computers over the last two decades.

1.2.1 Various Modeling Approaches

Various approaches to modeling of jets in cross-flow have been made. Demuren (1994) reviewed that these approaches were grouped into four broad classes, namely: empirical models, integral models, perturbation models and numerical models.

Empirical models present the simplest means of predicting global properties of jets in cross-flow. This model depend largely on the correlation of experimental data and are mostly useful for the first-order estimates of global properties such as jet trajectory and centreline decay rates and as qualitative checks for results produced by other methods. Such models were reviewed in detail by Abramovich (1963), Rajaratnam (1976) and Schetz (1980).

Integral models are the first elaborate calculation procedures applied to predict the behaviour of jets in cross-flow. In these models, integral equations are derived either by considering the balance of forces and momentum changes over elementary control volume of the jet, or by integrating in two spatial directions, the three dimensional, partial differential equations governing the jet flow. Integral models allow more details of the flow field to be obtained; simpler versions have to assume similarity of velocity and temperature profiles, but more sophisticated ones can actually calculate these profiles. Furthermore, it may be difficult to prescribe cross-sectional profiles in complex situations. Integral model flourished in the early 1980's when the rapid growth in computing hardware and software made numerical computations of three dimensional flows feasible. Such models were conducted by Schatzmann (1979), Adler and Baron (1979), Isaac and Schetz (1982), Makihata and Miyai (1983). Some variation of this model gives quite good prediction of the three-dimensional flow fields of jets in cross-flow studied experimentally by Kamotani and Greber (1972).

Perturbation models require little empirical inputs, but the need for small parameters to ensure convergent expansion limit their application to either near-field and far field. Most applications of perturbation models have been to study the flow of strong jets in a weak cross-flow. The goal is to predict the main features of jets including trajectory, cross-sectional shape, velocity field, vorticity field, mixing, etc. with minimal empirical inputs. These are mostly of scientific interest, since drastic assumptions such as inviscid flow, negligible jet distortion, small deflection maybe required for the perturbation analysis. Therefore, perturbation models are mostly useful for the study of flow physics in limited regimes. Such models were made by Needham et al. (1988) and Coelho and Hunt (1989).

Numerical models have the most potential for wide generality and in principle can be applied to whole range of jet in cross-flow situations, confined or unconfined, low, medium or high jet to cross-flow velocity ratio, single or multiple jets, impinging on a wall or on other jets, swirling, homogeneous or heterogeneous cross-flow, compressible or incompressible, etc. The analysis starts from the general conservation laws stated in partial differential equation form, which are the Navier Stokes equations for the velocity fields and the corresponding energy or species equations for temperature or concentration fields, respectively. These equations which describe unsteady three-dimensional flow cannot be solved directly in practical applications for turbulent flows. For incompressible fluid flow, time-averaged forms and for compressible fluid flow, density weighted, time-average (Favre-averaged) forms of the equations are solved. The process of time-averaging introduces a closure problem due to non-linear correlation between fluctuating velocity and/or temperature/concentration fields. Turbulence models are required to determine these correlations, thereby affecting closure of the system of equations. These numerical models require little empirical input but the most computational efforts. Reliability and computational accuracy are expected to improve with further development in numerical techniques and turbulence models. However, although numerical models show great deal of promise for universality, none of them is indeed capable to predict the whole range of turbulent jets in cross-flow to a reasonable degree of accuracy. Fairly good prediction has been obtained in relatively few cases. Such models were

conducted by Andreopoulos and Rodi (1984), Demuren (1994), and many more. [Demuren, 1994]

1.2.2 Early Jet Mixing Researches

As a jet is injected into a cross-flow, it causes a blockage in the main stream which decelerates the flow and increases the pressure upstream of the jet. The pressure immediately downstream of the jet, however, decreases and this non-uniform pressure distribution, deflects the jet, creating the kidney shape structure characteristic of a jet in a cross-flow. Downstream of the injection point, the cross-flow forms a pair of vortices behind the jet which persist long after the original jet disappears. The rate of entrainment and large scale mixing between the two streams are determined by the action and strength of these vortices. Figure 1-4 illustrates the principle of a round jet injected into a cross-flow. [Hatch et al., 1996]

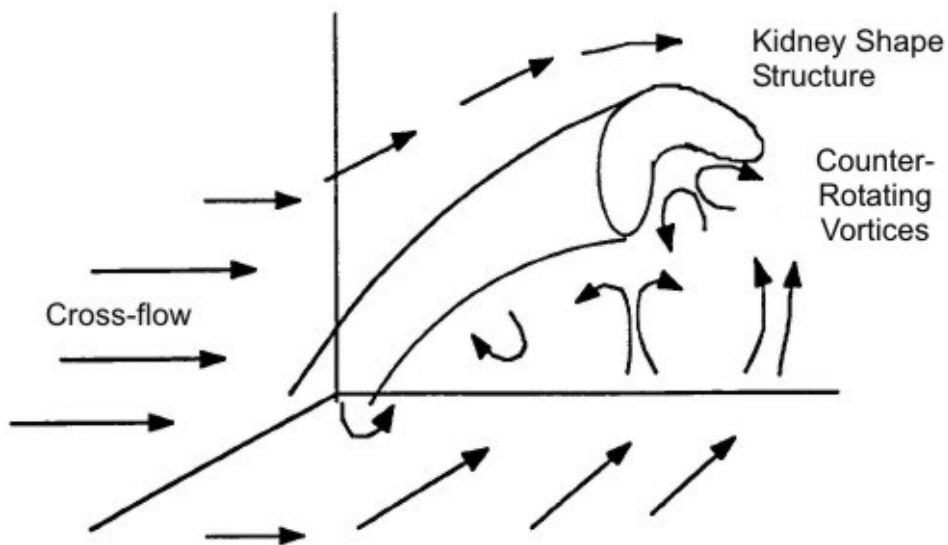


Figure 1-6: Principle of jet in a cross-flow. [Hatch et al., 1996]

Kamotani and Greber (1972) measured the velocity and temperature distribution downstream of a heated turbulent round jet injected into a subsonic cross-flow for several momentum-flux ratios. The results showed that the jet structure is primarily dominated by a vortex pair formed behind the jet. At lower momentum-

flux ratios, the jet is deflected sharply and the vortices do not have time to develop. Therefore, the kidney shape structure remains present into the far downstream. However at higher momentum flux ratios the vortices become stronger and dominate the flow field. The results also indicated that the jet velocity and temperature trajectories strongly depend upon the momentum flux ratio. Temperature trajectories are also dependent upon the density ratio. Turbulence intensity increases with increasing momentum ratio. Turbulence intensity distribution is qualitatively similar to temperature profiles. [Kamotani and Greber, 1972]

Fearn and Weston (1974) proposed two models to predict the location and strength of the vortices in order to present a quantitative measure of the vortex structure observed downstream of a jet injected into a cross-flow. In the vortex filament model, the strength and location of vortices are determined by the measured upwash velocities. In the other model, it is assumed that each vortex is composed of a Gaussian distribution of vorticity. The parameters used in each model are based on the measured velocity field in a vortex cross section. The models showed that the vortex pair is formed very close to the injection point, and the strength of the vortex structure is directly proportional to the orifice diameter and jet speed. [Fearn and Weston, 1974]

In order to predict the behavior of jets in a cross stream, various correlations have been proposed. Cox (1976) used the experimental data obtained from a single row of cold jets injected into a heated cross stream to develop a correlation to predict the temperature pattern inside the dilution zone of a gas turbine combustor. The experiments were performed in a rectangular geometry and the flow variables included jet to mainstream density ratio and velocity ratios. Geometric variables were jet diameter and spacing. The correlation accurately predicted the mixing characteristics of a single row of jets at conditions representative of gas turbine annular combustors. [Cox, 1976]

Holdeman and Walker (1977) used the same set of experimental data as Cox (1976) to develop an empirical model to: 1) predict the temperature downstream of the row of jets, and 2) study the effect of the independent variables on mixing. The independent flow and geometric variables included the momentum flux ratio,

the ratio of jet spacing to orifice diameter, the ratio of duct height to orifice diameter, and the ratio of the downstream distance to duct height. The scaling factors were expressed in terms of the independent flow and geometric variables. The model showed excellent agreement with experimental data except for the cases that resulted in strong impingement on the opposite wall. The study also concluded that the momentum-flux ratio was the most significant parameter that influences the penetration and mixing. Density ratio on the other hand, appeared to have only a second order effect on mixing for the range examined. [Holdeman et al., 1984]

Holdeman, Srinivasan, and Berenfeld (1984) extended the experimental variations to include variable density ratio, flow area convergence, variable mainstream temperature, and opposed in line and staggered injection to examine the mixing characteristics of jets in a rectangular duct at conditions representative of gas turbine combustors. Flow area convergence, especially injection wall convergence, significantly improved downstream mixing. [Holdeman et al., 1984]

The mixing of coolant air jets with the hot gas exiting the primary zones is of major importance to the combustor exit temperature profile. Wittig, Elbahar, and Noll (1983) reported that the geometry and momentum flux ratio are the dominant parameters. A theoretical and experimental study of a single as well as opposite wall injection into a hot cross-flow reveals the applicability and limitations of existing correlations. Modified correlations were presented for opposite wall injection with jets of different momentum flux ratios. [Wittig et al., 1984]

Andreopoulos and Rodi (1984) reported on measurement in flow generated by a jet issuing from the circular outlet in a wall into a cross-stream along this wall. The results had given quantitative picture of complex three-dimensional mean flow and turbulence field, and the various phenomena as well as their dependence on the velocity ratio were discussed in details. [Andreopoulos and Rodi, 1984]

Yoshida and Goldstein (1984) reported the velocity fields above an adiabatic flat plate through which air is injected via row of circular injection holes inclined at an angle of 35 deg to the surface. Key findings are that laminar jet can penetrate

into the main flow with smaller mass flux than the turbulence jet and a turbulent approaching boundary layer generates wider domain of interaction between the jets and the mainstream than a laminar approaching boundary layer for the same blowing rate. [Yoshida et al., 1984]

Holdeman, Srinivasan, Coleman, Meyers, and White (1987) extended the experimental and empirical model results that extended previous studies of mixing of single-sided and opposed rows of jets in a confined duct flow to include effects of non circular orifices and double rows of jets. Analysis of the mean temperature data obtained in these investigations showed that effects of orifice shape and double rows were significant only in the region closed to injection plane provided the orifices were symmetric with respect to the main flow direction. [Holdeman et al., 1987]

Pietrzyk, Bogard, and Crawford (1988) presented the results of a detailed hydrodynamic study of row of inclined jets issuing into a cross flow. Laser-Doppler anemometry was used to measure the vertical and streamwise components of the velocity for three jet to mainstream velocity ratios. The results, which have application to film cooling give a quantitative picture of entire flow field, from approaching flow upstream of the jet through the interaction region of the jet and mainstream to the relaxation region downstream where the flow field approaches that of a standard turbulence boundary layer. The data indicated the existence of the separation region in the hole from which the jets issues, causing high levels of turbulence and relatively uniform mean velocity profile at the jet exit. [Pietrzyk et al., 1988]

Detailed velocity and Reynolds stress measurements of twin jets injected normally to a cross-flow was performed by Isaac and Jakubowski in 1985. Their results showed a striking similarity in terms of mean velocities and turbulent parameters between the tandem jets and a single jet in a cross-flow. [Hatch et al., 1996]

Mixing characteristics of small aspect ratio elliptic jets were the subject of experimental investigation by Ho and Gutmark (1987). The results showed a significant increase in cross-flow entrainment for small aspect ratio elliptic jets

(2:1-3:1) as compared to circular holes. Most of the mass entrainment for this geometry occurred around the jet minor axis. [Hatch et al., 1996]

The influence of swirl and high turbulence was investigated in an experimental study conducted by Kavsaoglu and Schetz (1989). Pressure and velocity distributions were obtained for a 90° circular hole at low and high-exit turbulence and different swirl levels. The results showed that both swirl and high turbulence decrease jet penetration to center of the main flow and reduces the negative pressure regions on the surface. Inlet swirl also introduces asymmetries into the flow field, the effects of which were more pronounced at low velocity ratios. [Hatch et al., 1996]

Numerical studies by Smith (1990) examined the mixing patterns of opposed, staggered holes in a rectangular geometry, to determine the effects of jet inlet turbulence and holes spacing. Both symmetric and asymmetric flow patterns were seen for the conditions numerically tested. Jet mixing was strongly influenced by the type of flow pattern where improved mixing occurred for symmetric flow patterns. The result suggested that there was an optimum holes spacing for a given flow condition and geometry, and that mixing improved as the jet inlet turbulence is increased. [Hatch et al., 1996]

The impact of momentum flux ratio on mixing and NO formation in can geometry was numerically investigated by Talpallikar, Smith, and Lai (1990). Momentum-flux ratios of 32 and 40 produced the "best" mixing for 12-slot geometry under non-reacting and reacting conditions, respectively. The study also investigated the mixing characteristics of two asymmetric geometries designed to produce large scale vortices. The overall mixing was improved for the asymmetric configurations, but higher NO was calculated due to the presence of hot spots. [Talpallikar et al., 1990]

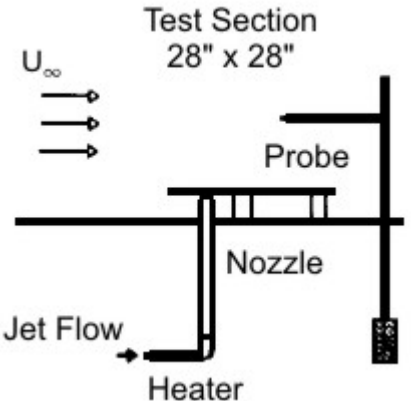
Smith, Talpallikar, and Holdeman (1991) conducted a CFD study to examine the effect of reduced flow area on mixing and NO_x emissions. Their calculations showed that mixing is unaffected by the reduction in the flow area, while NO_x formation was reduced due to shorter residence time. [Smith et al., 1991]

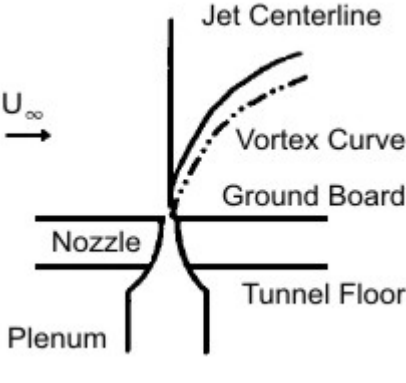
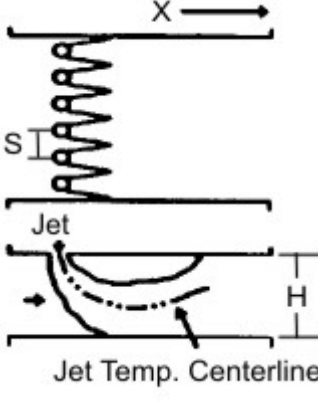
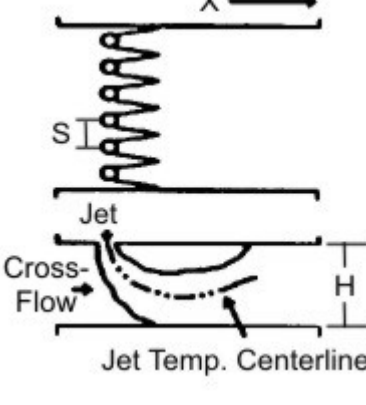
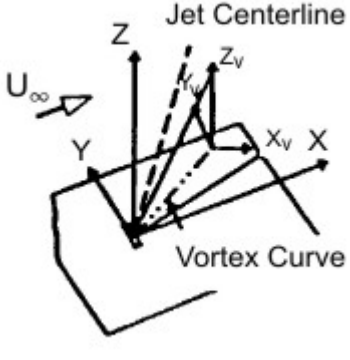
Nishiyama, Ota, Hamada, and Takahashi (1991) described the characteristics temperature fluctuations of slightly heated two dimensional jets issuing normally to a laminar or turbulent cold cross flow at different blowing rates. Some statistical properties of temperature fluctuations were classified in the direction normal to the jet axis for the potential core region and for the temperature decay one respectively, corresponding to the typical jet flow pattern. [Nishiyama et al., 1995]

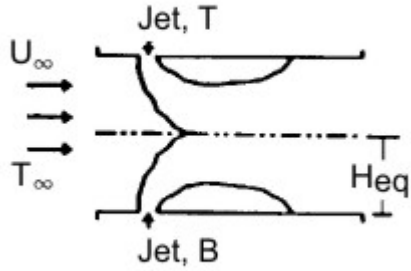
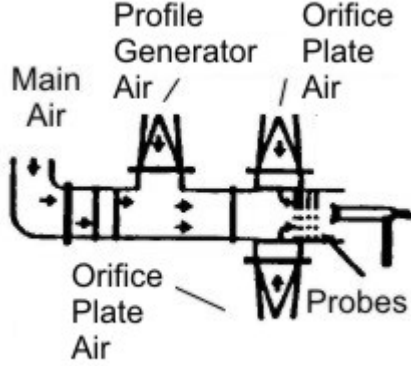
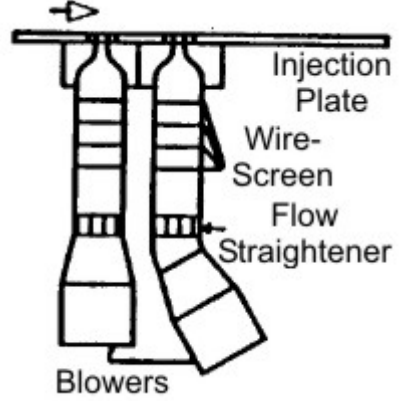
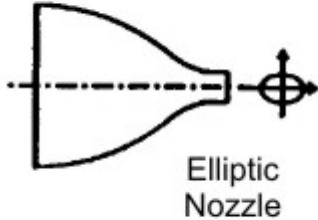
One of the few experimental studies of jet mixing in a cylindrical duct was conducted by Vranos, Liscinsky, True, Holdeman (1991). The primary variables in this experiment were the momentum-flux ratio, injector geometry, and density ratio. Planar digital imaging was used to measure the concentration of an aerosol seed uniformly mixed with the jet stream, in several planes downstream of the mixing orifices. The first axial location examined in this experiment was 1.2-radius downstream of the injection point. The results showed that for an axis-symmetric geometry, mixedness was more sensitive to circumferential uniformity rather than jet penetration. Therefore, above a certain momentum-flux ratio, mixing with slanted slots was better than with round holes. [Vranos et al., 1991]

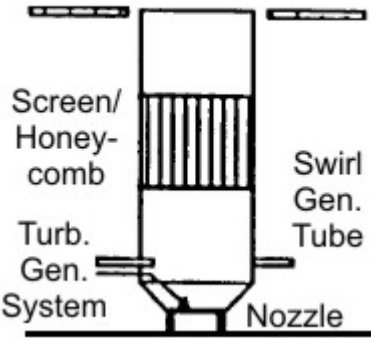
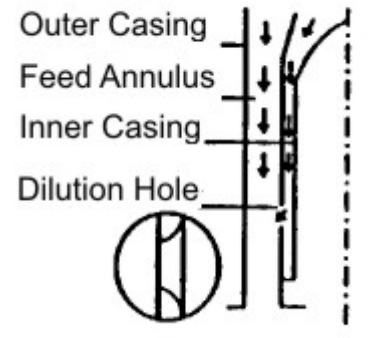
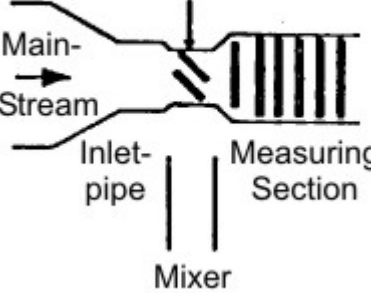
Table 2-1 summarizes selected experimental studies of jet mixing taken from [Hatch et al., 1996]. It shows the principle configurations and major conclusions of the selected studies conducted by researchers previously mentioned.

Table 2-1: Summary of Selected Jet Mixing Researches. [Hatch et al., 1996]

Reference	Configuration	Major Conclusion
Kamotani and Greber (1972)		<ul style="list-style-type: none"> ▪ Momentum flux ratio determines the jet trajectory. ▪ Turbulent intensity increases with momentum flux ratio. ▪ Temperature trajectory is a weak function of density ratio. ▪ Downstream temperature and velocity distribution is dominated by vortex motion.

<p>Fearn and Weston (1974)</p>		<ul style="list-style-type: none"> ▪ Developed two models to define counter-rotating vortices. ▪ The pair of vortices is then dominant feature of flow field. ▪ The vortex pair is formed close to injection point. ▪ Vortices initial strength is proportional to nozzle diameter and jet speed.
<p>Cox (1976)</p>		<ul style="list-style-type: none"> ▪ Developed a correlation method to predict temperature field downstream of one row of closely spaced holes injected into a hot confined cross-flow. ▪ The model provided good comparison between predicted and measured flow field within the range of parameters representative of GTE combustor.
<p>Holdeman and Walker (1977)</p>		<ul style="list-style-type: none"> ▪ Developed an empirical model to predict mixing of one row of jets injected into a hot cross-flow. ▪ The model provided good comparison between predicted and measured flow field. ▪ Momentum flux ratio was found to be the most important factor influencing mixing.
<p>Weston and Thames (1979)</p>		<ul style="list-style-type: none"> ▪ Penetration and vortex strength of blunt jets are less than those of streamwise jets. ▪ Nominal properties of streamwise jets are similar to those of circular jets. ▪ Rectangular jets decay much faster than round jets due to the increased viscous effects on larger perimeter.

<p>Wittig et. al. (1984)</p>		<ul style="list-style-type: none"> ▪ One sided wall injection correlations can be used for opposite-wall jet injection at low momentum flux ratios. ▪ Modified correlations to give better agreement at higher momentum flux ratios.
<p>Holdeman et. al. (1985)</p>		<ul style="list-style-type: none"> ▪ Density ratio has a second order effect on mixing. ▪ Injection wall convergence significantly improves mixing. ▪ Optimum orifice spacing for opposed in-line jets is half of the optimum value for single sided case. ▪ For staggered jets the optimum value is twice the one of single side injection.
<p>Isaac and Jakubowski (1985)</p>		<ul style="list-style-type: none"> ▪ Similarity was observed in details of flow within the cross sections of single and tandem jets. ▪ The transverse velocity profiles were found to be significantly different than axial and vertical profiles. ▪ Initial conditions are important in determining the jet trajectory.
<p>Ho and Gutmark (1987)</p>		<ul style="list-style-type: none"> ▪ Mass entrainment by a 2:1 aspect ratio elliptic jet is significantly higher than of a round hole.

<p>Kavsaoglu and Schetz (1989)</p>	<p>Top of Test Section</p> 	<ul style="list-style-type: none"> Swirl and high turbulence reduce penetration and decrease negative pressure surface area. Swirl produces asymmetry in pressure distribution, especially for low velocity ratios and high swirl ratios.
<p>Stevens and Carrote (1990)</p>		<ul style="list-style-type: none"> Developed an empirical model to predict mixing of one row of jets injected into a hot cross-flow. The model provided good comparison between predicted and measured flow field. Momentum flux ratio was found to be the most important factor influencing mixing.
<p>Vranos et. al. (1991)</p>	<p>Seeded Jet Flow</p> 	<ul style="list-style-type: none"> Slanted slots are better mixers above a certain momentum flux ratio. Mixing decreases at increased density ratios. Mixedness is independent of mass flow rate.

1.2.3 Recent Jet Mixing Researches

Over the past decade, various attempts have been made to improve the mixing efficiency of a jet in cross-flow. The majority of these studies have focused on the numerical analysis of the flow field.

Howe, Li, Shih, and Nguyen (1991) developed a computer program to investigate the mixing characteristics for both reacting and non-reacting conditions in a configuration simulating the quick mix region of a RQL combustor. Jet to mainstream momentum flux ratio was shown to have a significant impact on jet penetration depth while reaction appeared to reduce the penetration depth. No NO_x measurements were reported for this study. [Howe et al., 1991]

Chao and Ho (1992) numerically investigated a heated and unheated lateral jets discharging into a confined swirling cross flow. Emphases are placed on the effects of the temperature difference on the trajectories and mixing characteristics of the lateral jet in the swirling cross flow and the detailed impingement process of the opposed jets in the cross flow. Parameter variations studied include jet temperature, jet-to-cross flow velocity ratio, and jet number and swirl strength. The results show that pressure forced caused by the presence of the opposing jets will hinder the penetration and increase the velocity as jets impinge. The jet decaying process is almost independent of the temperature difference between the heated jet and the cross flow. The jet spreading process is dependent on the inlet mass flux ratio and the mixing conditions. [Chao et al., 1992]

Hatch, Sowa, Samuelsen, and Holdeman (1992) examine the mixing characteristics of jet in axis symmetric can geometry, temperature measurements were obtained downstream of a row of cold jets injected into a heated cross stream. Parametric, non reacting experiments were conducted to determine the influence of geometry and flow variations on the mixing pattern in a cylindrical configuration. Results show that jet-to-mainstream momentum flux ratio and orifice geometry significantly impact the mixing characteristics of jets in can geometry. [Hatch et al., 1992]

To examine the mixing characteristics of jets in a cylindrical duct, Oechsle, Mongia, and Holdeman (1993) describe the interaction of some important parameters affecting the mixing process in a quick mixing region of a rich burn/quick mix/lean burn RQL Combustor and reported that the optimum jet penetration for round jet requires a parameter $C=2.5$ using the design correlation: $n = \pi\sqrt{2J}/C$. [Oechsle et al., 1993]

Holdeman (1993) summarizes experimental and computational results on the mixing of single, double and opposed rows of jets with an isothermal or variable temperature mainstream in a confined subsonic cross flow. The studies from which these results came were performed to investigate flow and geometric variations typical of complex three dimensional flow fields in the dilution zone of combustion chamber in gas turbines. The main conclusions from these experimental results are variations in momentum flux ratio, orifice size and spacing have a significant effect on the flow distribution. Similar distributions can be obtained, independent of orifice diameter, when orifice diameter is inversely proportional to the square-root of the momentum flux ratio. Flow area convergence, especially injection wall convergence, significantly improves the mixing. [Holdeman, 1993]

Chang and Chen (1994) presented a numerical study on the mixing of opposing heated line jets discharged normally or at an angle into horizontal cold cross flow rectangular channel. The $k-\epsilon$ turbulence model is adopted and simulation is performed for the jet to cross-flow momentum flux ratio. The results show that there is a strong recirculation near the downstream region of the nozzle opening and the temperature field behaves like a deflected plume. The turbulence kinetic energy is high in the region where vertical velocity gradient is steep. Corrections for the jet temperature and velocity trajectories, the penetration and circulation depths, the jet half-width and the reattachment point are divided in terms of the momentum flux ratio, the downstream distance and the incident angle. As compare to the case of a one side line jet, the opposing jets will hinder the vertical penetration but increases the horizontal velocity when jet impinge on each other: Better thermal mixing can be achieved at higher momentum flux ratio and incident angle. [Chang et al., 1994]

Bain, Smith, and Holdeman (1995) analyzed 3-D turbulence reaction with CFD on transverse jets injected into annular and cylindrical can confined cross flows. The goal of this study was to identify and access mixing differences between annular and can geometry. The result showed that the optimum condition which gave the lowest NO_x emissions for a cylindrical geometry configuration required a

parameter $C=3.5$ for design correlation: $C = S/H\sqrt{J}$ where S/H was defined as the nozzle spacing to duct height ratio. [Bain et al., 1995]

Doerr, Blomeyer, and Hennecke (1995) investigated experimentally a non-reacting multiple jet mixing in a confined cross-flow. Flow and geometric conditions were varied in order to examine favorable parameters for mixing. The requirement for a rapid and intense mixing process originates from combustions applications, especially RQL combustion concept. Thus, the jets were perpendicularly injected out of one opposed row of circular orifices into a heated cross-flow in a rectangular duct. Spacing and hole size were varied within the ranges referring to combustor applications. The results presented were restricted to an inline orientation of opposed jet axis. Temperature distribution, mixing rate and standard deviation were determined at discrete downstream locations. Uniform mixing can be observed strongly depending on momentum flux ratio. Too high ratios deteriorate the mixing process due to the mutual impact of the opposed entraining jets along with a thermal stratification of the flow field. Corrections were introduced describing the dependency of optimum flux ratio on mixing hole geometry. [Doerr et al., 1995]

Doerr, Blomeyer, and Hennecke (1995) had conducted experimental investigation of a non-reacting mixing process of jets in a cross. The jets were perpendicularly injected through one stage of opposed row of circular orifices into a heated cross-flow in a rectangular duct. All geometries were tested with staggered arrangements of the centerlines of the oppose jets. The temperature distribution was measured and from that the mixing rate was determined for parametric variation of the flow and geometric conditions. The experimental study provides the data base for a correlation of best mixing depending on geometric conditions for staggered mixing configurations. [Doerr et al., 1996]

Holdeman, Liscinsky, and Bain (1999) summarizes experimental and computational results on the mixing of opposed rows of jets with confined subsonic cross flow in rectangular ducts. The principle observation was that momentum flux ratio and the orifice spacing was the most significant flow and geometric variables. Jet penetration was critical and penetration decreased as either momentum flux ratio or orifice spacing decreased. It is also appeared that

jet penetration remained similar with variations in orifice size, shape, spacing and momentum flux ratio when the orifice spacing was inversely proportional to square root of the momentum flux ratio. Three-dimensional flow was a key part of efficient mixing and was observed for all configurations. [Holdeman et al., 1997]

He, Guo, and Hsu (1999), studied the effect of Schmidt number on turbulent scalar mixing in a jet-in-cross flow. The adequacy and accuracy of the constant Schmidt number assumption in predicting turbulent scalar fields in jet-in-cross flows are assessed in that work. A round jet injected into a confined cross flow in a rectangular tunnel had been simulated using Reynolds-averaged Navier-Stokes equation with the standard $k-\epsilon$ turbulence model. The principle observations was that the turbulence Schmidt number had a significant effect on the prediction of the species spreading rate in jet-in-cross flows, especially for the cases where the jet-to-cross flows momentum flux ratios are relatively small. [He et al., 1999]

Tao, Adler, and Specht (2002) numerically investigated a confined cylindrical cross flow using the control-volume-based method. Interest was focused on determining the relationship between the temperature trajectory and the upstream flow and geometric variables. Parameter variations studied include nozzle diameter, number of nozzles, duct radius, jet and mainstream volume-flow, temperature ratio and dynamic pressure ratio. It was found that the dynamic pressure ratio, the number of nozzles and nozzle spacing are significant. A logarithmic function describing the relationship between penetration depth and dynamic pressure divided by the square of the number of nozzles is derived by fitting the data of the computation results. The values for penetration depth and the nozzle spacing are described for optimum mixing. A suggested design procedure is presented which can be used as a first approach in configuration design. [Tao et al., 2002]

Wegner, Huai, and Sadiki (2004) conducted a comparative study of turbulent mixing in jet in cross flow configurations using large eddy simulation (LES). After validating the computations against measurement made by Andreopoulos and Rodi (1984), both qualitative and quantitative comparisons were made to study the mixing process for three configurations with different angles. It shown those

inclinations influence the characteristics of vortical structures and secondary motion which in turn have an effect on the mixing process. [Wegner et al., 2004] Muppidi (2006) studied the different aspects of round single jets in a cross-flow using direct numerical simulation (DNS). Trajectories and the near-field were carefully studied. A length scale is proposed to describe the near-field of the jet. An analytical expression is proposed for this length scale which is a measure of the relative inertias of the jet and the crossflow. Muppidi pointed out that as a jet issues into the cross-flow, it deflects in the direction of the cross-flow then a pair of counter rotating vortices is generated. The counter-rotating vortex pair (CVP) has been considered to be a dominant feature of this flow and has been observed to persist far downstream. Figure 1-7 shows some DNS results made by Muppidi. It shows an isometric view of the flow field showing a) the center of streamlines and CVP, and b) the streamlines that originate in the pipe indicating the motion of the jet fluid.

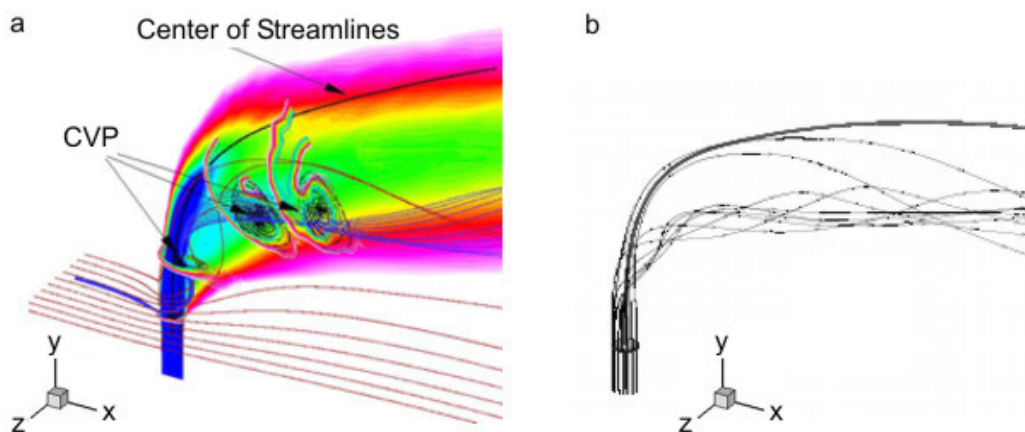


Figure 1-7: Contours of velocity and streamlines of jet in cross-flow originating from a round pipe. [Muppidi, 2006]

Additional Figure 1-7 shows that the trajectories of streamlines that do not originate on the symmetry plane are shallower than the trajectory of the center streamline. This situation results in the jet being wider on the leeward side of the center streamline. Also note that the cross-flow fluid has a higher momentum at the upstream side of the jet (negative x side of the jet centerline) as compared to the downstream side of the jet. This difference in momentum could also aid in accentuating the asymmetry in the jet width. Close to the jet-exit, the jet cross-

section is circular, and fluid with the highest velocity is seen towards the center. The trailing edge flattens as the jet cross-section deforms to a kidney shape. Away from the jet-exit, the high velocity contours are seen toward the edges of the jet, while the fluid towards the center appears to have a relatively lower velocity. At these cross-sections, streamlines show the stages of formation of the CVP. Shortly after jet-exit, streamlines show a small region of vorticity toward the trailing edge of the jet. As it moves further, the CVP increases in size.

1.3 Overview of this Research

As discussed in the previous section, it is clear that there are still very few studies that have been carried out in the field of chemical and thermal industrial applications. Thus some uncertainties still exist as to whether these previous studies can be directly transferred into this field of industrial applications. Therefore more studies must be conducted in order to ensure its uses and to investigate further the influences of many industrial parameters and geometrical configurations to the mixing quality which mostly were not taken into account due to their different applications.

Many of the studies previously mentioned have been made for single jet in a cross-flow and some were made for multiple jets in cross-flow. Some sophisticated studies using LES and DNS were also made, however these types of studies were conducted for only a single jet in a cross-flow.

There are a number of possible geometries for jet injection systems in a cylindrical chamber. Figure 1-8 shows choices among potential designs which may depend on the desired mixing characteristics. As can be seen, the typical design of jet injection is a design of multiple jets oriented perpendicular to the chamber centerline. There can be two types of injections for such a case which are external and internal injections. For the external type of injections one possibility involves the use of single row of nozzles, further possibilities involve the use of double or multiple rows of jets oriented along the cylindrical chamber. For the internal type of injections, one may also involve nozzles which are made in the inner pipe near the head of the cylindrical chamber.

This work reports the results of numerical investigations using CFD especially the influences of these multiple jets configuration on mixing in a cylindrical duct or chamber. Studies were made for both non-reactive and reactive (i.e. Combustion) flows. Since the combustion in kilns are mostly a non-premixed combustion which means that both the fuel and oxidizer flow into the reaction in a separate stream, therefore this work concentrates only on a case of non-premixed combustion.

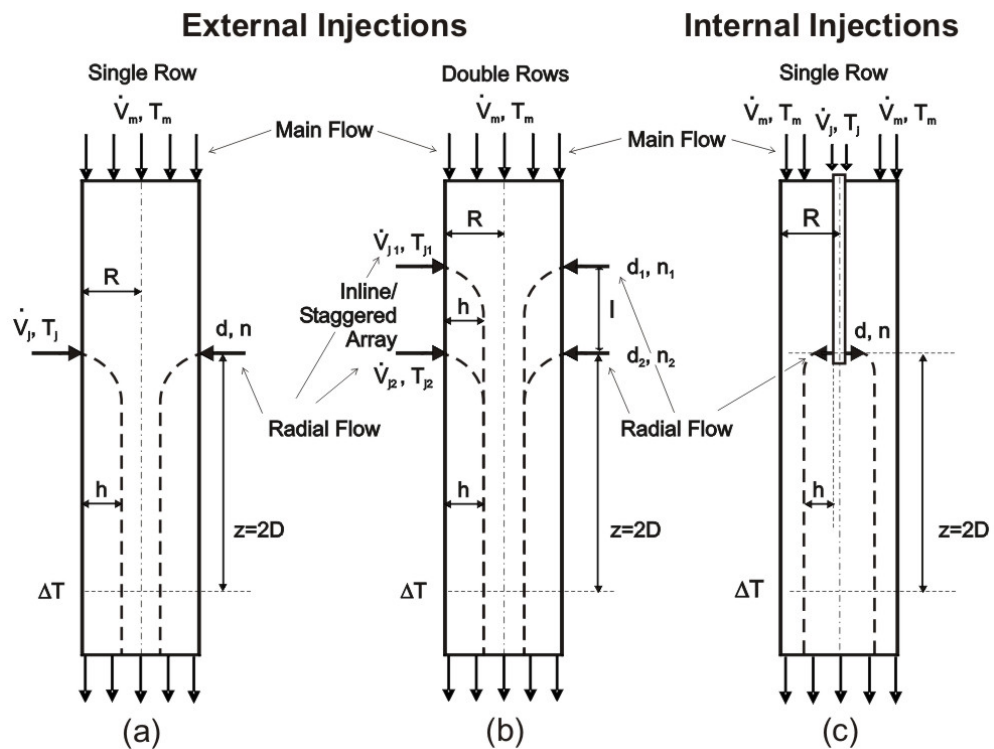


Figure 1-8: Choices among potential designs which depend on the desired mixing characteristics.

Verifications with other commercial CFD codes and validations with experimental results were also made to ensure further uses of the simulation results. Special cares are given for the assessment on mixing quality for both reactive and non-reactive flows at a downstream distance of twice the chamber diameter after the injection points. This chosen downstream distance is mainly based on numerous industrial experiences which need intensive and rapid mixing.

C H A P T E R 2

COMPUTATIONAL FLUID DYNAMICS SIMULATION

The design, scale-up, and running of unit operations in chemical process industries rely heavily upon empiricism and correlations of overall parameters for non-ideal or non-equilibrium conditions. Many equipment designs in use are based on the experience of experts applying rules of thumb, resembling art more than science. Processes that are sensitive to local phenomena and reactant concentrations are often difficult to design or scale up, because the design correlations do not take local effects into account. Non-idealities introduced by scaling up of lab or pilot scale equipment are difficult, if not impossible to predict accurately.

Researchers, equipment designers, and process engineers are increasingly using computational fluid dynamics (CFD) to analyze the flow and performance of process equipment, such as chemical reactors, stirred tanks, fluidized beds, cyclones, combustion systems, spray dryers, pipeline arrays, heat exchangers, and other equipment. CFD allows for in depth analysis of the fluid mechanics, local effects, and chemistry in these types of equipment such as turbulence and combustion. CFD can be used when design correlations or experimental data are not available. It provides comprehensive data that are not easily obtainable from experimental tests. It highlights the root cause, not just the effect and many 'what if' scenarios can often be analyzed in a short time. This method reduces scale-up problems, because the models are based on the fundamental physics and are scale-independent.

CFD is basically the science of predicting fluid flow, heat transfer, mass transfer, chemical reactions, and related phenomena by solving the mathematical equations that govern these processes using numerical algorithm. It is the merger of the classical branches of theoretical and experimental science, with the infusion of the modern element of numerical computation. The results of CFD analyses are relevant engineering data used in conceptual studies of new designs, detailed product development, troubleshooting, and redesign. In many cases, CFD results in better insight, improved performance, better reliability, more confident scale-up, improved product consistency, and higher plant productivity.

The progress of CFD during the last fifty years has been extraordinary. Much of this progress has been driven by the phenomenal increases in digital computing speed. The continual and exponential increase in computing power, improved physical models in many CFD codes, and better user interfaces now enables non-experts to use CFD as a design tool on day-to-day basis. As a consequence, CFD has progressed from the domain of mainframe to the high-end engineering workstation and even to laptop PCs. This power of digital computing has transformed research and engineering especially in fluid mechanics, just as it has in virtually all fields of human endeavors.

2.1 Phases of Modeling and Simulation

There has been a long history of efforts to establish the basic concepts and terminology in modeling and computer simulation. The identification of the fundamental issues and debates began two decades ago in the operation research community, long before there was such concern in the CFD community. The term model, modeling, and simulation are used in a wide range of disciplines. Consequently, these terms have a range of meanings that are both context-specific and discipline-specific. Model is a representation of a physical system or process intended to enhance our ability to understand, predict, or control its behavior. Modeling is the process of construction or modification of a model. Simulation is the exercise or use of a model. [AIAA, 1998]

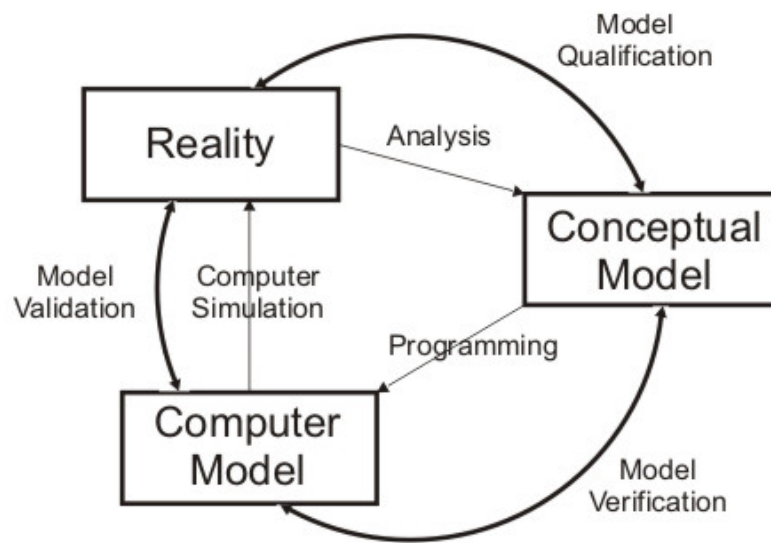


Figure 2-1: Phases of modeling and simulation. [AIAA, 1998]

The basic phases of modeling and simulation have been identified by operation research community. Figure 2-1 shows these basic phases and processes. It identifies two types of models: a conceptual model and a computer model. The conceptual model is composed of all the information, mathematical modeling data, and mathematical equations that describe the physical system or process of interest. The conceptual model is produced by analysis and observations of the physical system. In CFD, the conceptual model is dominated by partial differential equations (PDEs) of conservation equations of mass, momentum, and energy. The computer model is an operational computer program that implements a conceptual model. Modern terminology refers to the computer model as computer code.

Although CFD simulations are widely conducted in industry, government and academia, there is presently little agreement on procedures for assessing their capability. There is no fixed level of credibility or accuracy that is applicable to all CFD simulations. The accuracy level required of simulations depends on the purposes for which the simulations are intended to be used.

The two main principles that are necessary for assessing credibility are verification and validation. Verification is the process of determining if a

computational simulation accurately represents the conceptual description of the model and the solution to the model, but no claim is made of the relationship of the simulation to real world. Validation is the process of determining if a computational simulation accurately represents the real world from the perspective of the intended uses of the model. The definition of verification and validation also stress the evaluation of accuracy. In verification activities, accuracy is generally measured with the respect to benchmark solutions of simplified model problems. In validation activities, accuracy is measured with respect to experimental data, which represent the reality. [AIAA, 1998]

As represented in Figure 2-1, verification addresses the question of fidelity of the computational or computer model to conceptual model. Validation addresses the issue of fidelity of the computational model or its simulation results to the real world. The term model qualification refers to the issue of fidelity of the conceptual model to reality. Model verification, validation, and qualification are processes of determining. Therefore these processes are ongoing activities that do not have a clearly defined completion point. Completion or sufficiency is usually determined by practical issues such as budgetary constraints and intended uses of the model.

Uncertainty and error can be considered as the broad categories that are normally associated with the loss in accuracy in modelling and simulation. Uncertainty is defined as a potential deficiency in any phase or activity of the modelling process that is due to lack of knowledge. Lack of knowledge is commonly caused by incomplete knowledge of a physical characteristic or parameter. Lack of knowledge can also be caused by the complexity of a physical process, for example in the case turbulent combustion. Error is defined as a recognizable deficiency in any phase or activity of modelling and simulation that is not due to the lack of knowledge. Error can be categorized as either acknowledged or unacknowledged. Examples of acknowledged errors are round-off error in a digital computer and physical approximations made to simplify the modelling of a physical process. Unacknowledged errors include blunders and mistakes such as programming errors.

In CFD simulations, there are four predominant sources of error, namely insufficient spatial discretization convergence, insufficient temporal discretization convergence, lack of iterative convergence, and computer programming. The most important activity in verification testing is to systematically refining the grid size and the time step. The objective of this activity is to estimate the discretization error of numerical solution. As the grid size and time step approach zero, the discretization error should asymptotically approach zero. In verification activities, comparing a computational solution to a highly accurate solution is the most accurate and reliable way to quantitatively measure the error in the computational solution. However highly accurate solutions are known for a relatively small number of simplified problems. These highly accurate solutions can be classified into three types: analytical solutions, benchmark numerical solutions to ordinary differential (ODEs), and benchmark numerical solutions to partial differential equations (PDEs).

2.2 CFD Calculation

CFD is applied by first dividing or discretizing the geometry of interest into a number of computational cells. Discretization is the method of approximating the differential equations by a system of algebraic equations for the variables at some set of discrete locations in space and time. The discrete locations are referred to as the grid or the mesh.

The continuous information from the exact solution of the Navier-Stokes partial differential equations is now replaced with discrete values. The number of cells can vary from a few thousands for a simple problem to millions for very large and complicated ones. Cells have a variety of shapes. Triangular and quadrilateral cells are generally used in 2D problems. For 3D problems, hexahedral, tetrahedral, pyramidal, and prismatic shaped cells can be used.

In the past, CFD codes required the use of structured grids containing one cell type, such as brick-shaped hexahedral elements, in which the cells were positioned in regular pattern. Current codes allow cells to be located in an irregular, unstructured pattern, giving much greater geometric flexibility. Additionally, a good CFD code can accept grids consisting of a combination of

different cell types, or hybrid grids, to address complex geometries, providing flexibility to the CFD analyst. Geometries are often created using computer aided design (CAD) software. The geometry, either a wireframe or solid model is exported to the grid-generation software program to create the CFD quality grid. A few packages have combined both functions of CAD geometry creation and mesh generation into a single interface. With the grid created, the boundary conditions such as pressures, velocities, mass flows, and scalars specified, and physical properties defined, the CFD calculations can start. The CFD codes will solve the appropriate conservation equations for all grid cells using iterative procedure. Typical chemical process applications involve solving for: mass conservation (using a continuity equation), momentum (using Navier Stokes equations), enthalpy, turbulent kinetic energy, turbulent energy dissipation rate, chemical species concentrations, local reaction rates, and local volume fractions for multiphase problems.

There are many commercial CFD packages for modeling and analyzing system involving fluid flow, heat transfer and associated phenomena such as chemical reaction. Some popular CFD packages include: FLUENT, CFX, PHOENICS and ANSYS. All these commercial CFD codes contain three main elements: Pre-processor, Solver and Post-processor. This study concentrates on the use of FLUENT software package to simulate the flow and mixing behaviour especially for chemical and thermal industrial applications. But comparisons with some of these popular commercial CFD codes were also necessary to be made in order to verify the results made by FLUENT CFD code.

2.3 FLUENT Software Package

FLUENT is a CFD software package that can be used for modeling fluid flow and heat transfer in complex geometries. It provides complete mesh flexibility, solving the flow problems with unstructured meshes that can be generated about complex geometries with relative ease. It uses a CFD code based on finite-volume method for solving transport equation of mass, momentum and energy conservation. The basic idea of a finite-volume method is to satisfy the integral form of the conservation law to some degree of approximation for each of many contiguous control volumes which cover the domain of interest. Here the domain

is discretized into a finite set of computational cells as control volumes. Figure 2-2 shows the fluid region of a pipe flow which is spatially discretized into a number of computational cells as control volume.

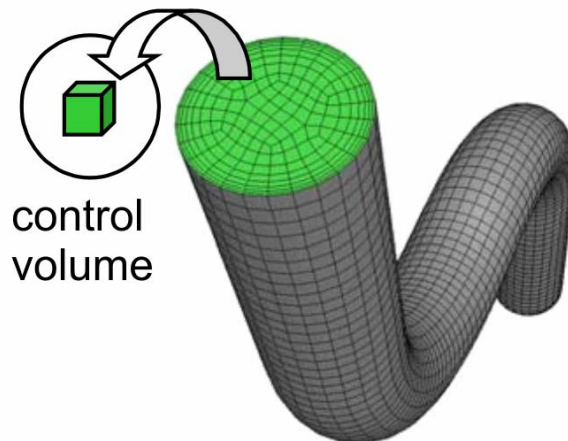


Figure 2-2: Fluid region of pipe flow discretized into finite set of control volumes. [FLUENT, 2003]

Supported mesh types include 2D triangular/quadrilateral, 3D tetrahedral, hexahedral, pyramid, wedge, and mixed i.e. hybrid meshes and body-fitted, block-structured meshes. It uses unstructured meshes in order to reduce the amount of time for generating meshes, simplify the geometry modeling and mesh generation process, model more-complex geometries easily with conventional, multi-block structured meshes, and easily to adapt the mesh to resolve the flow-field features. All types of meshes can be adapted in FLUENT in order to resolve large gradients in the flow field, but the mesh must always be initially generated whatever the element types used outside of the solver, using GAMBIT, TGrid, or one of the CAD systems for which mesh import filters exist.

FLUENT solves transport equations for mass, momentum, energy, etc. which is applied in each cell. The general transport equation for each cell:

$$\frac{\partial}{\partial t} \int_V \rho \phi dV + \oint_A \rho \phi \mathbf{V} \cdot d\mathbf{A} = \oint_A \Gamma \nabla \phi \cdot d\mathbf{A} + \int_V S_\phi dV \quad (2-1)$$

where ϕ is a quantity which is 1 for continuity equation, u for x-momentum equation, v for y-momentum equation, and h for energy equation. On the left side of Equation 2-1, the first part of the equation is to account for an unsteady condition and second part is to account for a convective behavior. On the right side of the Equation 2-1, the first part is to account for a diffusive behavior, and the second part is to account for generation of quantity (ϕ) inside the cell. Each transport equation is then discretized into algebraic form. The discretized equations require field data (material properties, velocities, etc.) which are stored at cell centers; and also require face values which are interpolated in terms of local and adjacent cell values. The Equation is written out for every control volume in domain resulting in an equation set. The set of equations are then solved to render flow field. The basic program structure of FLUENT software package is shown in Figure 2-3.

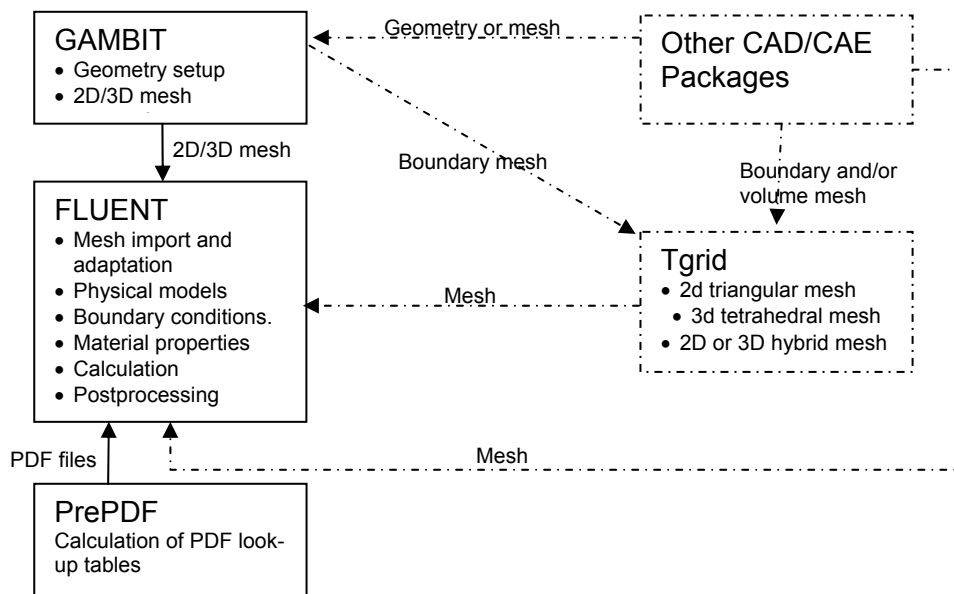


Figure 2-3: Basic program structure of FLUENT software package.

2.3.1 Problem Solving Steps in FLUENT

Having determined the important features of the problem to be solved, then the following basic procedural steps should be followed.

1. Create the model geometry and grid in the Gambit.
2. Start the FLUENT by selecting the appropriate solver for 2D or 3D modeling.
3. Import the grid.
4. Check the grid.
5. Select the solver formulation.
6. Choose the basic equations to be solved: laminar or turbulent, chemical species or reaction, heat transfer models, etc. Identify additional models needed: fans, heat exchangers, porous media, etc.
7. Specify material properties.
8. Specify the boundary conditions.
9. Adjust the solution control parameters, initialize the flow field and calculate a solution by iteration.
10. Examine and write the results.

If necessary, refine the grid or consider revisions to the numerical or physical model.

2.3.2 FLUENT Numerical Solvers

FLUENT has two major numerical solvers; namely, Segregated solver and Coupled solver – Implicit and Explicit. In either of these methods, FLUENT will solve the governing integral equations for the conservation of mass and momentum, and energy(when appropriate) and other scalars such as turbulence and chemical species and in both cases a control-volume-based technique is used. For this work segregated solver was used.

Segregated Solver

In this approach, the governing equations are solved sequentially (i.e., segregated from one another), because the governing equations are non-linear (and coupled), several iterations of the solution loop must be performed before a converged solution is obtained.

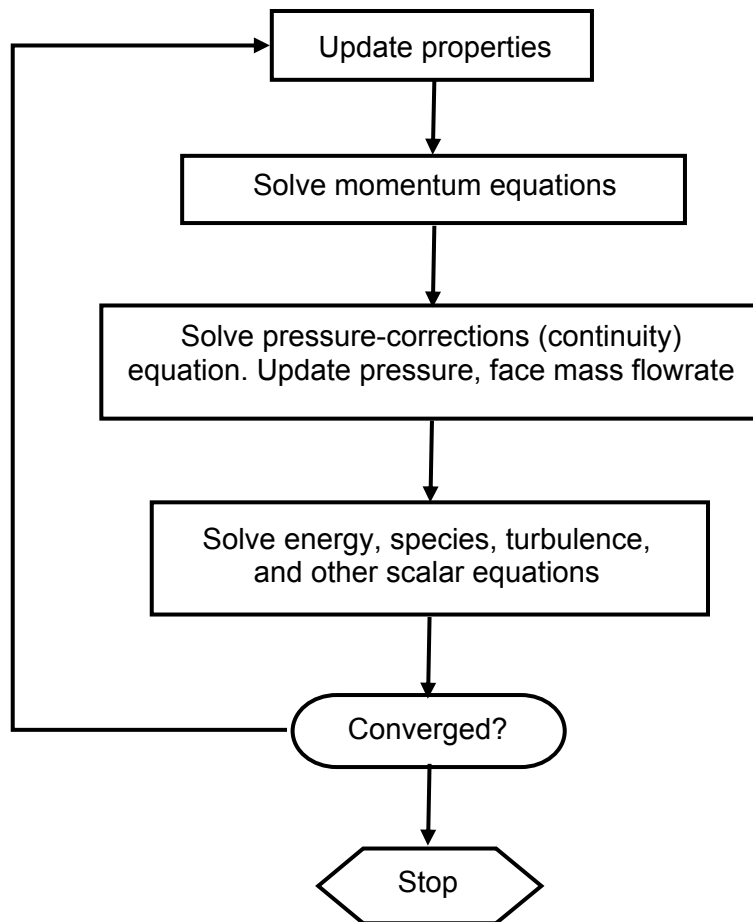


Figure 2-4: Overview of the segregated solution method.

Figure 2-4 give an overview of the segregated solution method in the following steps:

1. Fluid properties are updated, based on the current solution. (If the calculation has just begun, the fluid properties will be updated based on the initialized solution.)
2. The u , v , and w momentum equations are each solved in turn using current values for pressure and face mass fluxes, in order to update the velocity field.
3. Since the velocities obtained in Step 2 may not satisfy the continuity equation locally, "Poisson-type" equation for the pressure correction is derived from the continuity equation and the linearized momentum equations. This pressure correction equation is then solved to obtain the necessary corrections to the pressure and velocity fields and the face mass fluxes such that continuity is satisfied.

4. Where appropriate, equations for scalars such as turbulence, energy, species, and radiation are solved using the previously updated values of the other variables.
5. When interphase coupling is to be included, the source terms in the appropriate continuous phase equations may be updated with a discrete phase trajectory calculation.
6. A check for convergence of the equation set is made.

The iteration process is continued until the convergence criteria are met.

Coupled Solver

The coupled solver solves the governing equations of continuity, momentum, and energy (where appropriate) and species transport simultaneously (i.e., coupled together). Governing equations for additional scalars will be solved sequentially (i.e., segregated from one another and from the coupled set) using the procedure described for the segregated solver above because the equations are non-linear (and coupled), several iterations of the solution loop must be performed before a converged solution is obtained.

2.4 Combustion Modeling using FLUENT

FLUENT provides several models for chemical species transport and chemical reactions. FLUENT can model species transport with or without chemical reactions. Chemical reactions that can be modelled in FLUENT include the following: gas phase reactions that may involve NO_x and other pollutant formation; surface reactions (e.g., chemical vapor deposition) in which the reaction occurs at a solid (wall) boundary; particle surface reactions (e.g., coal char combustion) in which the reaction occurs at the surface of a discrete-phase particle.

FLUENT provide five approaches to modeling gas phase reacting flows which are: generalized finite-rate model, non-premixed combustion model, premixed combustion model, partially premixed combustion model, composition probability density function (PDF) transport model. The generalized finite-rate model is suitable for wide range of applications including premixed, partially premixed, and non-premixed combustion. Here the chemical reaction mechanism is user-

defined and the reaction rates that appear as source terms in the species transport equations are computed from equation such as from Arrhenius rate expressions. In the non-premixed combustion model, the individual transport equations are not solved. Instead, transport equations for one or two conserved scalars (the mixture fraction) are solved and individual component concentrations are derived from the predicted mixture fraction distribution. Here the reacting system is treated using flame sheet (mixed is burned) approach or chemical equilibrium calculations. In the premixed combustion model, perfectly mixed reactants and burned products are separated by a flame front. The reaction progress variable is solved to predict the position of this front. The influence of turbulence is accounted for by means of a turbulent flame speed. In the partially premixed combustion model, the mixture fraction equations and the reaction progress variable are solved to determine the species concentration and position of the flame front. Last but not least, the composition PDF transport model simulates realistic finite-rate chemistry in turbulent flames. Arbitrary chemical mechanism can be imported into FLUENT and kinetic effects such as non-equilibrium species and ignition/extinction can be captured. This model is applicable to premixed, non-premixed, and partially premixed flames. But one must note that this model is computationally expensive.

The first step in solving any problem involving species transport and reacting flow is to determine which model is appropriate. For cases involving the mixing, transport, or reaction of chemical species, or reactions on the surface of a wall or particle (e.g., chemical vapor deposition), the generalized finite-rate model can be used. For reacting systems involving turbulent diffusion flames that are near chemical equilibrium where the fuel and oxidizer enter the domain in two or three distinct streams, use the non-premixed combustion model. For cases with single, perfectly mixed reactant streams use the premixed combustion model. For cases involving premixed flames with varying equivalence ratio in the domain use the partially premixed combustion model. For turbulent flames where finite-rate chemistry is important, use laminar flamelet model, the eddy dissipation concept (EDC) model, or the composition probability density function (PDF) transport model.

The combustion reactions in kilns are mostly a non-premixed combustion; that is, both the fuel and oxidizer flow into the reaction in a separate stream. Under the assumption that elemental mass fractions are conserved scalar, since elements are neither created nor destroyed by chemical reaction, thermochemistry can be reduced to a single parameter called mixture fraction, f . The mixture fraction is the mass fraction that originated from the fuel stream or the local mass fraction of burnt and un-burnt fuel stream elements (C, H, etc.) in all species (CO_2 , H_2O , O_2 etc.). In other words mixture fraction is of the conserved scalar quantities and therefore its governing equation does not have a source term. Combustion is simplified to a mixing problem, and the difficulties associated with closing non-linear mean reactions rate are avoided.

The non-premixed modeling approach has been specifically developed for the simulation of turbulent diffusion flames with fast chemistry. The method offers many benefits over the finite rate formulation. The non-premixed model allows intermediate species (or radicals) prediction, dissociation effects, and rigorous turbulence-chemistry coupling. The method is computationally efficient in that it does not require the solution of a large number of species transport equations. When the underlying assumptions are valid, the non-premixed approach is preferred over the finite rate formulation.

The non-premixed modelling approach involves the solution of transport equations for one or two conserved scalars (the mixture fractions). Equations for individual species are not solved. Instead, species concentrations are derived from the predicted mixture fraction fields. The thermochemistry calculations are pre-processed in pre-PDF and tabulated for look-up in FLUENT. Interaction of turbulence and chemistry is accounted for with a probability density function.

The basis of the non-premixed modelling approach is that under a certain set of simplifying assumptions, the instantaneous thermo-chemical state of the fluid is related to a conserved scalar quantity known as the mixture fraction f . It can be defined as the ratio of mass of material having its origin in the fuel stream to mass of mixture.

$$f = \frac{Z_i - Z_{i,ox}}{Z_{i,fuel} - Z_{i,ox}} \quad (2-2)$$

where Z_i is elemental mass fraction for element, i . The subscript ox denotes the value at the oxidizer stream inlet and the subscript fuel denotes the value at the fuel stream inlet. The instantaneous mixture fraction value at each point in the flow field can be used to compute the instantaneous values of individual species mole fractions, density, and temperature.

2.5 Turbulence Modeling using FLUENT

Practically all technically relevant flows are indeed turbulent. In numerical simulations of such flows, a turbulence model has to be used in order to keep computing times reasonable. Special attention needs to be paid to accurate modeling of turbulence.

The presence of turbulent fluctuations, which are functions of time and position, contribute a mean momentum flux or Reynolds stress for which analytical solutions are nonexistent. These Reynolds stresses govern the transport of momentum due to turbulence and are described by additional terms in the Reynolds-Averaged Navier-Stokes (RANS). The RANS equations are as follows:

$$\rho \left(\frac{\partial U_i}{\partial t} + U_k \frac{\partial U_i}{\partial x_k} \right) = - \frac{\partial p}{\partial x_i} + \frac{\partial}{\partial x_j} \left(\mu \frac{\partial U_i}{\partial x_j} \right) + \frac{\partial R_{ij}}{\partial x_j} \quad (2-3)$$

where $R_{ij} = -\overline{\rho u_i u_j}$ is called the Reynolds stresses. The Reynolds stresses are additional unknowns introduced by the averaging procedure, hence they must be modeled (related to the averaged flow quantities) in order to close the equations. The purpose of a turbulence model is to provide numerical values for these Reynolds stresses at each point in the flow. The objective is to represent the Reynolds stresses as realistically as possible, while maintaining a low level of complexity.

In FLUENT, RANS modeling involve an ensemble averaging which may be used to extract the mean flow properties from the instantaneous. Figure 2-5 shows the method of ensemble averaging which follows by Equation 2-4 and Equation 2-5 that describe the mathematical expression of the figures.

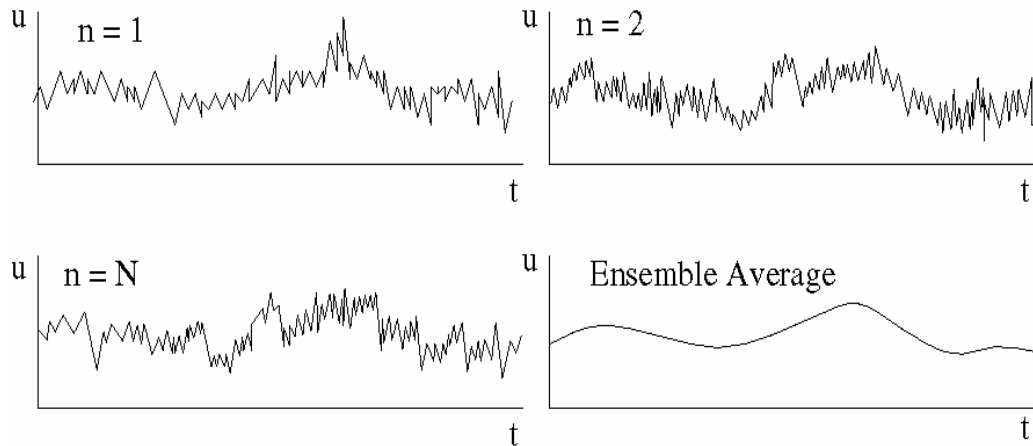


Figure 2-5: RANS modeling using an ensemble averaging

where:

$$U_i(\bar{x}, t) = \lim_{N \rightarrow \infty} \frac{1}{N} \sum_{n=1}^N U_i^{(n)}(\bar{x}, t) \quad (2-4)$$

$$u_i(\bar{x}, t) = U_i(\bar{x}, t) + u_i(\bar{x}, t) \quad (2-5)$$

with $U_i(\bar{x}, t)$ is the mean and $u_i(\bar{x}, t)$ is the fluctuation.

In complex flows having relevance to practical applications, turbulence plays a major role and its accurate representation is crucial for correct predictions. This is achievable by considering the effects of the whole spectrum of turbulent scales on the mean flows, a possibility reserved to direct numerical simulation (DNS) and large eddy simulation (LES). Unfortunately, these sophisticated prediction tools are computational costly (often 10 to 100 times more than RANS) and are not practical for industrial flows.

It is an unfortunate fact that no single turbulence model is universally accepted as being superior for all classes of problems. The choice of turbulence model will

depend on considerations such as the physics encompassed in the flow, the established practice for a specific class of problem, the level of accuracy required, the available computational resources, and the amount of time available for the simulation. A wide range of models is available, and understanding the limitations and advantages of the selected one is required if the best answer is to be obtained with the minimum computation. Table 2-1 summarize the RANS turbulence model description available in FLUENT which is then follow by Table 2-2 that summarize the RANS turbulence model behavior and usage.

Table 2-1: RANS turbulence model description. [FLUENT, 2003]

Model	Description
Spalart- Allmaras	A single transport equation model solving directly for a modified turbulent viscosity. Designed specifically for aerospace applications involving wall-bounded flows on a fine, near-wall mesh. Fluent's implementation allows use of coarser meshes. Option to include strain rate in k production term improves predictions of vortical flows.
Standard $k-\varepsilon$	The baseline two transport equation model solving for k and ε . This is the default $k-\varepsilon$ model. Coefficients are empirically derived; valid for fully turbulent flows only. Options to account for viscous heating, buoyancy, and compressibility are shared with other $k-\varepsilon$ models.
RNG $k-\varepsilon$	A variant of the standard $k-\varepsilon$ model. Equations and coefficients are analytically derived. Significant changes in the ε equation improves the ability to model highly strained flows. Additional options aid in predicting swirling and low Re flows.
Realizable $k-\varepsilon$	A variant of the standard $k-\varepsilon$ model. Its 'realizability' stems from changes that allow certain mathematical constraints to be obeyed which ultimately improves the performance of this model.
Standard $k-\omega$	A two transport equation model solving for k and ω the specific dissipation rate (ε/k) based on Wilcox. This is the default $k-\omega$ model. Demonstrates superior performance for wall bounded and low-Re flows. Shows potential for predicting transition. Options account for transitional, free shear, and compressible flows.
SST $k-\omega$	A variant of the standard $k-\omega$ model. Combines the original Wilcox model (1988) for use near walls and standard $k-\varepsilon$ model away from walls using a blending function. Also limits turbulent viscosity to guarantee that $\tau_t \sim k$. The transition and shearing options borrowed from SKO. No compressibility option.

Reynold Stress Model	Reynolds stresses are solved directly with transport equations avoiding isotropic viscosity assumption of other models. Use for highly swirling flows. Quadratic pressure-strain option improves performance for many basic shear flows.
----------------------	--

Table 2-2: RANS turbulence model behavior and usage. [FLUENT. 2003]

Model	Behavior and Usage
Spalart- Allmaras	Economical for large meshes. Performs poorly for 3D flows, free shear flows, flows with strong separation. Suitable for mildly complex (quasi-2D) external/internal flows and b.l. flows under pressure gradient (e.g. airfoils, wings, airplane fuselage, missiles, ship hulls).
Standard $k-\varepsilon$	Robust. Widely used despite the known limitations of the model. Performs poorly for complex flows involving severe ∇p , separation, strong stream line curvature. Suitable for initial iterations, initial screening of alternative designs, and parametric studies.
RNG $k-\varepsilon$	Suitable for complex shear flows involving rapid strain, moderate swirl, vortices, and locally transitional flows (e.g., b.l. separation, massive separation and vortex-shedding behind bluff bodies, stall in wide-angle diffusers, room ventilation)
Realizable $k-\varepsilon$	Offers largely the same benefits and has similar applications as RNG. Possibly more accurate and easier to converge than RNG.
Standard $k-\omega$	Superior performance for wall-bounded b.l., free shear, and low Re flows. Suitable for complex boundary layer flows under adverse pressure gradient and separation (external aerodynamics and turbomachinery). Can be used for transitional flows (though tends to predict early transition). Separation is typically predicted to be excessive and early.
SST $k-\omega$	Similar benefits as SKO. Dependency on wall distance makes this less suitable for free shear flows.
Reynold Stress Model	Physically the most sound RANS model. Avoids isotropic eddy viscosity assumption. More CPU time and memory required. Tougher to converge due to close coupling of equations. Suitable for complex 3D flows with strong streamline curvature, strong swirl/rotation (e.g. curved duct, rotating flow passages, swirl combustors with very large inlet swirl, cyclones).

2.6 CFD Simulation of this Work

The CFD calculations in this study were carried out using the FLUENT 6.x package. For the reactive flows, the oxidation is a non-premixed combustion; that means both the fuel and the air flow into the chamber in separate streams which is the general case in chemical processing applications. As combustion gas, waste gas was used, which is typical for the application studied here. The composition consists of CO, H₂, CO₂, H₂O, N₂ and small amount of hydrocarbon of CH₄. The combustible component of CO, H₂, and CH₄ were varied to cover the range of heating value of typical waste gas.

Table 2-3: Compositions of the waste gas used for simulations.

No.	Compositions	Waste Gas [% vol]	
		$h_u = 2.4 \text{ MJ/m}^3$	$h_u = 4.7 \text{ MJ/m}^3$
1	CO	9.53	19.06
2	H ₂	6.60	13.20
3	CH ₄	1.60	3.2
4	CO ₂	11.71	8.1
5	H ₂ O	24.03	18.1
6	N ₂	46.53	38.34

The cylindrical chamber geometry used for this simulation includes a number of pipe junctions which made it difficult to create a high-quality mesh. Creating a structured hexagonal mesh which would give the most accurate results is very time consuming and does not lead to an ideal mesh in the region of the pipe junctions. Therefore, an unstructured T-Grid form was chosen and about five hundred thousand cells were used to mesh a part of the cylindrical chamber.

CFD calculations with the whole geometry of the cylindrical chamber as a computational domain was first made as preliminary calculations. Based on the CFD results using the whole geometry, no swirling exists. Therefore a

simplification using only a part of the full geometry with symmetrical boundary conditions can be made. One of the advantages of using only the part of the domain is that a very fine mesh can be constructed.

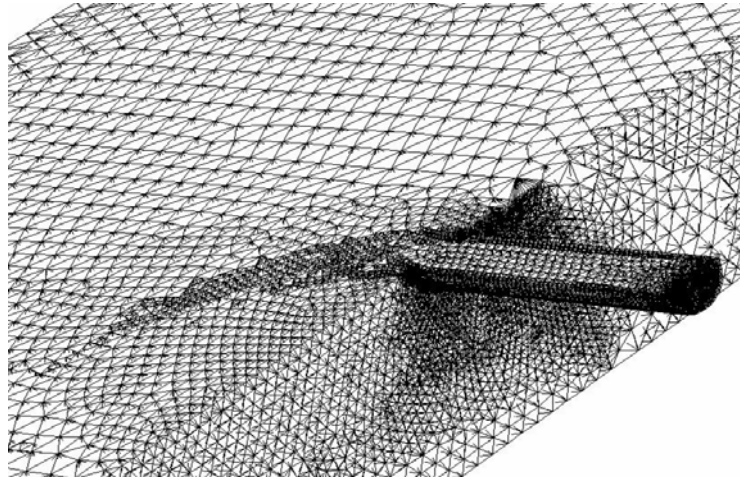


Figure 2-6: Typical grid used for the CFD calculation

Figure 2-6 shows the typical grid that was created in this study. It should be noted that to ensure a better resolution of the simulated results, a grid adaptation in each of the CFD calculations was also made. The adaptations were based on both velocity and temperature gradients as can also be seen in this figure.

EXTERNAL INJECTIONS WITH A SINGLE ROW OF JETS

As a basis of this research, a single row of non-reacting jets oriented perpendicular to the chamber wall and injected inwardly from the chamber wall to the centerline is chosen. The chamber diameter was varied from 0.3 m to 3 m, the number of nozzles from 4 to 32, and cases for both non-reactive and reactive flow were simulated and compared.

3.1 Influencing Parameters

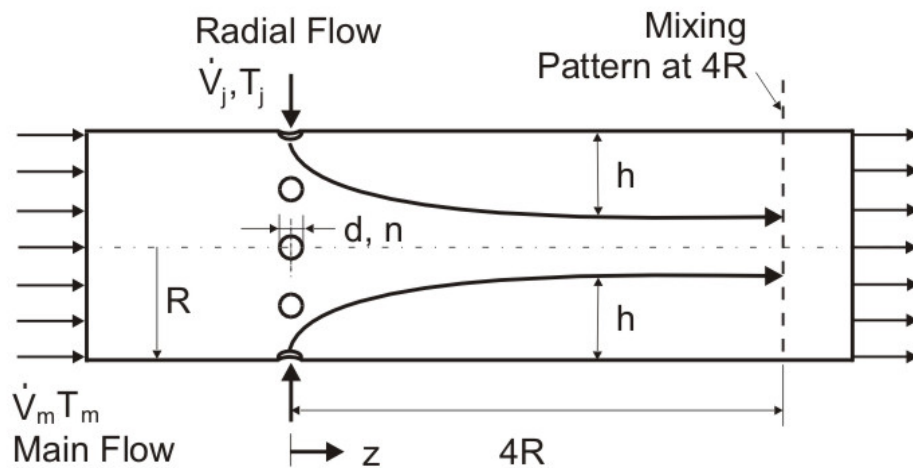


Figure 3-1: Principle of external injections with a single row of jets directed radially into a cylindrical chamber with its jets trajectories.

The influencing parameters are shown in Figure 3-1. Air with a volumetric flow rate \dot{V}_m and a temperature T_m enters along the cylindrical chamber with a diameter of $2R$ as the main input. After reaching a certain distance inside the chamber, a different air stream with a volumetric flow rate of \dot{V}_j and a temperature of T_j is injected radially through a single row of nozzles. The trajectory of the jets and the penetration depth (h/R) has to be determined. The mixing quality is analyzed by means of the difference between the maximum temperature (T_{max}) and the minimum temperature (T_{min}) in the cross-sectional area at a downstream distance of $4R$ after the injection.

From the numerous previous studies it is known that a dimensionless group which can be expressed as follows:

$$J = \rho_j v_j^2 / \rho_m v_m^2 \quad (3-1)$$

is of dominant influence for jets in a cross-flow. Here v and ρ are the velocity and the density for the jets and the mainstream. This group is named as the momentum flux ratio or dynamic pressure ratio [Reményi, 1987]. The velocities v_j and v_m in Equation 3-1 are not given in practical cases, but the volumetric flow rates under standard conditions and the temperatures are given. The velocities can be calculated using Equation 3-2 and Equation 3-3:

$$\dot{V}_m = \left(\pi \cdot D^2 / 4 \right) \cdot v_m \quad (3-2)$$

$$\dot{V}_j = n \cdot \left(\pi d^2 / 4 \right) \cdot v_j \quad (3-3)$$

where \dot{V}_m is the actual volumetric flow rate of the mainstream and D is the chamber diameter. On the other hand, \dot{V}_j is the actual volumetric flow rate for all nozzles, d is the nozzle diameter and n is the number of nozzles.

The actual density and the actual volumetric flow rate were replaced by the reference values under the standard operating conditions (subscripts 'o'), using Equation 3-4:

$$\rho = \rho_o \cdot (T_o/T) \quad ; \quad \dot{V} = \dot{V}_o \cdot (T/T_o) \quad (3-4)$$

where T is the absolute temperature of the mainstream or the jets.

The insertion of Equations 3-2 to 3-4 into Equation 3-1 gives:

$$J = \left(\frac{T_j}{T_m} \right) \cdot \left(\frac{\rho_{jo}}{\rho_{mo}} \right) \cdot \left(\frac{\dot{V}_{jo}}{\dot{V}_{mo}} \right)^2 \cdot \left(\frac{D^2}{nd^2} \right)^2 \quad (3-5)$$

The momentum flux ratio can now be calculated directly based on the inlet conditions and geometric configurations used in the chemical process industries. The variables investigated in this study include all seven variables of Equation 3-5 such as the number of nozzles, nozzle diameter, chamber diameter, jets and mainstream volumetric flow rates and inlet temperature.

3.2 Penetration Depth

The penetration depth is defined as the ratio of the distance between the wall and the maximum or minimum temperature position (h) to the radius of the chamber (R). The penetration depth of the jets can be determined quite accurately using the isotherm field contour such as shown in Figure 3-2. The penetration depth (h/R) was determined by measuring the distance from the wall to the highest or lowest temperature point in the cross-sectional of the temperature field contour.

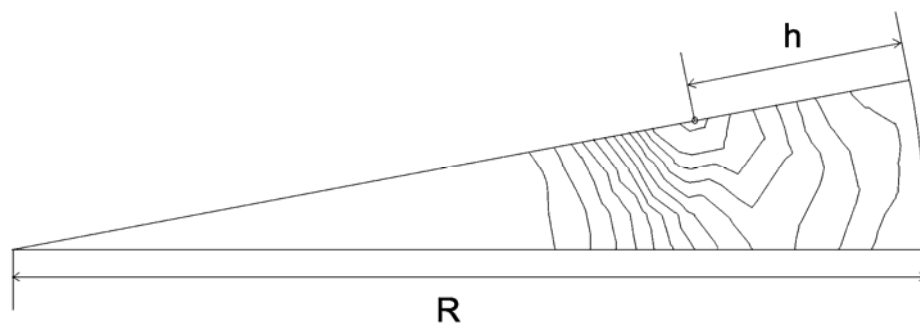


Figure 3-2: Example of isotherm field contour for the determination of the penetration depth.

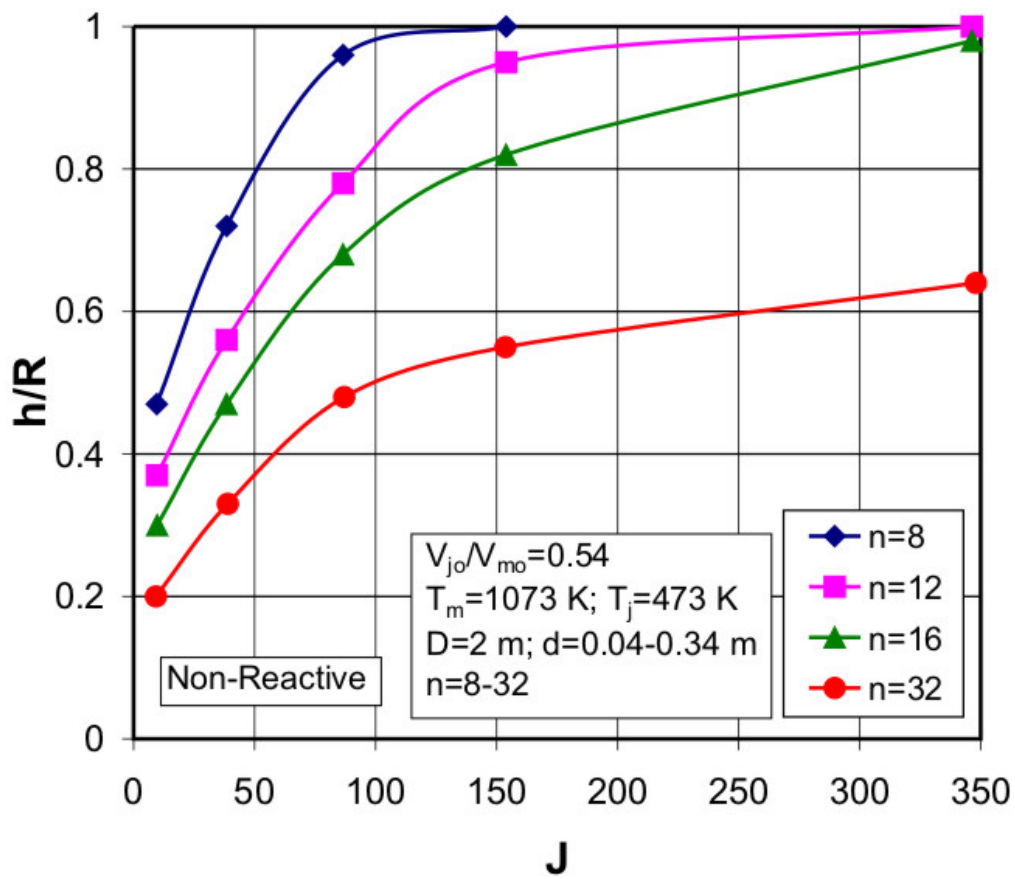


Figure 3-3: Penetration depth as a function of momentum flux ratio for various nozzle diameters of non-reactive flows.

Figure 3-3 shows the penetration depth (h/R) as a function of momentum flux ratio (J) for various nozzle diameters. Here relatively cold jets were injected into a hot and non-reacting cross-flow in a cylindrical chamber with diameter of 2 m. In order to maintain the same value of volumetric flow ratio of jet to mainstream (V_{j0}/V_{m0}) of 0.54, the nozzle diameter were varied between 0.04-0.34 m. It can be seen that by increasing J , the penetration depth also increases. But it is also clear that J is strongly dependent on the number of nozzle. Therefore, there is a need to introduce another parameter which will show less dependency on the number of nozzle.

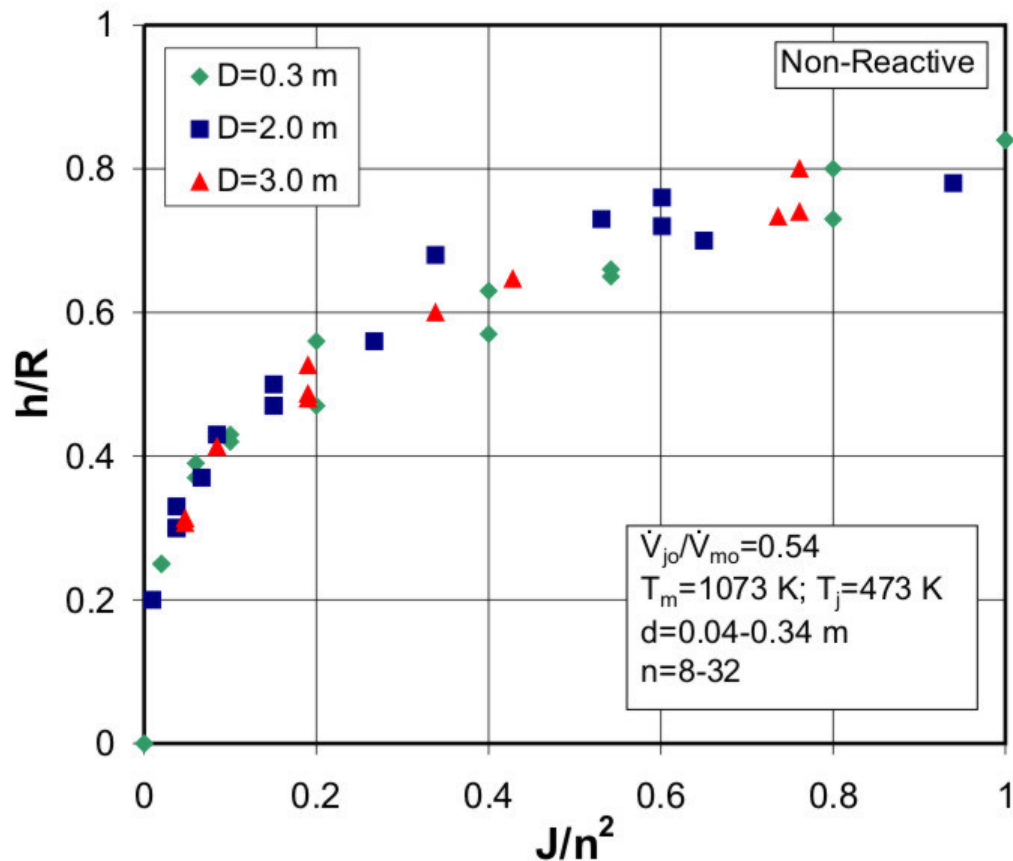


Figure 3-4: Penetration depth as a function of normalized momentum flux ratio for various chamber diameters of non-reactive flows.

Tao, Adler, and Specht (2002) reported that the normalised momentum flux ratio (J/n^2) is the main influencing parameter for the determination of penetration depth. Figure 3-4 shows the influence of J/n^2 on the penetration depth for the three chamber diameters of 0.3 m, 2 m, and 3 m at constant temperatures and volumetric flow ratio. To vary J/n^2 , the diameter and the number of nozzles were varied. It can be seen that J/n^2 is independent of the number of nozzles. Additionally, it can be concluded that the penetration depth is independent of the chamber diameter. Therefore a small chamber diameter of 0.3 will also produce similar penetration depth as large chamber diameter of 3 m. For penetration depths greater than 0.8, the multiple jets begin to meet on the centerline of the chamber, resulting backflows upstream. Therefore, penetration depths under such process conditions can not be accurately determined.

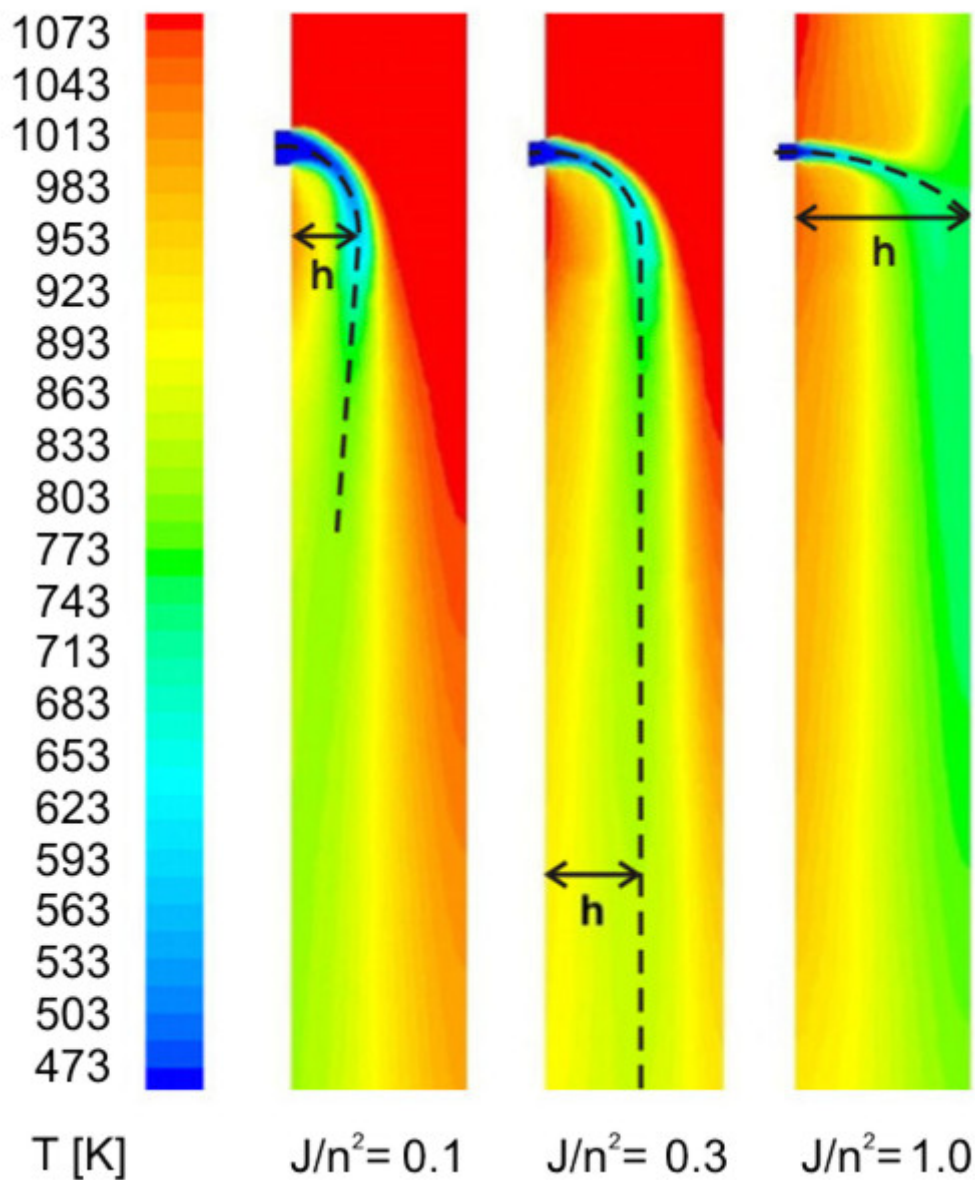


Figure 3-5: Influence of normalized momentum flux ratio of jets to mainstream on penetration depth for non-reactive flows with 12 nozzles.

The temperature field contour of Figure 3-5 shows the influence of this J/n^2 on the penetration depth for a non-reactive flow using 12 nozzles. It is obvious that at $J/n^2=0.1$, the jet can be considered as under-penetrated which results a bad mixing downstream. On the other hand, at $J/n^2=1.0$, the jets meet in the centerline which can be considered as over-penetrated. Unwanted backflows to the upstream occurs giving a bad mixing downstream. The desired condition which gives the optimum temperature homogenisation is somewhat as can be

found at $J/n^2=0.3$, which gives a moderate penetration depth into a cross-flow and gives best mixing downstream.

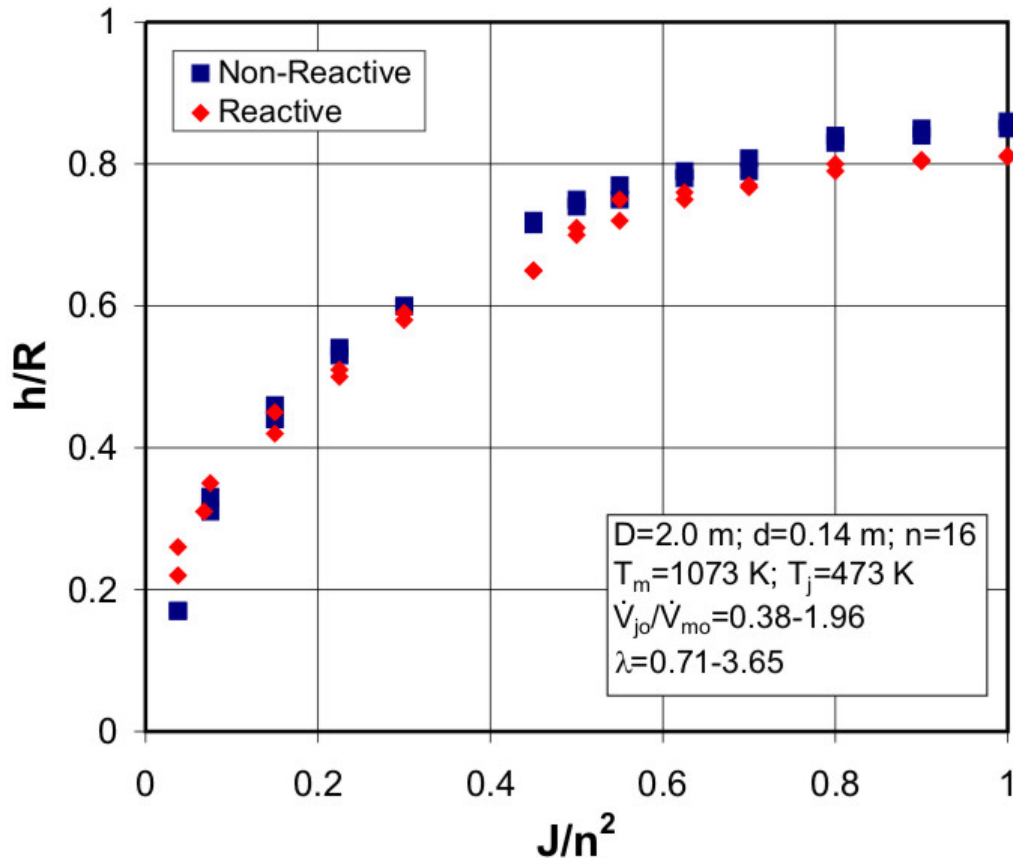


Figure 3-6: Penetration depth as a function of normalized momentum flux ratio for both non-reactive and reactive flows.

Figure 3-6 shows the influence of J/n^2 on the penetration depth such as in Figure 3-4 but for both reactive and non-reactive flows at various volumetric flow ratios of jets to mainstream. The chamber diameter is 2 m, the nozzle diameter is 0.14 m, and the number of nozzles is 16. Here the reactive flow is combustion of waste gas with composition which can be referred back in Table 2-3. In this case, J/n^2 was varied by changing the volumetric flow ratio. For the reactive case, a change in the volumetric flow ratio means a change in the excess air number (λ). All cases have the same profile. Both reactive and non-reactive cases have the same profiles. Therefore for both cases, similar value of J/n^2 will produce similar penetration depth.

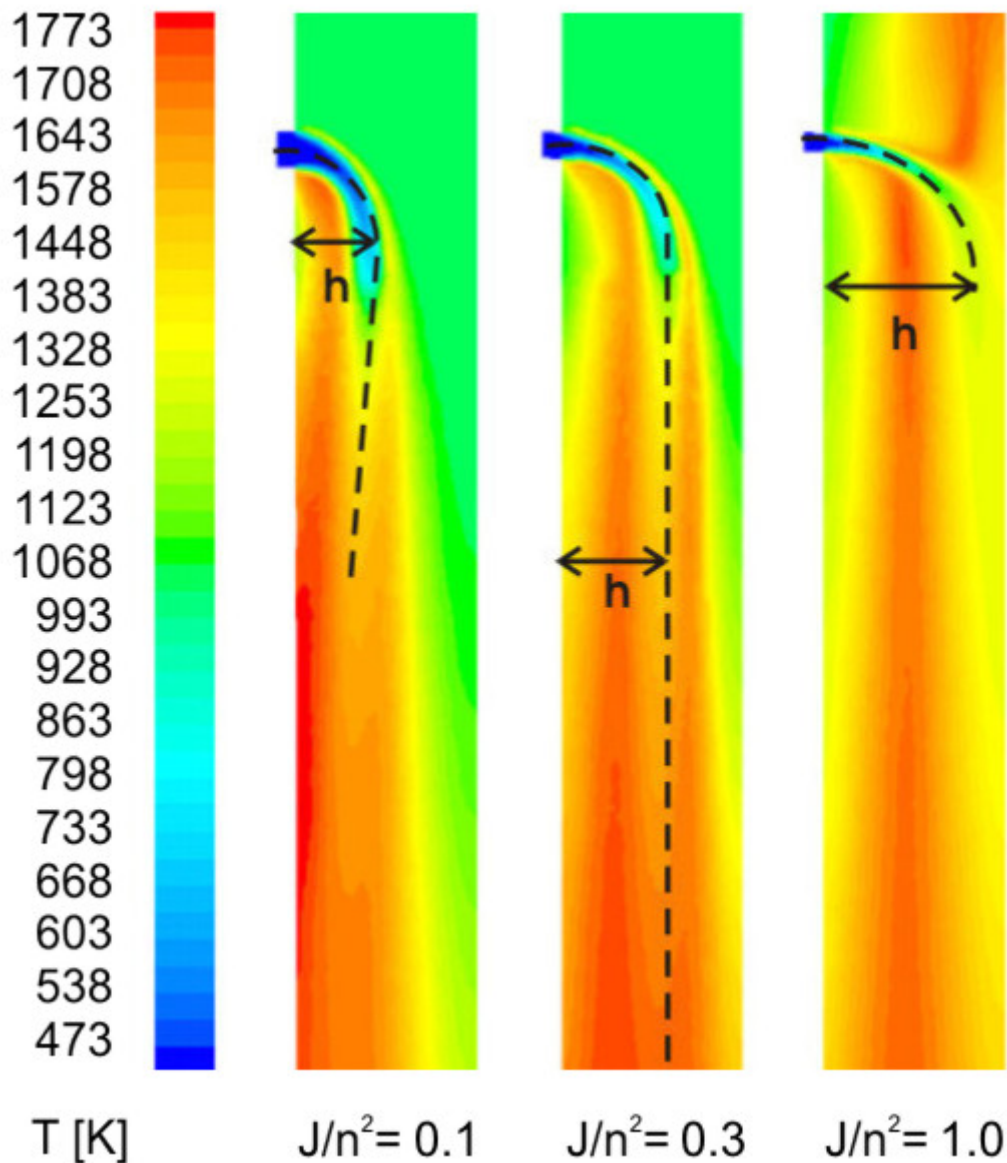


Figure 3-7: Influence of normalized momentum flux ratio of jets to mainstream on penetration depth for stoichiometric combustion of waste gas with 12 nozzles.

Figure 3-7 shows the influence of J/n^2 on the penetration depth but for a reactive flow with 12 nozzles and excess air number of 1. Similar situations occur as with the non-reactive flow of Figure 3-5 due to the same value of volumetric flow ratio of the jets to mainstream ($\dot{V}_{jo}/\dot{V}_{mo}$) of 0.54. The density ratio is nearly the same which is (ρ_{jo}/ρ_{mo}) of 1.01 for the reactive flow and unity for the non-reactive

flow.. It can also be seen that for a moderate penetration ($J/n^2 = 0.3$), the penetration depth remains approximately constant with increasing downstream distance.

3.3 Verifications with other Commercial CFD Codes

The penetration depth is the most important parameter for optimum mixing evaluation. Therefore, its value must be verified with other commercial CFD codes. Four different commercial CFD codes were used which were Phoenics 3.4, CFX-TASC Flow 2.11, CFX 5.5 and Fluent 6.0.

Here as the main input, air with a velocity of 3.1 m/s at 200 °C was used. Hot air at 1200 °C with a velocity of 14.5 m/s was injected radially through each of the 8 nozzles into a cylindrical chamber with a diameter of 2 m. The calculated penetration depths, which were determined are summarised in Table 3-1. It can be seen that the penetration depth deviations even using different grid type among the mentioned commercial CFD codes are not significant.

Table 3-1: Verification with other commercial CFD codes.

CFD Codes	Grid Type	Penetration Depth (h/R)
Phoenics 3.4	structured	0.53
CFX-TASC Flow 2.11	structured	0.54
CFX 5.5	unstructured	0.57
Fluent 6.0	unstructured	0.51

3.4 Mixing Criterion

Proceeding literatures such as [Hatch et al., 1995], [Doerr et al , 1995], [Holdeman et al. 1997], [Tao et al., 2002] had investigated parameters to evaluate mixing such as:

$$\text{Mixture fraction: } f = \left(\frac{T - T_j}{T_m - T_j} \right) \quad \text{or} \quad \theta = 1 - f = \left(\frac{T_m - T}{T_m - T_j} \right) \quad (3-6)$$

$$\text{Equilibrium mixture fraction: } f_{\text{equil}} = \left(\frac{T_{\text{equil}} - T_j}{T_m - T_j} \right) \quad (3-7)$$

Normalized maximum temperature difference:

$$\Delta T_m = \left(\frac{T_{\text{max}} - T_{\text{min}}}{T_m - T_j} \right) \quad (3-8)$$

Area weighted standard deviation created at each location z/R using:

$$\text{Mixture uniformity} = \sqrt{\frac{1}{A} \sum_{i=1}^n a_i (f_i - f_{\text{equil}})^2} \quad (3-9)$$

For this study, it is important to obtain flows with lowest temperature difference downstream. Therefore the first three definitions of Equations 3-6 up to 3-8 make no sense for reactive flows since T_m and T_j may have the same value in chemical industrial process applications. It should be noted here that the mixing temperature for reactive and non-reactive flows (T_{equil} or T) can be significantly different. For the case of non-reactive flow, the mixing temperature will always lay between the inlet temperatures (T_m and T_j). However for the case of reactive flow especially for combustion, the mixing temperature can be much higher than both inlet temperatures. Referring to Equation 3-9, one peak of temperature has virtually no influence on the area-weighted standard deviation. Beside this, a peak of temperature in any streamline could cause damage in the apparatus downstream as explained in the introduction.

The maximum temperature difference gives the difference between the maximum and the minimum local temperatures in the chamber cross-section area. This is the strongest condition for an optimum mixing. The downstream distance to evaluate the mixing was set at $z/D=2$ as explained before. Referring back to Figure 3-5 and 3-7, it can be seen that after this downstream distance, the mixing will not be significantly improved.

3.5 Mixing Conditions

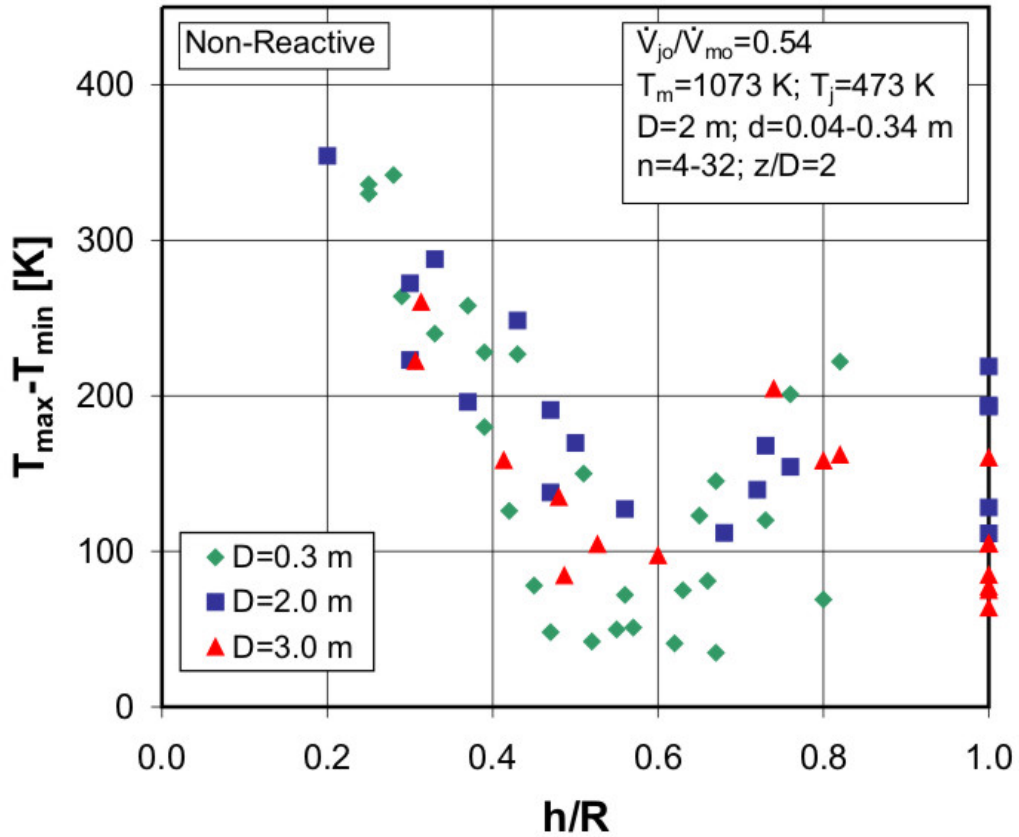


Figure 3-8: Temperature differences at $z/D=2$ as a function of penetration depth for various chamber diameters.

For this investigation the maximum temperature difference is chosen to evaluate the mixing quality. Figure 3-8 shows this temperature difference at a distance of $z/D=2$ as a function of penetration depth for various chamber diameters for $\dot{V}_{jo}/\dot{V}_{mo} = 0.54$, $T_j=473$ K and $T_m= 1073$ K. It can be seen that there is a clear minimum of temperature difference at a value h/R of about 0.6. The temperature difference will again reach a low value if the jet is over penetrated and meet in centerline. However, these high penetration depths require values of J/n^2 to be many times higher than those for $h/R=0.6$. As a consequence, a higher pressure drop is needed and the process will be considered as non-economical. Again, It should also be noted that the chamber diameter has no recognizable influence

Figure 3-9 also shows temperature difference at a distance of $z/D=2$ as a function of penetration depth for the same situation as in Figure 3-7, but for both non-reactive and reactive flows. It can be seen that there is also clear minimum of temperature difference at a value h/R of about 0.6.

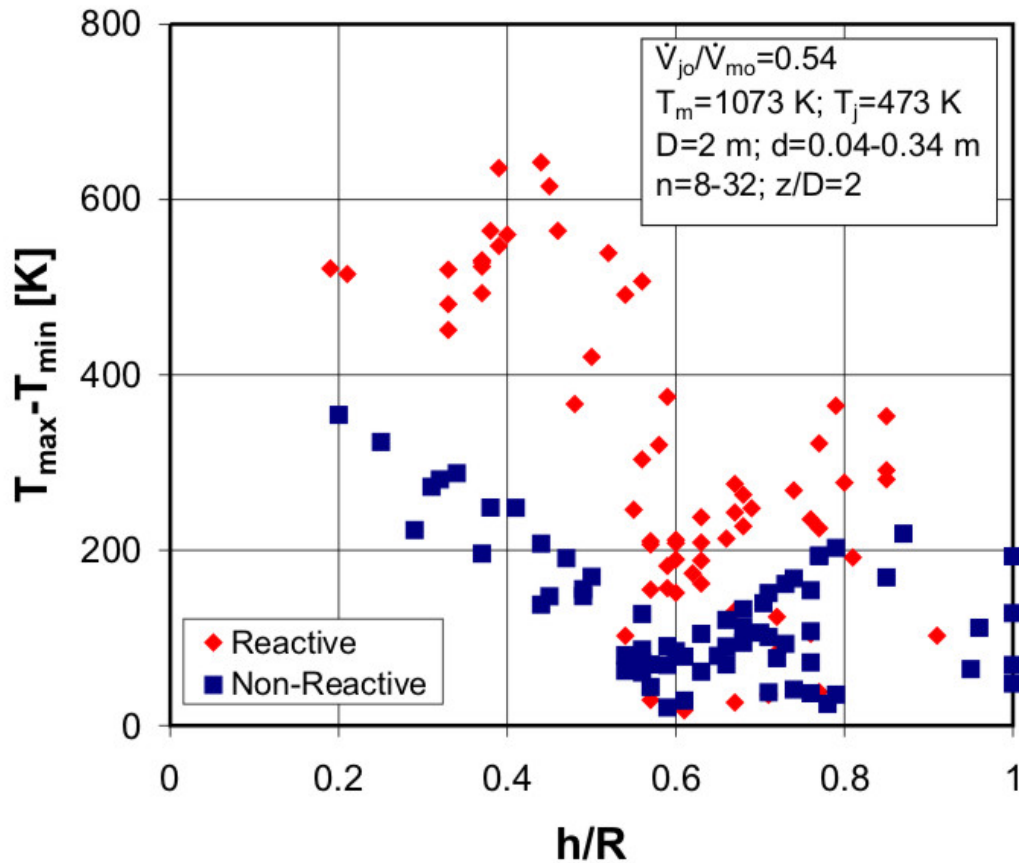


Figure 3-9: Temperature differences at $z/D=2$ as a function of penetration depth for both reactive and non-reactive flows.

3.6 Influence of Hot and Cold Injections

Figure 3-10 shows the temperature difference as a function of the penetration depth (h/R) for the case of non-reactive flow for various volumetric flow ratios of jets to mainstream. The chamber diameter is 2 m, a nozzle diameter is 0.14 m, and number of nozzles is 16. It can be seen that the minimum value of temperature difference for both cold and hot injections of air occurs at a penetration depth value of about 0.6. Referring back to Figure 3-4 which shows the dependency of J/n^2 toward h/R for the same case, it is clear that this minimum value of h/R corresponds to J/n^2 of about 0.3.

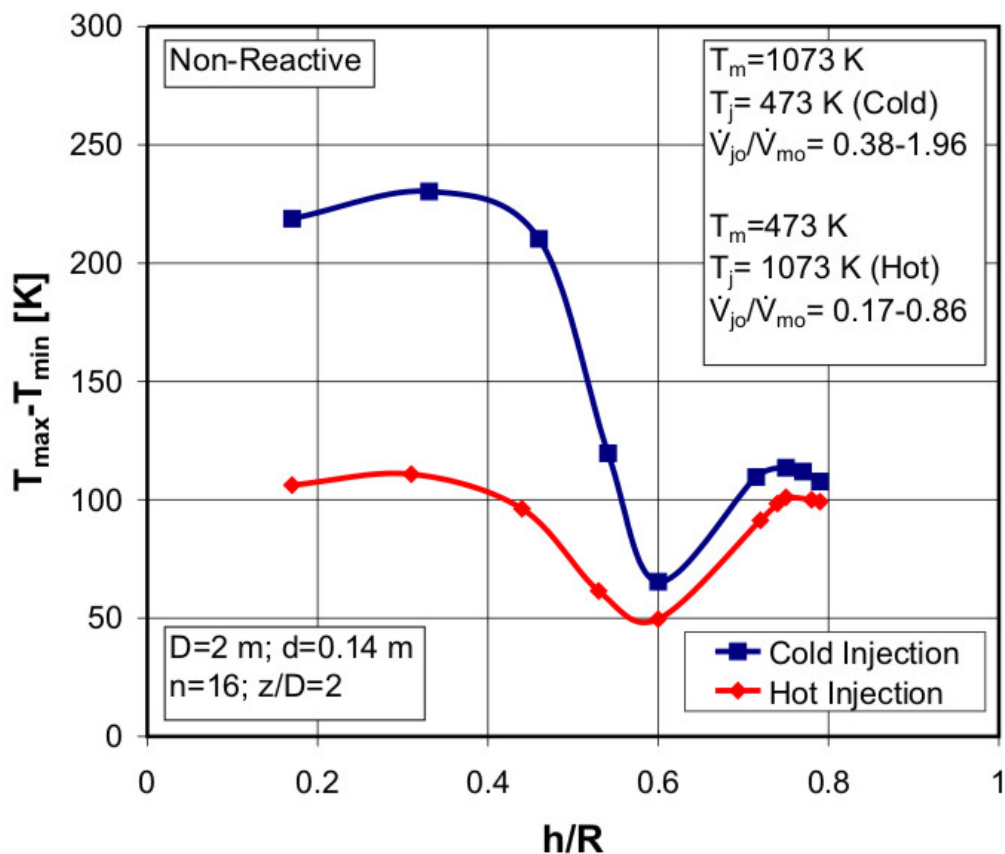


Figure 3-10: The temperature differences at $z/D=2$ for $n=16$ as a function of penetration depth for non-reactive flow for both cold and hot injection

3.7 Influence of the Heating Value

Figure 3-11 shows the temperature differences at a distance $z/D=2$ for 24 nozzles as a function of normalized momentum flux ratio for reactive case with two heating value at the same air excess number which is at a stoichiometric condition. The waste gas composition can be referred back to Table 2-3. It is obvious that a higher heating value results in higher maximum temperature difference. However the optimum mixing condition still has the same range of normalized momentum flux ratio.

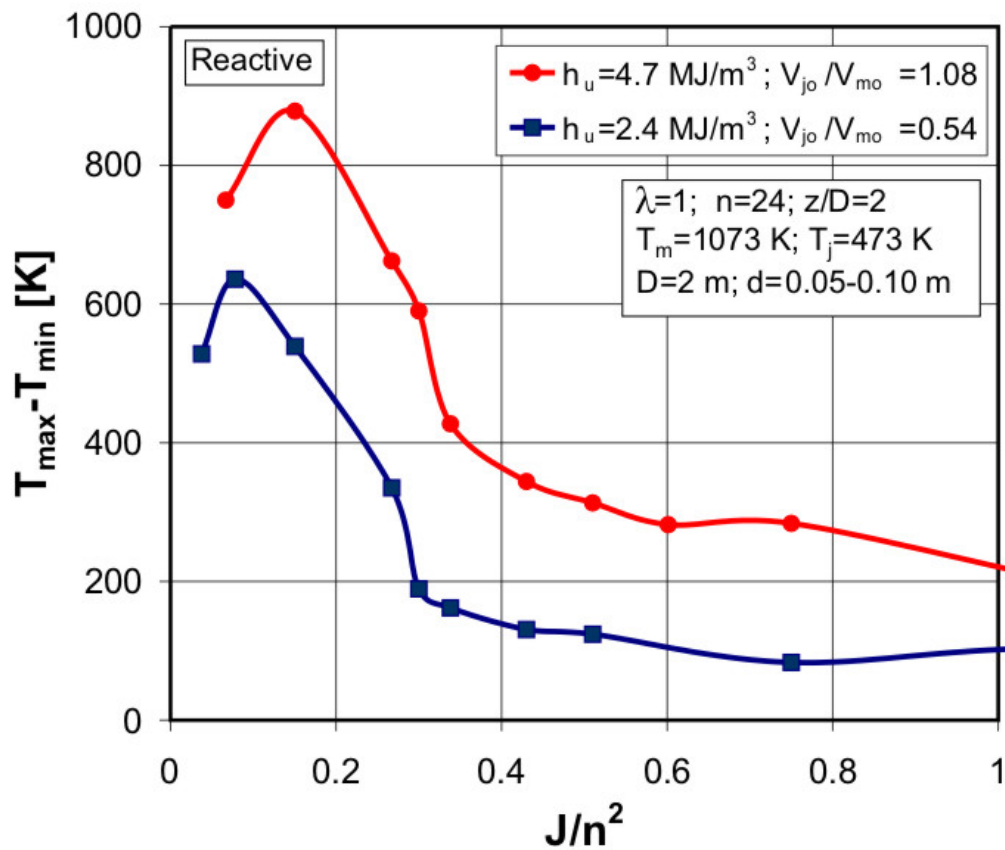


Figure 3-11: Temperature differences at $z/D=2$ for $n=24$ as a function of normalized momentum flux ratio for reactive flow with different heating value.

3.8 Influence of the Number of Nozzles

Although for different parameters and application, this study show no significant deviations with the optimum condition obtained from studies reported by Oechsle et al. (1993) and Bain et al. (1995) as mentioned before. By converting into the parameter used in this study, their results correspond to $J/n^2 \approx 0.32$ and $J/n^2 \approx 0.31$ respectively. Therefore it is clear this optimum condition also apply to chemical industrial process. However the influence of the operating parameters on this optimum condition differs. In the gas turbine or turbo propulsion engine application as for the previous researches, J/n^2 is independent of the power of the engine. Referring back to Equation 3-5, it can be seen that J depends on the ratio of $\dot{V}_{jo} / \dot{V}_{mo}$, which is the volumetric flow ratio of the air to the fuel. This ratio is constant during operation, and it is independent of the power of the engine. Therefore the optimum condition can be obtained by setting the diameter and the number of nozzles for a given chamber diameter. A different situation exists in the chemical process industries because of the ever changing flow parameters such as compositions, flow rates, and temperatures. Here the combustible components varies with time, therefore the injected air flowrate must also be change for a complete combustion. As consequences, the ratio of $\dot{V}_{jo} / \dot{V}_{mo}$ and therewith J depends on time. But one must note that a small change in J/n^2 can significantly result in much higher temperature difference. Hence it is impossible during the operation to regulate to a fixed value of $J/n^2=0.3$ by changing the diameter and the number of nozzle. As a result, a broad range of J/n^2 is required to obtain a good mixing for the chemical industrial application.

In order to have a broad range of J/n^2 , the influence of the number of nozzles on the mixing quality will be now discussed in detail. Figure 3-12 shows the temperature difference as a function of the normalised momentum flux ratio (J/n^2) for a small scale of chamber diameter of 0.3 m. The number of nozzles for this chamber diameter was varied from 4 to 16.

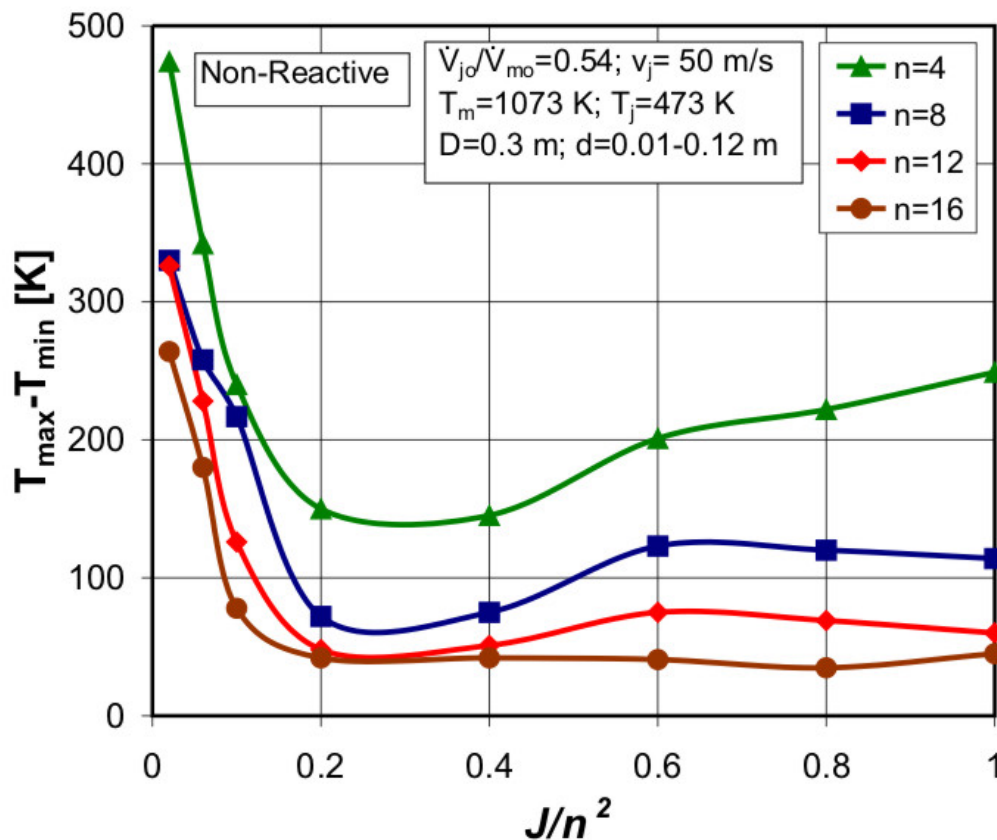


Figure 3-12: The temperature differences for $D=0.3$ m at $z/D=2$ as a function of normalized momentum flux for various numbers of nozzles of non-reactive flow.

It is obvious that the optimum value for all number of nozzles which gives the lowest temperature difference was found again at a value J/n^2 of about 0.3. However, it can be seen that with an increasing number of nozzles the mixing quality will be improved. An increase in the number of nozzle from 4 to 8 results in a strong improvement of the mixing quality. With an increase from 8 to 12 only a slight improvement can be achieved. A further increase of the number of nozzles will then give no significant improvement on the mixing. It is obvious that for a number of nozzles equal to or greater than 12, the mixing quality is nearly independent for values of J/n^2 greater than 0.3. Therefore for a small chamber diameter of 0.3 m, in order to attain a wide range of temperature difference for example of about 40 K, a number of nozzles equal to or greater than 16 with values of J/n^2 greater than 0.3 must be used.

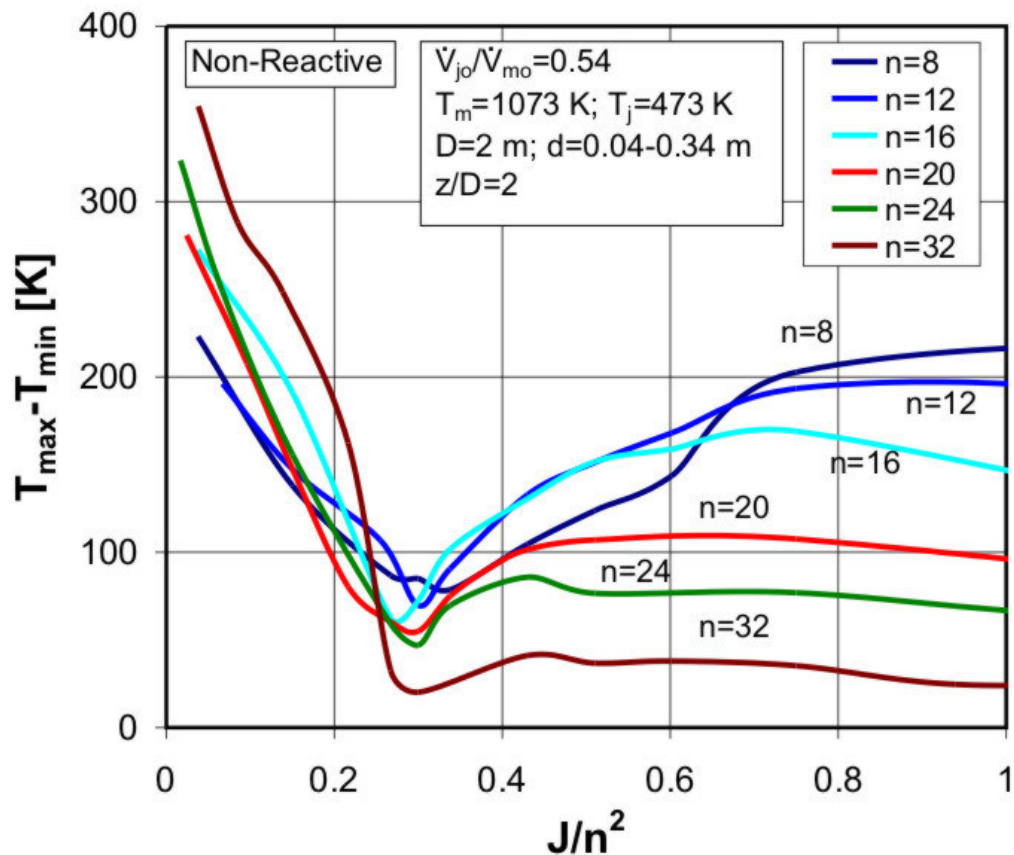


Figure 3-13: The temperature differences for $D=2$ m at $z/D=2$ as a function of normalized momentum flux for various numbers of nozzles of non-reactive flow.

Figure 3-13 shows the influence of the number of nozzles on the temperature difference as a function of the normalised momentum flux ratio (J/n^2) for a large scale of chamber diameter of 2.0 m, which are normally used in chemical process industries. The number of nozzles was varied from 8 to 32, and a lot more of CFD calculations were made since this study is aimed for this scale of chamber diameter. It is obvious, that the optimum value for all number of nozzles was again found at a value J/n^2 of about 0.3. An increase in the number of nozzles also results in an improvement of the mixing quality. But it is obvious here that the number of nozzles also has another influence on the level of temperature differences. For this chamber diameter, a number of 16 nozzles results in much higher temperature differences. Thus for a large chamber diameter of 2.0 m, in order to reach a similar temperature difference for example of about 40 K, as for small chamber diameter of 0.3 m, about 32 number of nozzles are necessary instead of about 16 number nozzles. Therefore, the larger the chamber diameter

is, the higher must be the number of nozzles to obtain similar mixing quality as the smaller chamber diameter. It can also be seen that the mixing quality becomes nearly independent for values of J/n^2 greater than 0.3 with number of nozzles equal to or greater than 24.

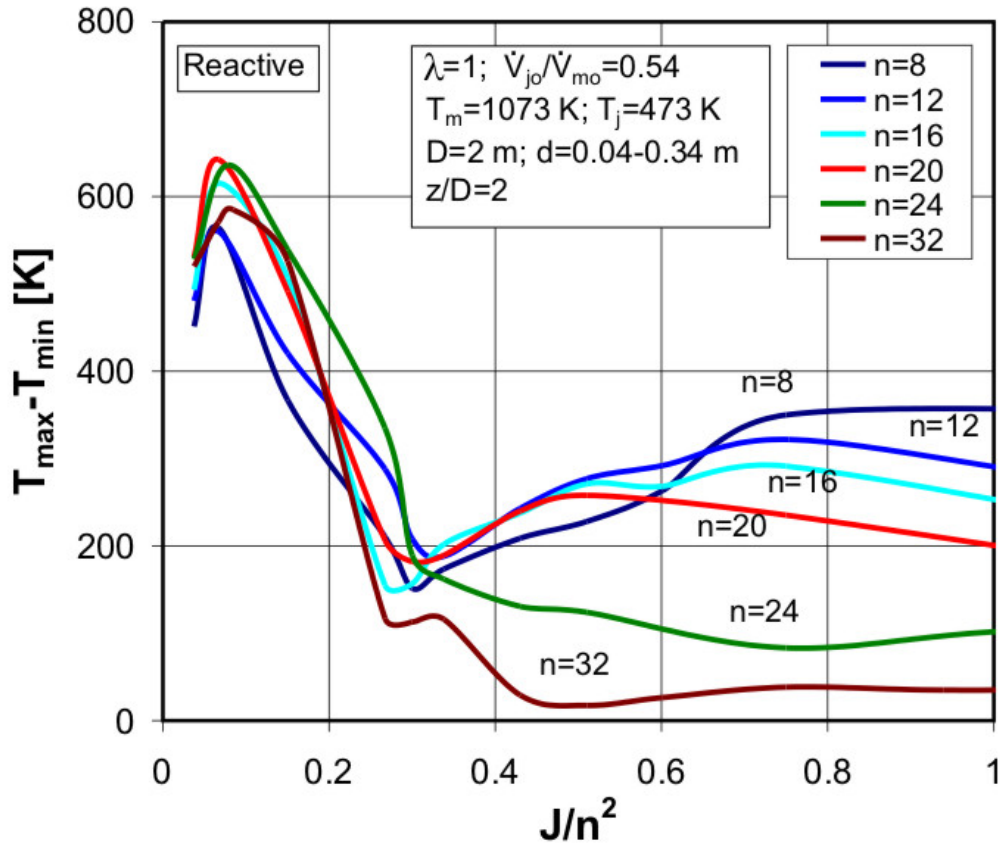


Figure 3-14: The temperature differences for $D=2$ m at $z/D=2$ as a function of normalized momentum flux for various numbers of nozzles of reactive flow.

Figure 3-14 shows the temperature difference as a function of J/n^2 using the same parameters as before but for the reactive case. The optimum is again found at a value of J/n^2 of about 0.3 for all number of nozzles. However as for the non-reactive case, the mixing quality becomes nearly independent for values of J/n^2 greater than 0.3 with number of nozzles equal to or greater than 24.

This result is important for the design of mixing chambers for both reactive and non-reactive cases, because in the chemical processing industry a wide range of regulation of power and mass throughput is necessary as previously explained.

Therefore, it is not possible to adjust the optimum value of the momentum flux ratio at $J/n^2=0.3$ for all required process conditions. As a consequence, a higher number of nozzles are needed to obtain a wide range of J/n^2 to ensure optimum mixing. The additional condition is that the momentum flux ratio (J/n^2) must always be greater than 0.3.

A high number of nozzles and a high value of J/n^2 result in a high pressure drop caused a high jet velocity. Figure 3-15 shows the jet velocity as a function of the normalized momentum flux ratio with the number of nozzles as parameter. It can be seen that the velocity increases with J/n^2 and with the number of nozzles. Thus, some considerations to find a suitable trade off must be made, since higher the number of nozzles means higher jet velocity, and lower number of nozzles means having a bad mixing downstream.

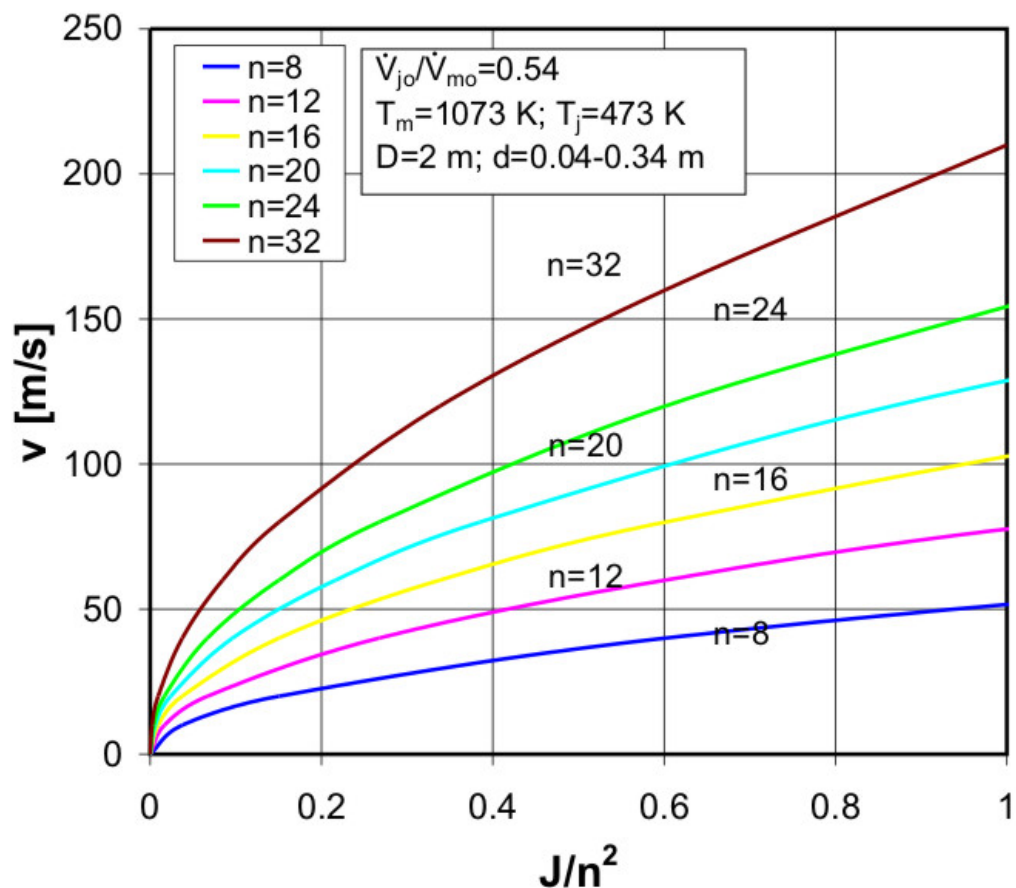


Figure 3-15: The jet velocity as function of normalized momentum flux ratio for various number of nozzles.

EXTERNAL INJECTIONS WITH DOUBLE ROWS OF JETS

A practical example of a reacting jets in a cross-flow using double rows of radial air injections is shown in Figure 4-1. It is combustion of waste gas with composition that can be referred to Table 2-3. The temperature downstream should not exceed 1300 °C to avoid emissions of NO_x but also should not be less than 1200 °C to completely destroy all the hydrocarbons.

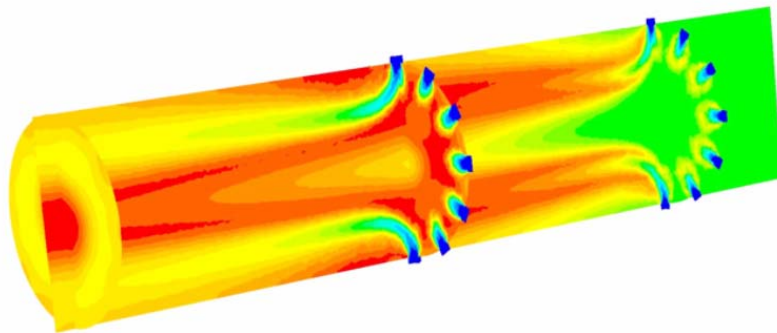


Figure 4-1: Practical example of jets in cross-flow in using double rows of radial air injections.

Two arrangements of the double rows had been studied here. These arrangements were the staggered arrangement and the inline arrangement. The number of nozzles in each row is half the number of nozzles of the single row. For staggered arrangement the nozzles of the second row were shifted angularly in comparison with the nozzles of the first row. Therefore if the spacing distance

between these two rows is zero, then it will be exactly the same arrangement as the single row.

4.1 Influencing Parameters

The influencing parameters are shown in Figure 4-2. Air with a volumetric flow rate \dot{V}_m and a temperature T_m enters along the cylindrical chamber with a diameter of $2R$ as the main input. After reaching a certain downstream distance inside the chamber, a different air stream with a volumetric flow rate of \dot{V}_{j1} and a temperature of T_{j1} is injected radially through the first row of nozzles. Furthermore after reaching a distance l , another or the same air stream as the first row with a volumetric flow rate of \dot{V}_{j2} and a temperature of T_{j2} is injected radially through the second row of nozzles. The trajectory of the jets and the penetration depth (h/R) for each row has to be determined. The mixing of the gases for this type of cylindrical chamber is analyzed by means of the difference between the maximum temperature (T_{max}) and the minimum temperature (T_{min}) in the cross section at a certain downstream distance of $4R$ after the last injection.

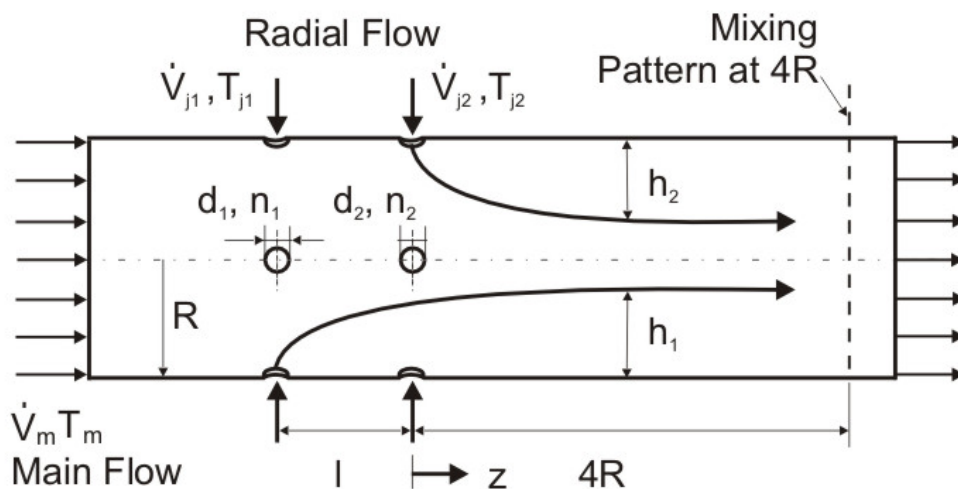


Figure 4-2: Principle of double rows of jets directed radially into a cylindrical chamber with its penetration depths

4.2 Experimentation

The principle of the experimental facility used in the laboratory at Lurgi Bischoff GmbH is illustrated in Figure 4-3 Cold ambient air at a temperature of 20 °C and a flow rate of 1.3 m³/s was used as the main input. A flow patternator was installed to create a plug flow at the inlet. Hot air at a temperature of 385 °C and a total flow rate of 200 m³/s was distributed over the two rows of jets and injected radially into the chamber.

**all dimensions are in mm*

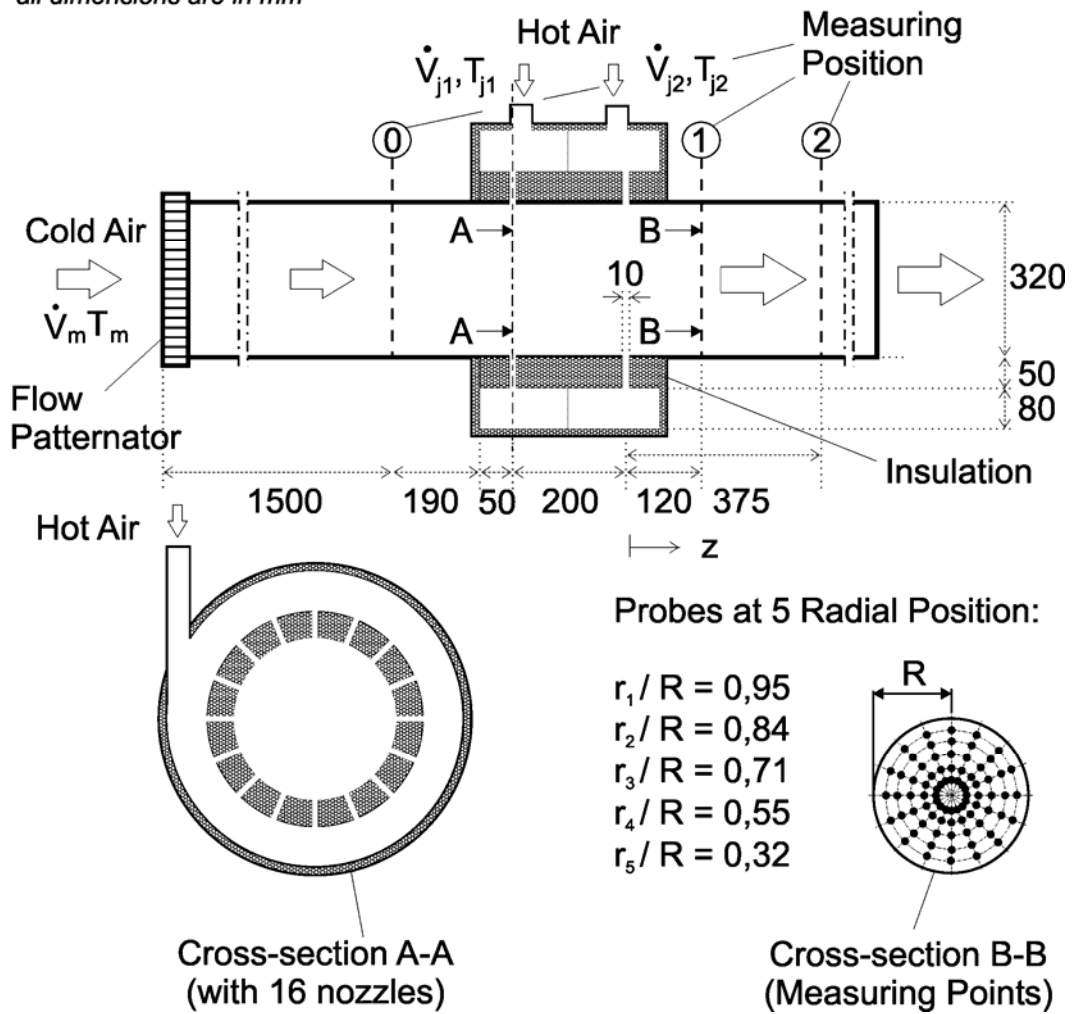


Figure 4-3: Principle of the experimental facility

The cross section A-A shows that the injected hot air was injected tangentially into an annular ring pipe. This purpose was to give an equally distributed flow condition at each of the 16 nozzles. Three measuring positions along the

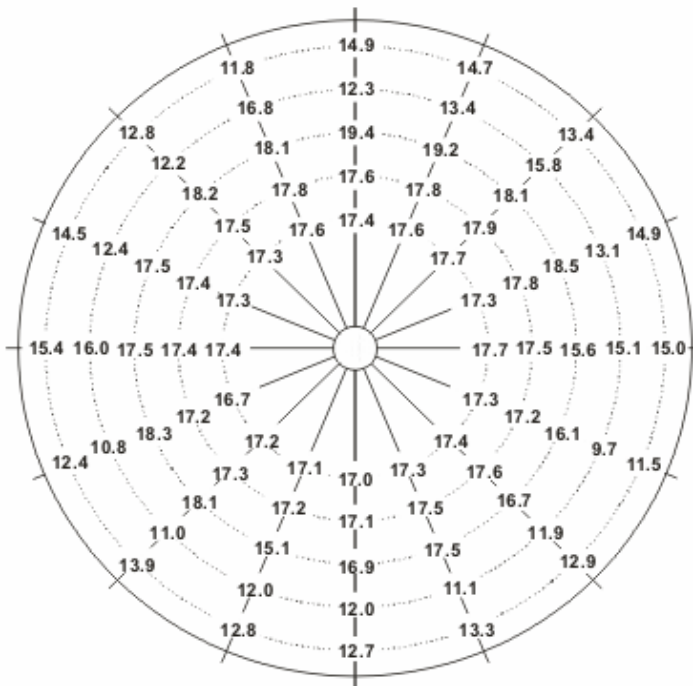
cylindrical chamber were chosen for both velocity and temperature, which were: position 0 at $z/D=-1.4$, position 1 at $z/D=0.4$ and position 2 at $z/D=1.2$. The local velocities were measured using hot wire anemometer and the local temperatures were measured using thermocouples. The measuring orifices were installed in 16 circumferential positions, as shown in Figure 4-3 at the cross section B-B. The measuring values were taken at five radial distances.

Table 4-1: Parameters used for the experiment.

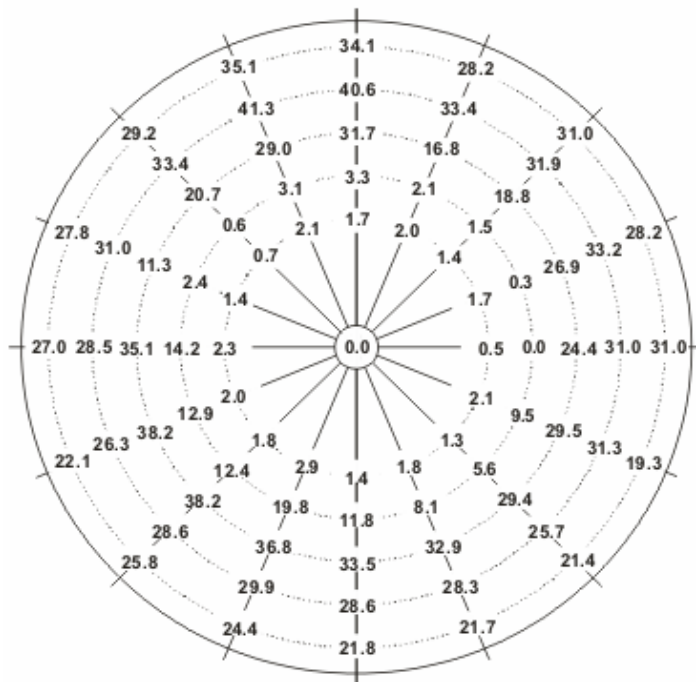
Parameter	Case 1	Case 2	Case 3
$\dot{V}_{j01} / \dot{V}_{j02}$	1/3	2/1	1/1
$\dot{V}_{j01} + \dot{V}_{j02}$ [m ³ /s]	200.2	200.2	200.2
v_{j1} [m/s]	25.7	72.5	53.5
v_{j2} [m/s]	80.6	36.0	53.9
\dot{V}_m [m ³ /s]	1.3	1.3	1.3
D [mm]	320	320	320
$d_{j1} = d_{j2}$ [mm]	10	10	10
$n_{j1} = n_{j2}$	16	16	16
T_m [°C]	20	20	20
$T_{j1} = T_{j2}$ [°C]	385	385	385

Table 4-1 shows the parameters that were varied during the experiment. The volumetric flow ratio of the first and second rows of jets was varied. Three ratios were taken while the other parameters were kept constant. A cylindrical chamber of 320 mm in diameter was used. Two rows of jets with a distance of 200 mm with 16 nozzles in each row were chosen for the experimental study. The second row of jets was inclined angularly by 11.25° to the first row of jets creating a staggered arrangement.

Measuring Position at $z/D=0.4$ (Position 1)



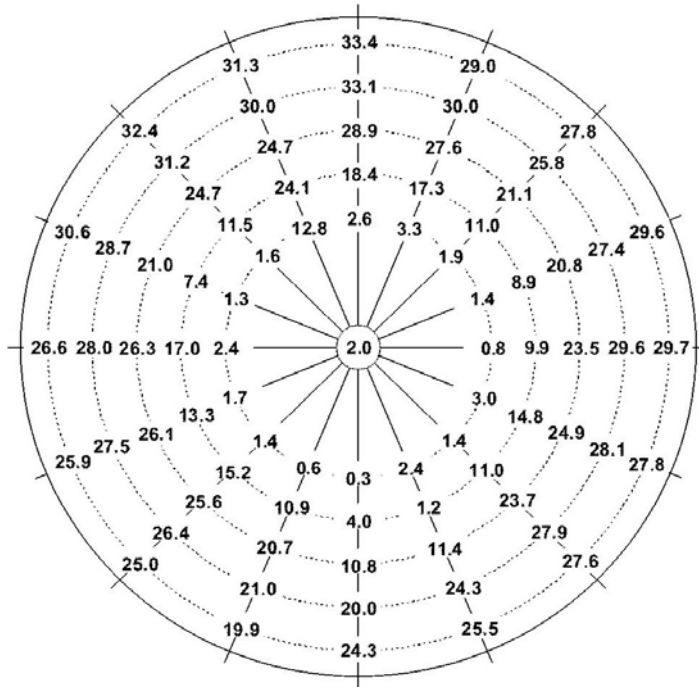
$(T-T_a)$ average : 18.4 °C
 Relative Standard Deviation: 72.3 %



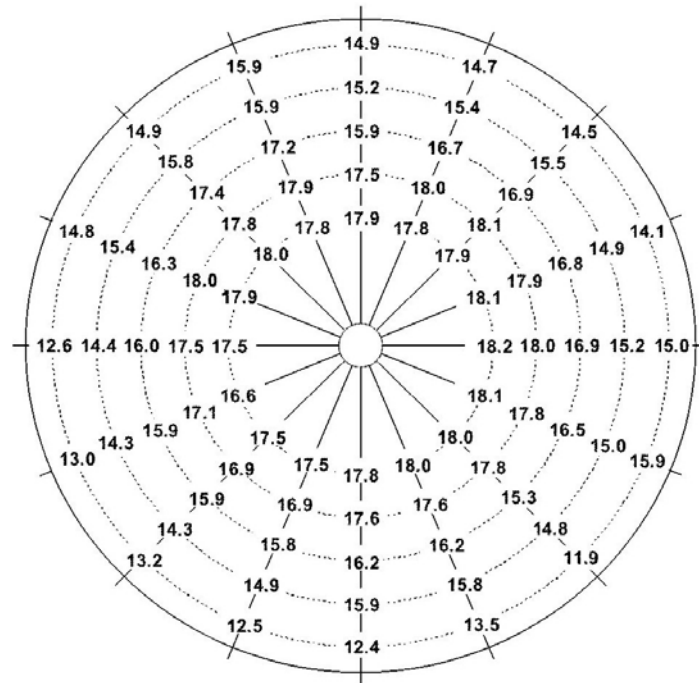
v_w average: 15.8 m/s
 Relative Standard Deviation: 15.3 %

Figure 4-4: Experimental result of v and $(T-T_a)$ at $z/D=0.4$ for Case 1.

Measuring Position at $z/D=1.2$ (Position 2)



$(T-T_a)$ average [°C] 18.3
 Relative Standard Deviation [%] 59.0



v_m average [m/s] 16.3
 Relative Standard Deviation [%] 15.8

Figure 4-5: Experimental result of v and $(T-T_a)$ at $z/D=1.2$ for Case 1.

Example of the experimental data of the measured velocities and temperatures are shown in Figure 4-4 and Figure 4-5. The profiles correspond to probe measurements at $z/D=0.4$ (position 1) and at $z/D=1.2$ (position 2). The difference between the local temperature and the ambient temperature was used because the ambient temperature was not constant. It can be seen that the values of $T-T_a$ at each radial distance scatters very strongly in a circumferential direction. This scattering occurred even where the injections were made symmetrically. At $z/D=0.4$ both temperatures and velocities scattered quite strongly, but as it moves further downstream, such as at $z/D=1.2$, the scattering is reduced. Because of this scattering, it was nearly impossible to evaluate the mixing and to determine the criterion to ensure an optimum condition. It will be shown later that the simulated results based on the CFD calculations reveal the same tendencies.

4.3 CFD Calculations

The CFD calculations were carried out using the FLUENT 6.x package. The chamber geometry includes a number of pipe junctions, which made it difficult to create a high-quality mesh. Creating a structured hexagonal mesh which would give the most accurate results is very time consuming and does not lead to ideal mesh in the region of the pipe junctions. Therefore, an unstructured T-Grid form was chosen and about five hundred thousand cells were used to mesh a part of the cylindrical chamber.

A CFD calculation with the whole geometry of the cylindrical chamber as a computational domain was first made. Based on this result as can be seen in Figure 4-1, a simplification using a part of the whole geometry with symmetrical boundary conditions was found to be acceptable for accuracy. One of the advantages of using only the part of the domain is that a very fine mesh can be constructed. Figure 4-6 shows the typical grid that was created in this study. It should be noted that to ensure a better resolution of the simulated results, a grid adaptation in each of the CFD calculations was also made. The adaptations were based on both velocity and temperature gradients.

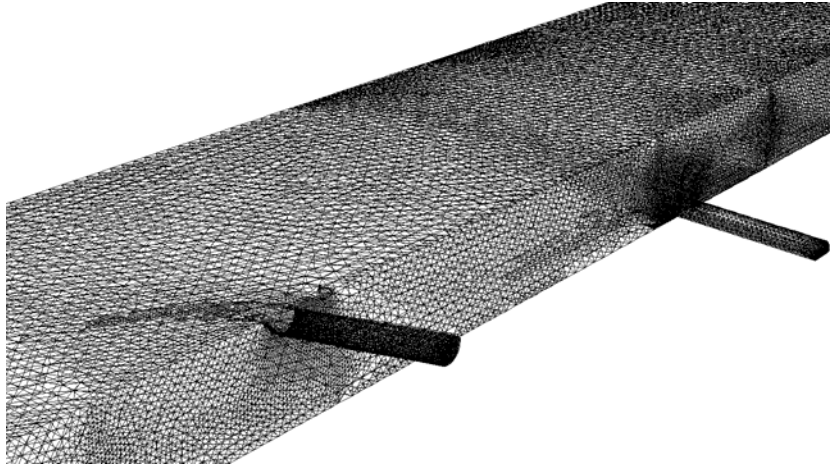


Figure 4-6: Typical grid used for the CFD calculation.

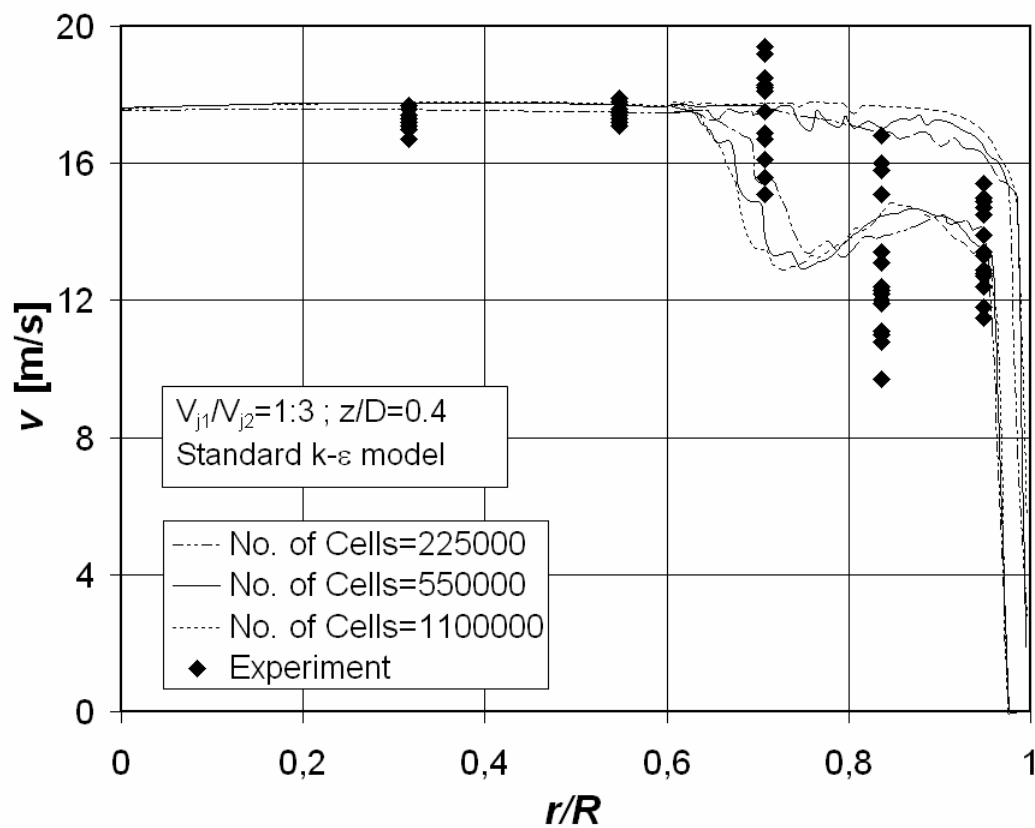


Figure 4-7: Influence of the grid sizes (Max-Min Values).

A grid independence study was performed using total numbers of cells for the whole computational domain of about 225000, 550000 and 1100000. Figure 4-7

shows the velocity profiles along the radial distance for different numbers of cells for $\dot{V}_{j01}/\dot{V}_{j02}$ of 1/3 at $z/D=0.4$. The local velocities of the CFD calculations were selected for both maximum and minimum values in order to show only their range. This was considered necessary in order to visualise the principal results and to compare them with the measured values, as will be explained later. It can be seen that the profiles for each number of cells show a similar range of results, and therefore the different sizes of grid are not significant. However, since the CPU time for calculation with a number of cells of about 550000 is quite moderate, all of the calculations here were then performed using this grid.

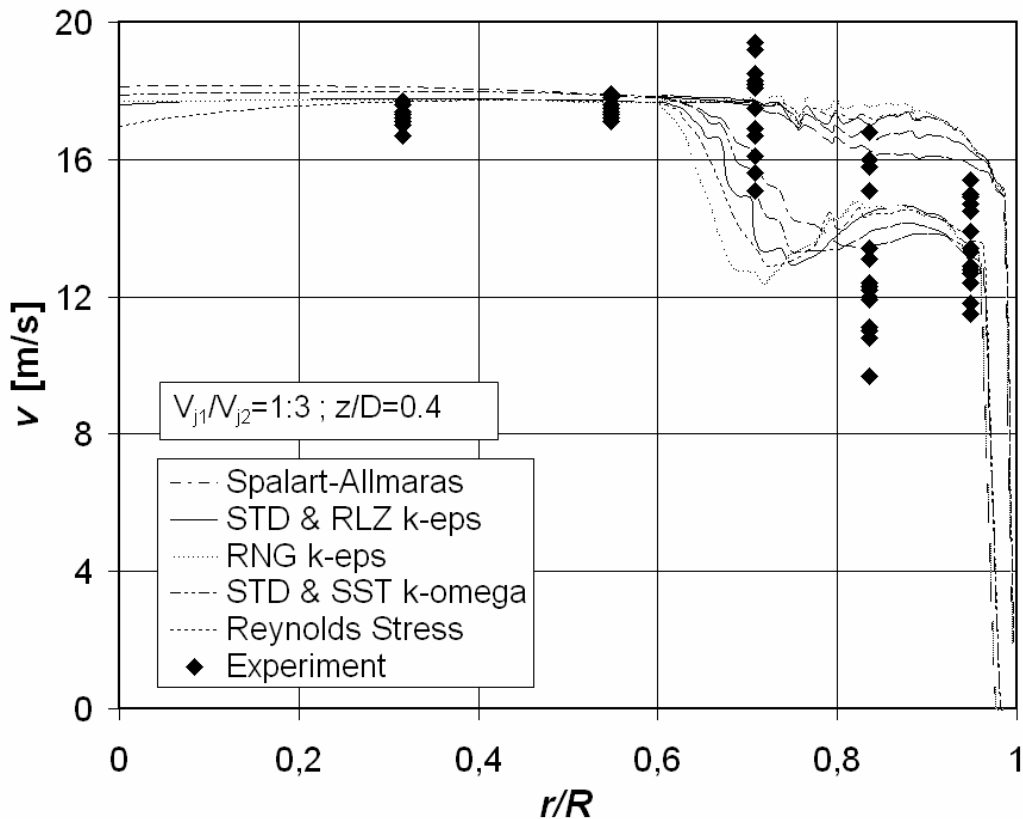


Figure 4-8: Influence of the turbulence models (Max-Min Values).

A number of calculations were carried out to study the influence of different turbulence models. All of the Reynolds Averaged Navier Stokes (RANS) turbulence models available in FLUENT were used to study their influence. Figure 4-8 shows the velocity profiles along the radial distance for $\dot{V}_{j01}/\dot{V}_{j02}$ of 1/3 at $z/D=0.4$ for several of the turbulence models. The values of the standard

(STD) and the realisable (RLZ) $k-\varepsilon$ model are somewhat similar, as are the values for the Standard $k-\omega$ model and the Shear-Stress-Transport (SST) $k-\omega$ model. Although other turbulence models showed similar results, the robustness and the stability of the standard $k-\varepsilon$ model, especially during iterations and further grid adaptations, should also be taken into consideration. The Reynolds stress model is perhaps the most sound of the RANS models, but unfortunately, it requires more CPU time. The standard $k-\varepsilon$ model was used for all CFD calculations in this study.

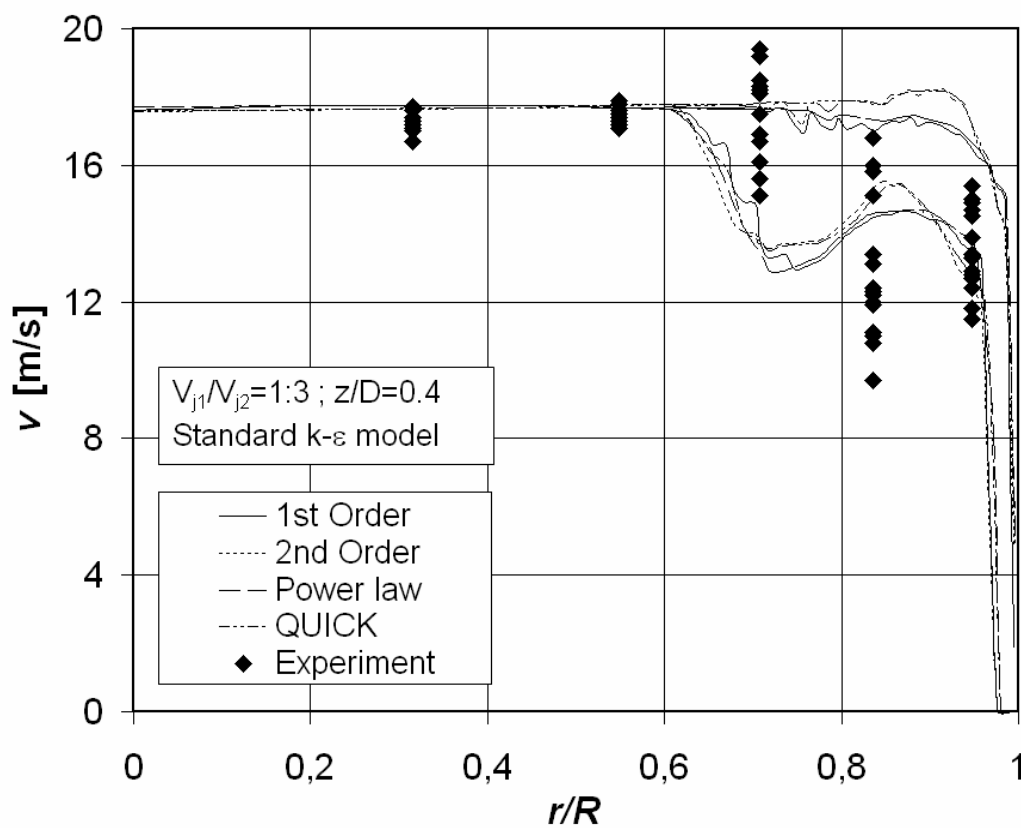


Figure 4-9: Influence of the discretization schemes (Max-Min Values).

Calculations using different orders of discretisation scheme were also made. Figure 4-9 shows the velocity profiles along the radial distance for different orders of discretisation scheme. Calculations using Power law and QUICK discretization schemes were somewhat similar to the 1st and 2nd order discretisation schemes, respectively. Figure 4-9 also includes the experimental values, for example, of $\dot{V}_{j01}/\dot{V}_{j02}$ of 1/3 at $z/D=0.4$. It can be seen that the 2nd order discretisation

scheme, although more accurate than the 1st order discretisation scheme, gives only a slightly different profile from $r/R = 0.6$. Therefore for practical industrial purposes, the 1st order discretisation scheme can also be made to save computation time.

4.4 Validation with Experiments

The measured and the calculated values for the velocities and the temperatures will be compared for different positions. The velocities were measured at five radial distances, which are at r/R of 0.32, 0.55, 0.71, 0.84 and 0.95. All radial positions show the scattering in a circumferential direction. In the region from the chamber centreline up to $r/R=0.55$ the scattering is low. However, in the penetration region at radial distances of 0.71, 0.84 and 0.95 a high range of scattering in a circumferential direction exist. At the radial distance of 0.84, about half of the measured values were below the minimum values of the CFD calculations.

Figure 4-10 again shows the scattering of the velocities in a circumferential direction at five radial distances for the same volumetric flow ratio $\dot{V}_{j01}/\dot{V}_{j02}$ of 1/3 but for a further downstream distance of $z/D=1.2$. The range of the measured values is much smaller when compared with the range at $z/D=0.4$ which could be seen in Figures 6 to 8. The same tendencies were found for the scattered values of the CFD calculations. After a distance of $z/D=1.2$ the jet has been turned to the axial direction. As a consequence, the turbulent scattering becomes low. However, in the jet region with the changing gradient of the jet direction, the turbulent scattering in the circumferential direction is much stronger.

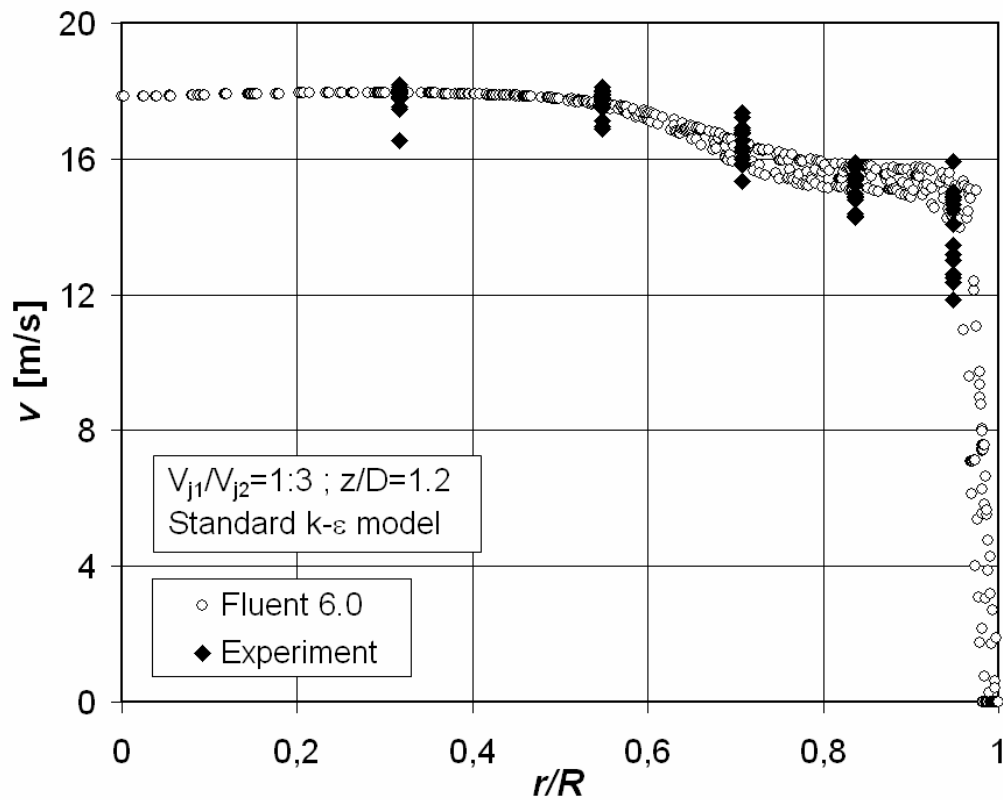


Figure 4-10: Scattered velocities in circumferential direction for $\dot{V}_{j01}/\dot{V}_{j02}$ of 1/3 at $z/D=1.2$.

Figure 4-11 shows the scattering of the temperatures in the circumferential direction at the five radial distances for $\dot{V}_{j01}/\dot{V}_{j02}$ of 1/3 at $z/D=0.4$. At a radial distance of 0.32, which is greater than the penetration distance, the scattering is small. However, in the range of the jets penetration ($0.6 < r/R < 1$) the scattering is again relatively higher. The measured and calculated values show good agreement except at a radial distance of 0.55. Here, the calculated penetration depth is a little bit smaller than the measured one.

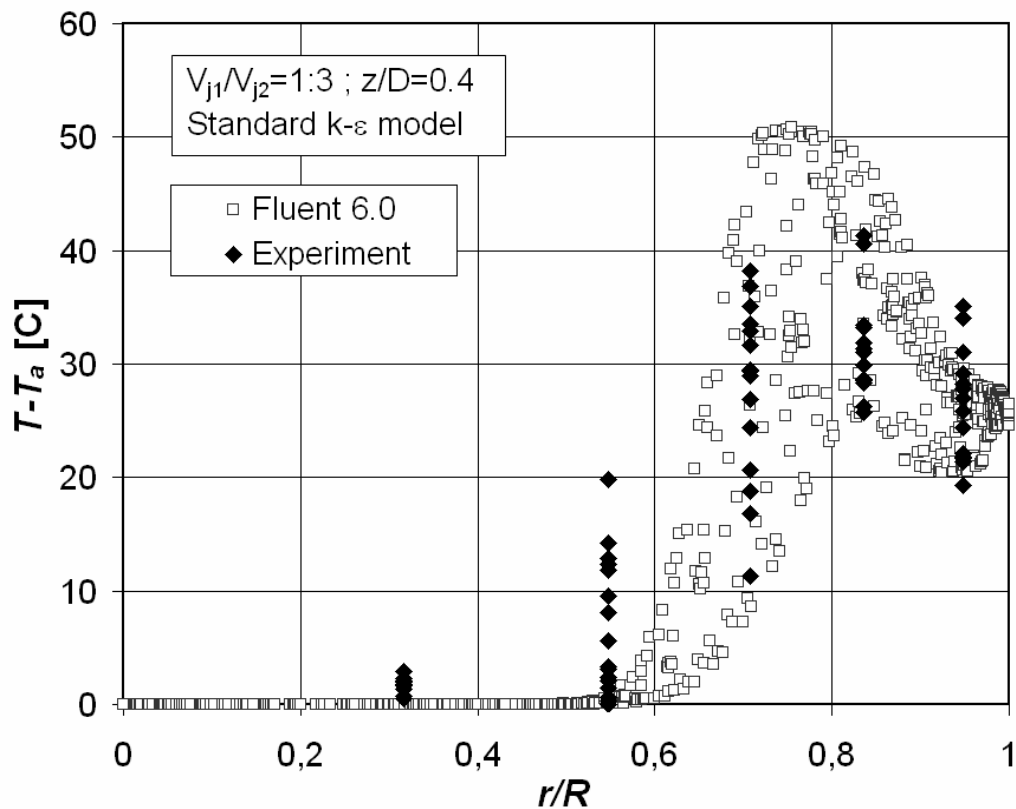


Figure 4-11: Scattered temperatures in circumferential direction at various radial distances for $\dot{V}_{j01}/\dot{V}_{j02}$ of 1/3 at $z/D=0.4$.

Figure 4-12 shows the scattering temperatures as before for $\dot{V}_{j01}/\dot{V}_{j02}$ of 1/3, but at a further downstream distance of $z/D=1.2$. As was the case for the velocities, the scattering at this further axial distance is again smaller compared with the condition shortly after the jet entrance. The tendencies of the calculated and measured values match except at the position $r/R=0.55$, as was the case for velocity.

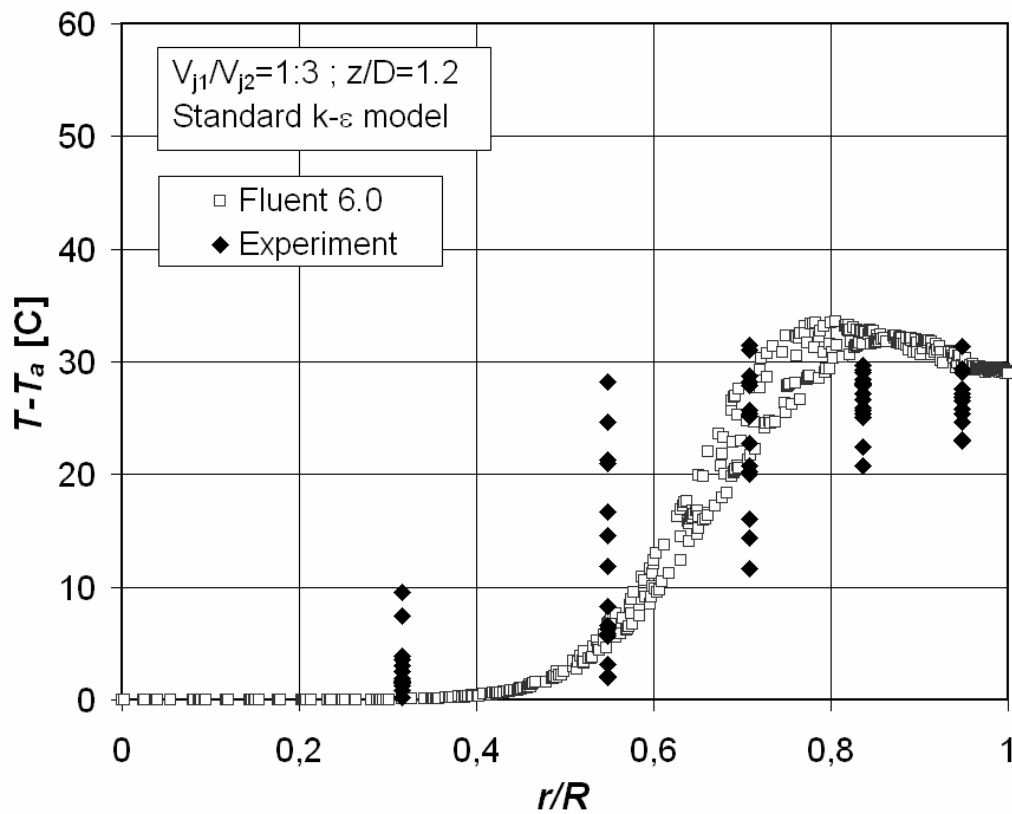


Figure 4-12: Scattered temperatures in circumferential direction at various radial distances for $\dot{V}_{j01}/\dot{V}_{j02}$ of 1/3 at $z/D=1.2$.

Figure 4-13 depicts the scattered temperatures at $z/D=0.4$ for the ratio of the volumetric flow $\dot{V}_{j01}/\dot{V}_{j02}$ of 2:1. In this case, the second injection has a flow rate which is less than the first one. The measured and calculated results again have the same range of scattering in the region near to the wall and in the core range ($r/R < 0.4$). Again at the positions $r/R=0.55$ and $r/R=0.71$, the measured values scatter much more than the calculated ones.

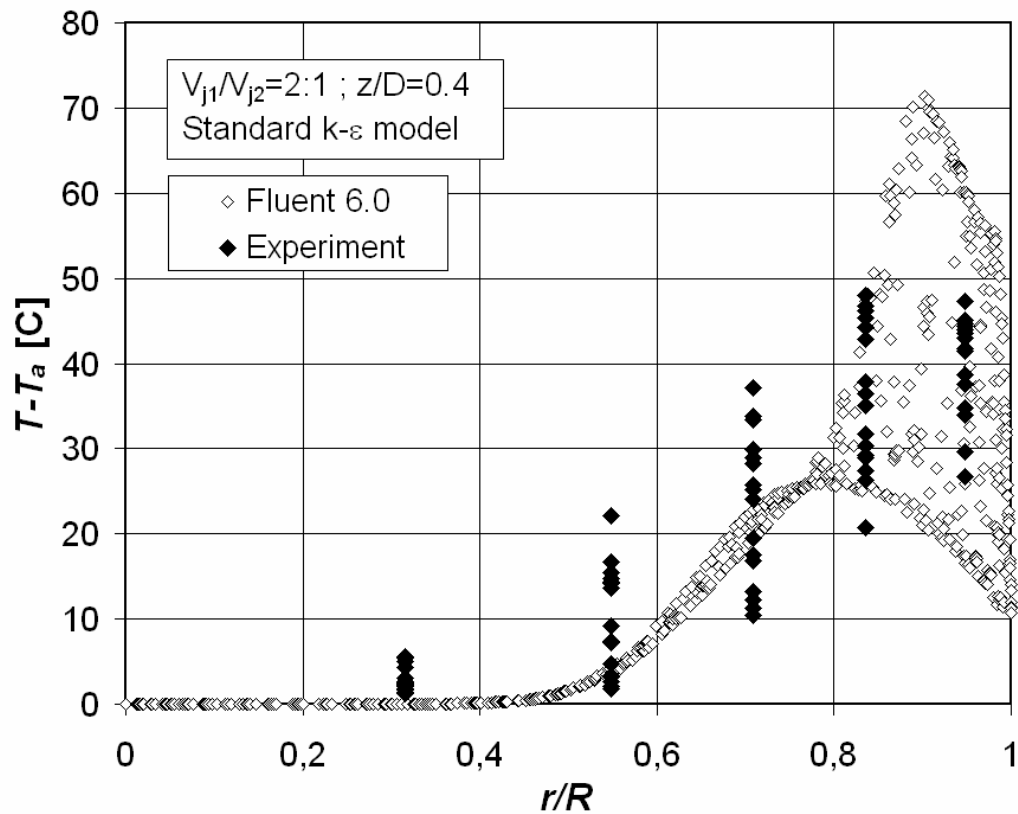


Figure 4-13: Scattered temperatures in circumferential direction at various radial distances for $\dot{V}_{j01}/\dot{V}_{j02}$ of 2:1 at $z/D=0.4$.

Figure 4-14 shows the scattered temperatures at a further downstream distance of $z/D=1.2$ for the ratio of the volume flow $\dot{V}_{j01}/\dot{V}_{j02}$ of 2:1. As was the case before, the scattering is reduced. Based on Figures 4-10 to 4-14, it can be concluded that all of the CFD calculation results give about the same tendencies as the experimental results.

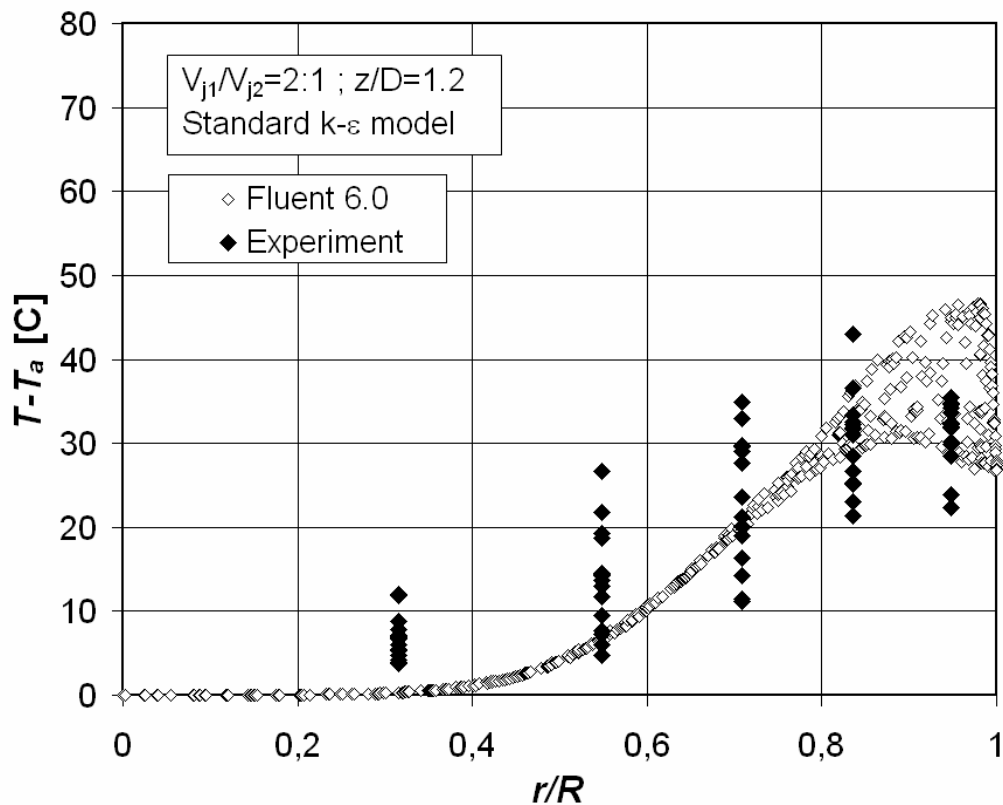


Figure 4-14: Scattered temperatures in circumferential direction at various radial distances for $\dot{V}_{j01}/\dot{V}_{j02}$ of 2:1 at $z/D=1.2$.

4.5 Influence of the Double Rows of Jets

The influence of double rows of jets will now be discussed. For the comparison between the single row and the double rows of jets, all of the parameters such as the volumetric flow rate ratio $\dot{V}_{jo}/\dot{V}_{mo}$ and temperature ratio between the jet and the mainstream were kept constant. It should be noted that the number of nozzles in each row for the double rows arrangements were half of the single row, but the total number of nozzles were the same as the single row.

Figure 4-15 shows the temperature differences as a function of the spacing distance between the two rows for staggered and inline arrangement of the double rows with equal volumetric flow in each row ($\dot{V}_{j01} = \dot{V}_{j02}$). The single row case is used here as the basis. The limiting value $l/D=0$ represents the single row case with the optimum condition of $J/n^2=0.3$. It can be seen that with increasing

spacing distance for both staggered and inline arrangements, the temperature differences increase. Therefore the double rows arrangements for equally distributed flows result in worse mixing conditions than the single row case. For staggered arrangement, a very small increase in spacing distance has a significant effect, because the temperature difference increases dramatically. It can also be seen in this figure that the inline arrangement results in lower temperature difference than the staggered arrangement.

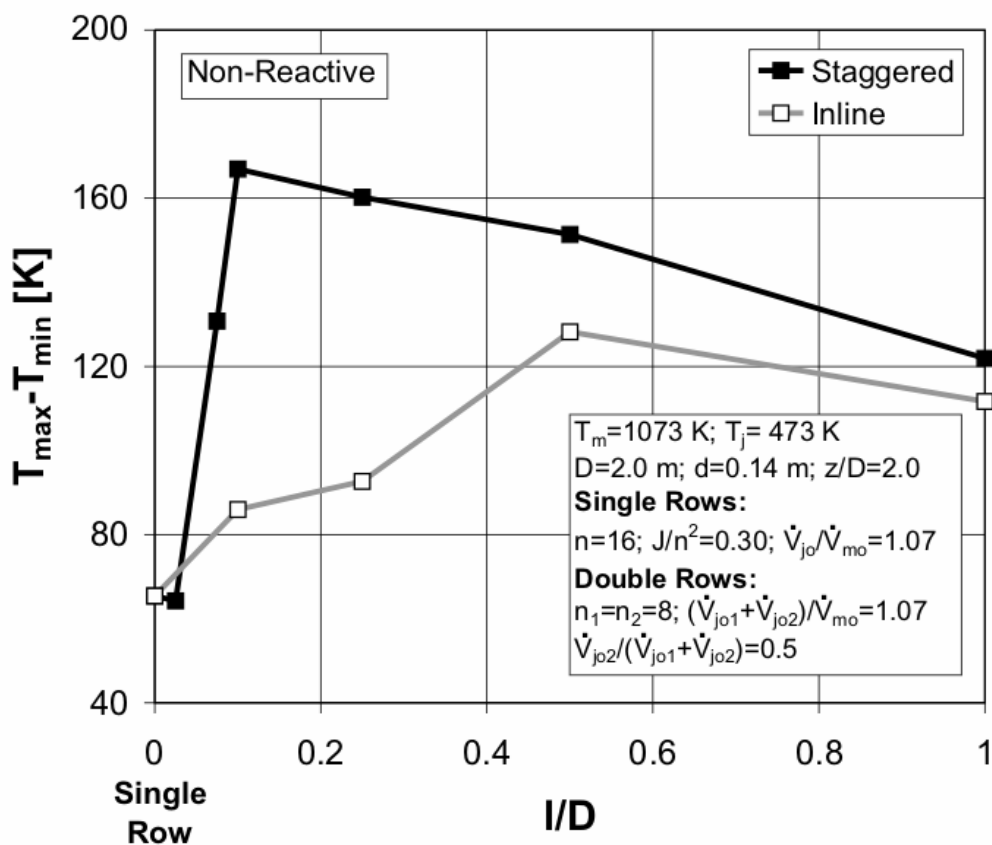


Figure 4-15: Influence of the double rows arrangement at $z/D=2$ and $\dot{V}_{j02}/(\dot{V}_{j01} + \dot{V}_{j02})=0.5$ on the temperature differences as a function of the spacing distance between the rows.

Now the influence of flow distribution will be discussed which results in different penetration depth of the jets in each row. Figure 4-16 shows the temperature differences as a function of the volumetric flow fraction of the second row for a spacing distance of 0.5. Both of the limiting values of $\dot{V}_{j02}/(\dot{V}_{j01} + \dot{V}_{j02})$ at 0 and 1

represent the single row case with optimum condition of $J/n^2=0.3$. The behavior for the staggered and the inline arrangement is quite different. For the staggered arrangement, the temperature differences are always much higher than the single row case. It can be concluded from both Figures 4-15 and 4-16, that a staggered arrangement always deteriorates the mixing quality in comparison with the single row case. The inline arrangement however has two minimum values where the temperature difference is even lower as for the single row. These minimum values occur for volumetric flow fraction of the second row, $\dot{V}_{j02}/(\dot{V}_{j01} + \dot{V}_{j02})$ of about 0.25 and 0.75, or using the expression of volumetric flow rate distribution $\dot{V}_{j01}/\dot{V}_{j02}$ of about 3/1 and 1/3. Therefore a better temperature homogenization can be only achieved if the flow rates are distributed with these ratios. These results will be discussed in the following.

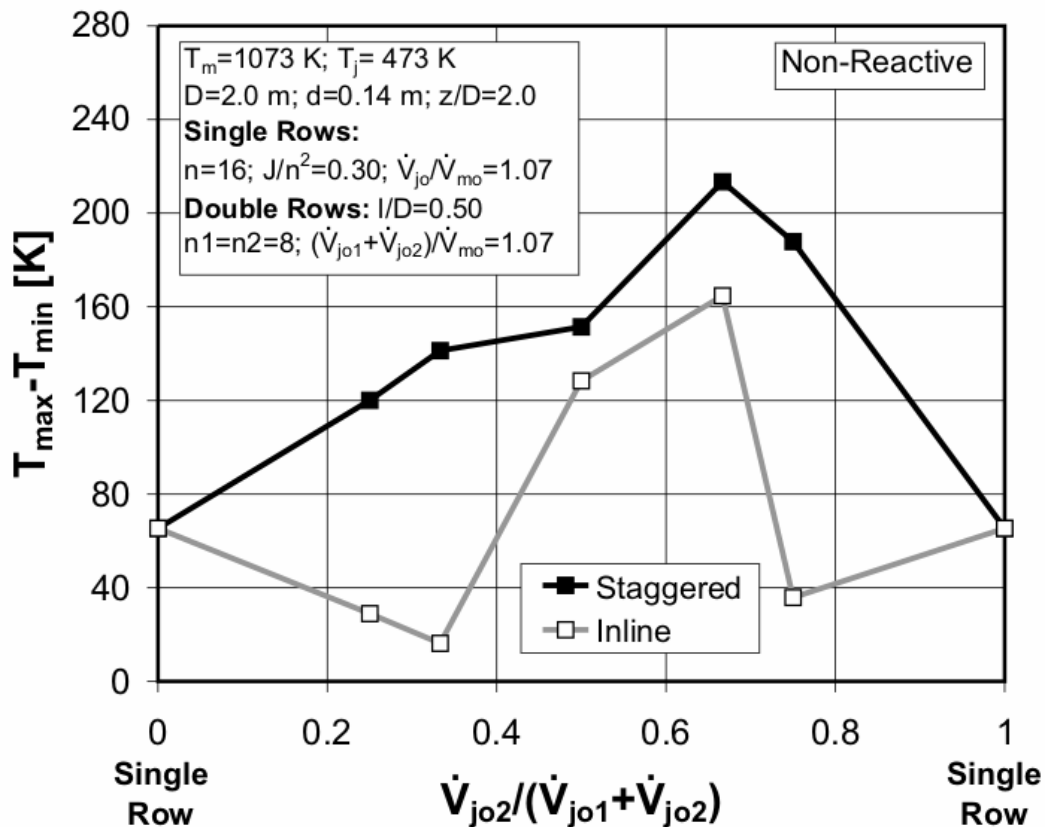


Figure 4-16: Influence of the double rows arrangement at $z/D=2$ on the temperature differences as a function of volumetric flow fraction of the second row.

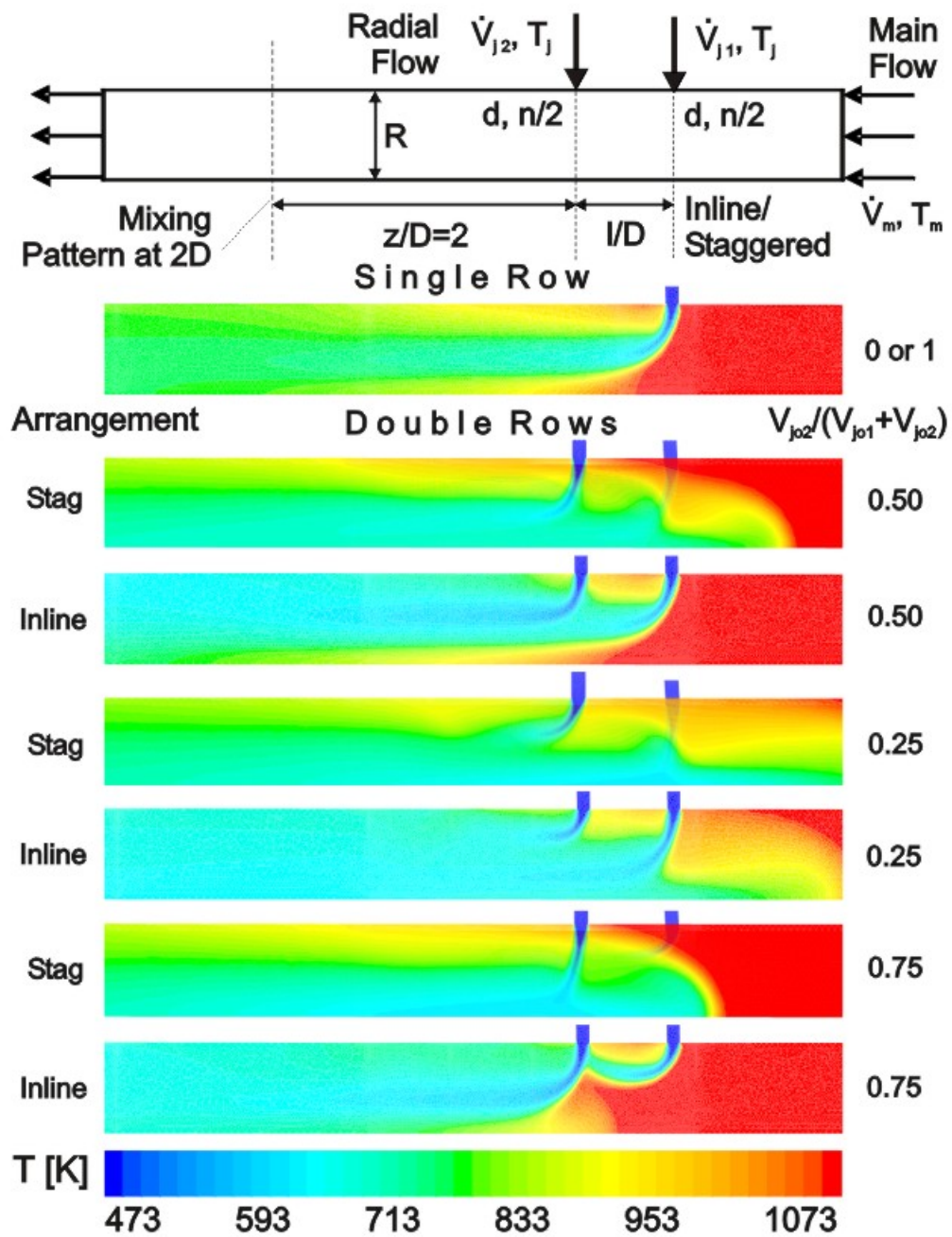


Figure 4-17: The temperature contours of single and double rows of jets for different rows arrangement and volumetric flow fraction of the second rows.

Figure 4-17 shows the temperature contours of double rows of jets for different rows arrangement and volumetric flow fractions of the second row with the single row case as basis. The single row with 16 nozzles and $\dot{V}_{j01}/\dot{V}_{j02}$ of 1.07 for the optimum mixing condition of $J/n^2=0.3$ is shown on the top. The double rows

cases have 8 nozzles in each row and the same nozzle diameter as the single row case. The hot mainstream temperature of 1073 K and the cold inlet temperature of 473 K are the limits of the scale. The volumetric flow fraction of the second row is used as parameter. The spacing distances of 0.5 were kept constant. The single row temperature contour of Figure 4-17 shows a jets penetration with $h/R=0.6$ for the optimum condition with $J/n^2=0.3$. The first two temperature contours of the double rows arrangements represent the equally distributed flows with $\dot{V}_{j02}/(\dot{V}_{j01} + \dot{V}_{j02})$ equal to 0.5. Both staggered and inline arrangements show similar jet penetrations as the case with single row. But it can be seen that the staggered arrangement has a hotspot near the wall and the inline arrangement near the axis. In this study, the mixing quality was evaluated with the difference of the maximum and the minimum temperature in any location in the cross-section. The next two contours in Figure 4-17 are for the fractions of 0.25 which means that the flow rate of the first row is three times higher than the second row. This results in an over-penetration jets of the first row and under-penetration jets of the second row. For the inline arrangement, it is obvious that the temperature contour is more homogeneous directly after the second than that of the single row. But for the staggered arrangement again a hot spot near the wall occurs. The last two contours show contours are for the fractions 0.75 which results in contrary as before with an under-penetration jets of the first row and over-penetration jets of the second row. The inline arrangement has again a homogeneous profile directly after the second row and the staggered arrangement has hot spot near the wall. Based on these previous figures, it can be said here that the double rows of jets using an inline arrangement with $\dot{V}_{j02}/(\dot{V}_{j01} + \dot{V}_{j02})$ of 0.25 or 0.75 can be recommended to provide better mixing condition than the single row case.

4.6 Double Rows of Jets Simulation

Finally principle example of double rows of jets simulation will be shown here. The mixing process with combustible components is described schematically for example for the blast furnace gases by burning of its CO and H₂ components, which can be found in the furnaces of the metallurgical industry. These gases are burned out by radial injecting of preheated air into the cylindrical combustion

chamber. In many cases, the combustion-air is supplied two stages in form of primarily air and secondary air.

Figure 4-18 shows the principle of such a combustion chamber with a diameter of 3.5 m with the primarily and secondary air supplied in a distance of 5 m with 12 nozzles each. The waste gas as the main stream is blown at a velocity of 40 to m/s and a temperature of 800 °C. The volumetric flow rate of the radial supplied primarily air corresponds to an air excess number of 0.9, and the volumetric flow rate of the secondary air corresponds to air excess number of 1.5. The combustion air is preheated and has a temperature of 200°C.

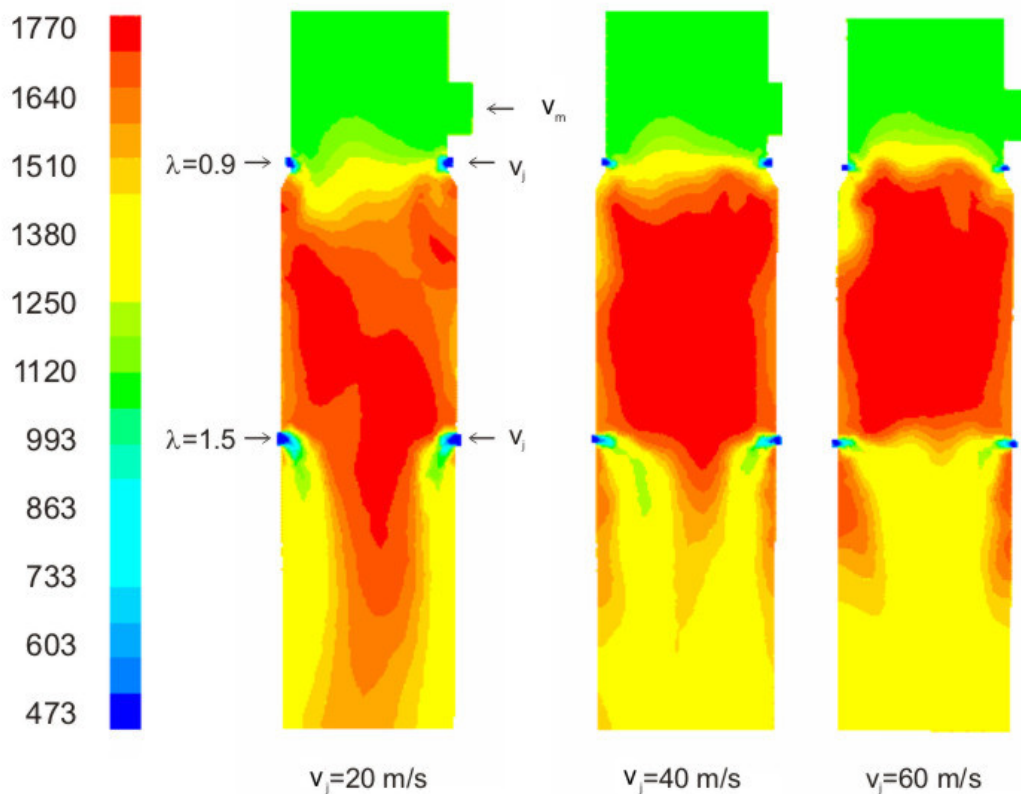


Figure 4-18: The principle design of a combustion chamber with the primarily and secondary air injections.

The temperature fields are shown in Figure 4-18 for radial jet velocity of 20, 40 and 60 m/s respectively. Thus with an air excess number of 0.9 can cause only one below stoichiometric combustion condition. For this case, penetration-depths of the radial streams are to be only recognized which is directly close to the

injection point. With velocities of 40 and 60 m/s, a homogeneous temperature field develops almost in the whole reduction-area of the combustion chamber. Although with a velocity of 20 m/s, it can be seen that bad mixing occurs. For the secondary air supply which corresponds to an air excess number of 1.5, the penetration depths of the radial streams are to be clearly recognized. With 20 m/s (Figure 4-18a) the penetration-depth is lower than $h/R=0.6$ therefore creating a relatively hot stream in the core region of the chamber and a relatively cold stream near by the wall. If the jet velocity is to be increased about 3 times such as in the case of 60 m/s, the penetration-depth is higher than $h/R=0.6$, and the reversal phenomenon occurs, which is relatively cold flow of stream in the core region, and a relatively hot flow of stream nearby the wall (Figure 4-18c). Figure 4-18b shows the condition with 40 m/s which correspond approximately to $h/R=0.6$.

C H A P T E R 5

INTERNAL JET INJECTIONS

As mentioned before, a single jet or multiple of jets injected normally or at an angle into a cross-flow has motivated a number of studies over the past three decades. Most of these studies reported jets in cross-flow for rectangular duct, some investigated for cylindrical duct, but almost no report has been found discussing jets in cross-flow for cylindrical duct injected outwardly from the chamber centerline to wall. Therefore it is important to gain insight on its basic phenomenon especially the influence of parameters such as in the case of single row of jets radially injected outwardly from the chamber wall to the centerline.

Figure 5.1 shows an industrial example of swirl burner that employs the principle of internal jets injection. Here the fuel flows from inside a pipe which will be injected into a cross-flow of oxidizer through a number of nozzles as it reaches near the end of the pipe. The jets of fuels will be radially injected outwardly in the direction to the pipe wall. The oxidizer is forced into a swirl generator before it reacts with the fuel.

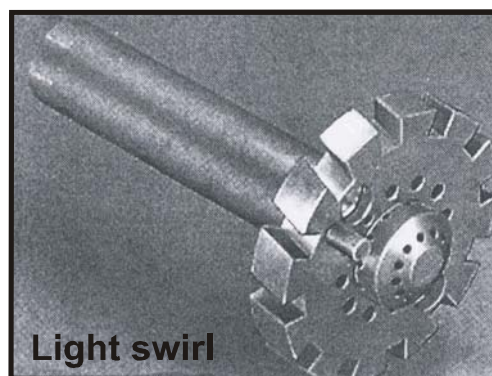
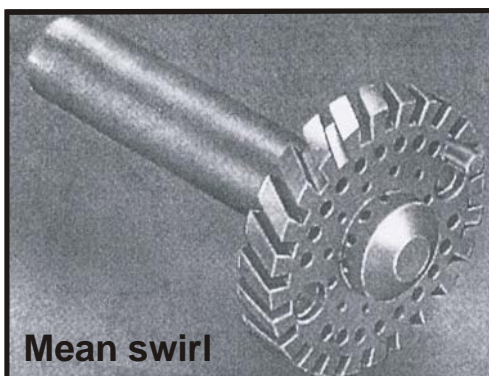
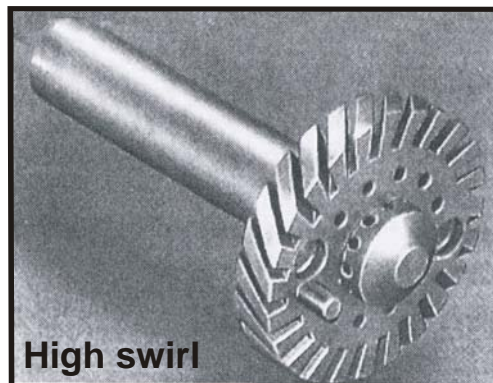
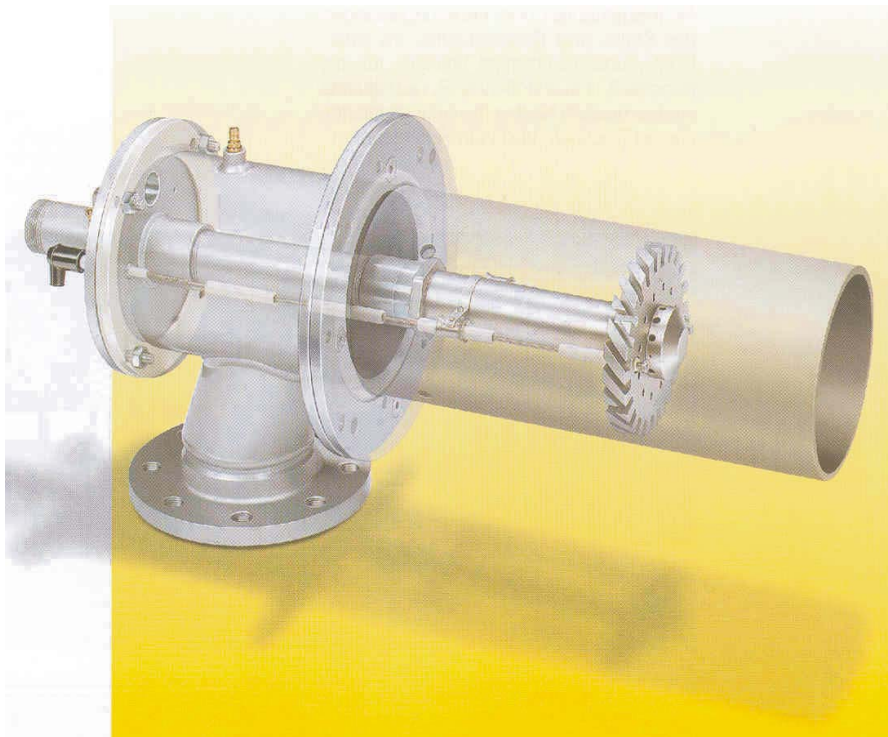


Figure 5-1: Industrial example of swirl burner that employs the principle of internal jets injection

5.1 Influencing Parameters

The influencing parameters are shown in Figure 5-2. Air with a volumetric flow rate \dot{V}_m and a temperature T_m enters along the cylindrical chamber with a diameter of $2R$ as the main input. After reaching a certain distance inside the chamber, a different air stream with a volumetric flow rate of \dot{V}_j and a temperature of T_j is injected through a small pipe with diameter d_p which centerline coincides with the chamber centerline. This pipe has n nozzles with diameter d installed just before reaching the closed end of the pipe. Therefore jets exit through these nozzles and are injected outwardly from the pipe centerline to the cross-flow. The trajectory of the jets and the penetration depth (h/R) has to be determined. The mixing quality is analyzed by means of the difference between the maximum temperature (T_{max}) and the minimum temperature (T_{min}) in the cross-sectional area at a downstream distance of $4R$ after the injection.

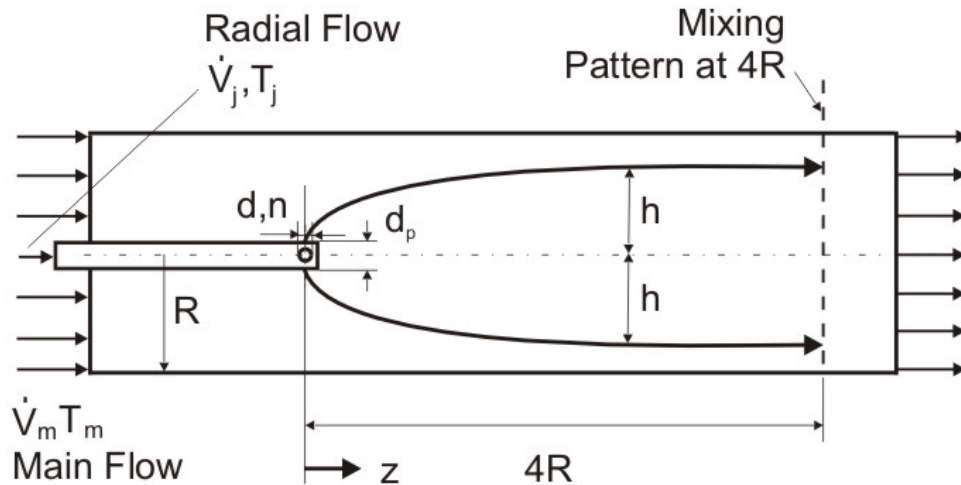


Figure 5-2: Principle of a single row of jets outwardly directed radially into a cylindrical chamber with its penetration depth (h/R)

The case of internal jets injection can not be approached in the same manner as with the case of external jets injection. Here the jets flow radially outward assumingly from the chamber centerline in the direction to the chamber wall,

which means to a larger cross-sectional area in the cylindrical chamber. Therefore higher jet impulse is needed to penetrate deeper into the cross-flow. But in order to compare the parametric influences of internal jets injection system with the basis case of external jet injection system, the pipe diameter whereas the jets exit should be made as small as possible in comparison with the chamber diameter. Smaller pipe diameter needs smaller nozzles diameter which in turn will produce small but stronger jets. Since higher jet velocity, for example higher than about 200 m/s, does not have any practical meaning in the industrial applications, the volumetric flow ratio of the jet to the mainstream will then be limited to a low value.

5.2 Penetration Depth

The penetration depth is defined as the ratio of the distance between the wall and the maximum/minimum temperature position (h) to the radius of the chamber (R). The penetration depth of the jets for outward flows from the chamber centerline is different than inward flows from the chamber wall. Here the jets do not exactly exit from the chamber centerline but from the wall of the internal pipe which its centerline coincides with the chamber centerline. If the diameter of pipe is very small in comparison to diameter of the chamber, then h can be determined from the chamber centerline. But for in order to use the same parameter as the case of external injection here the distance h is measured form the chamber centerline.

The temperature field contour of Figure 5-3 shows the influence of this J/n^2 on the penetration depth for a non-reactive flow with 16 nozzles. It is obvious that at $J/n^2=0.1$, the jet can be considered as under-penetrated which results a bad mixing downstream. On the other hand, at $J/n^2=0.9$, the jets almost hit the chamber wall which can be considered as over-penetrated. Unwanted back mixing occurs giving a bad mixing downstream. The desired condition which gives the optimum temperature homogenisation is somewhat as can be found at $J/n^2=0.4$, which gives a moderate penetration depth into a cross-flow and gives better mixing downstream.

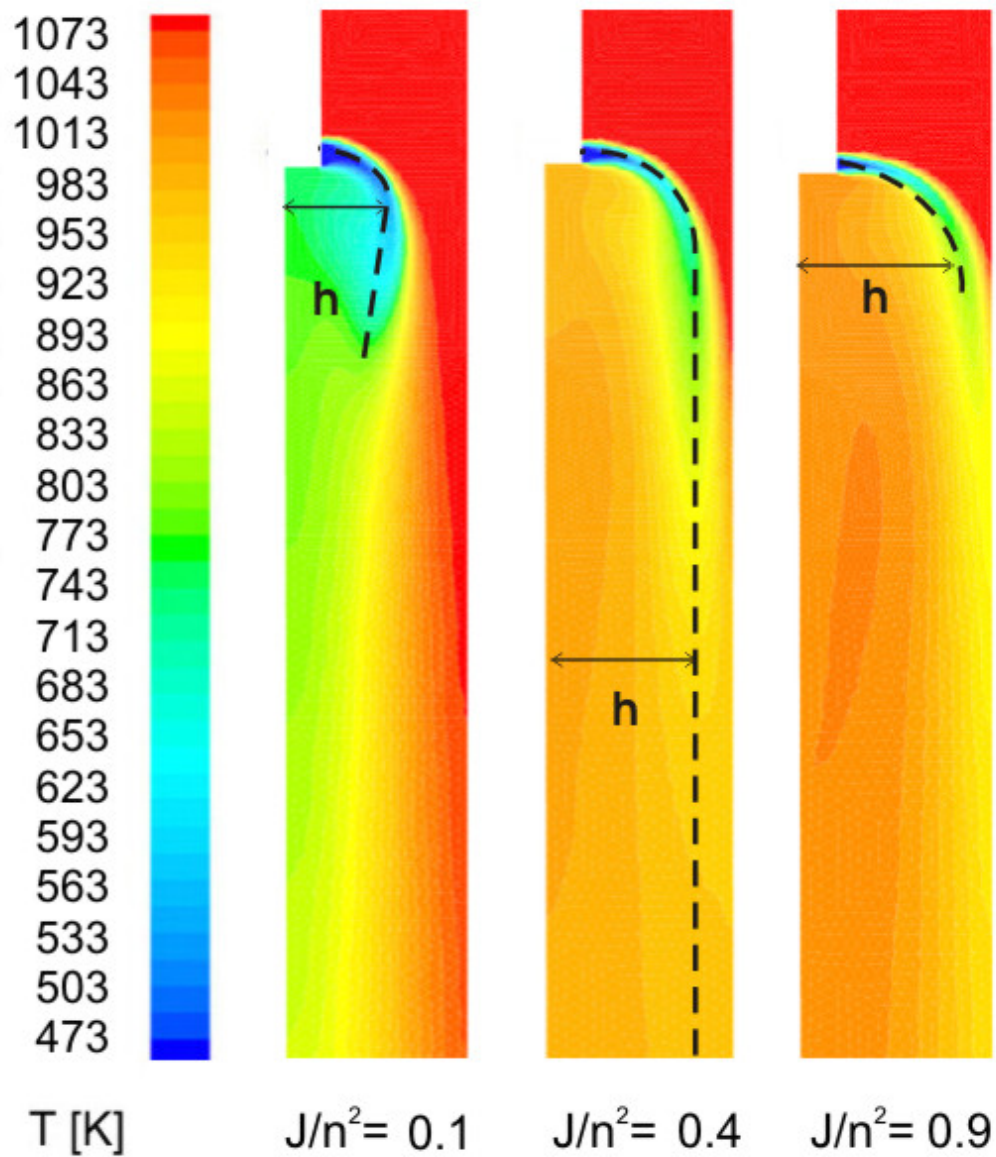


Figure 5-3: Influence of momentum flux ratio of jet to mainstream on penetration depth

Figure 5-4 shows the penetration depth as a function of normalized momentum flux ratio for different number of nozzle. Similar situation such as in the external injection occurs, but higher value of penetration depth is also found in comparison to the external injection case.

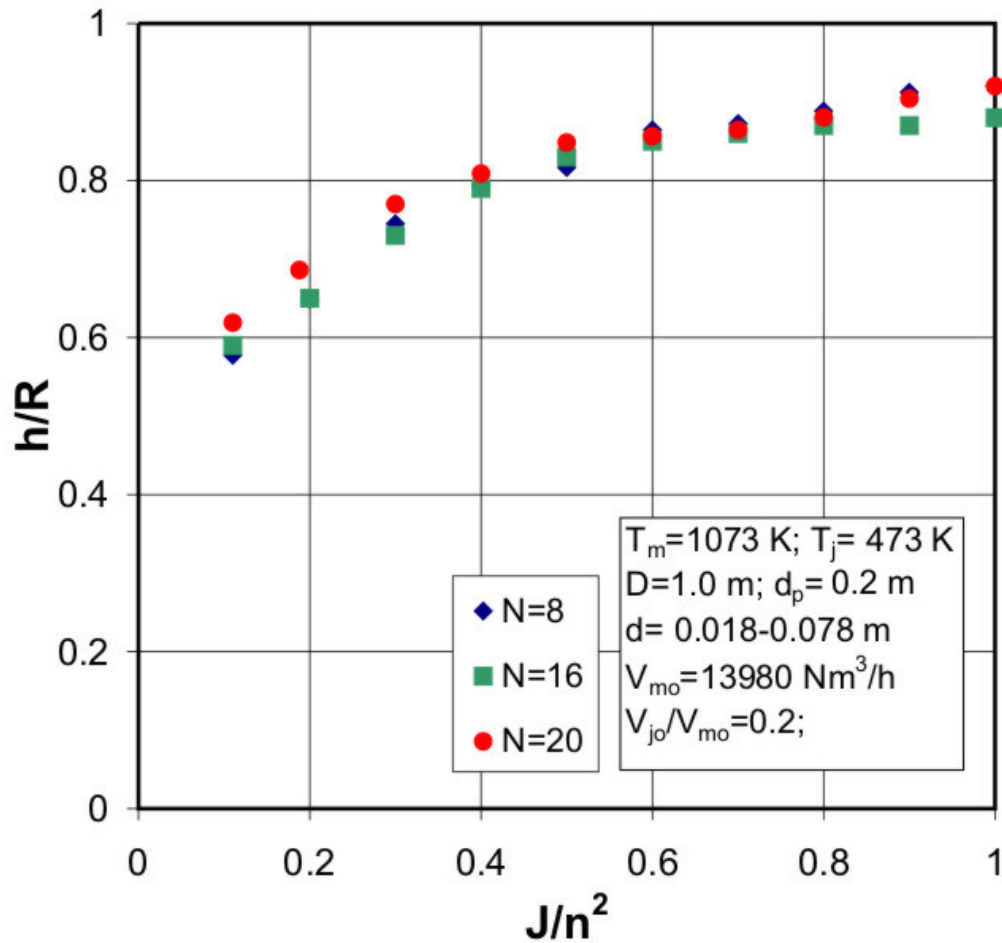


Figure 5-4: Penetration depth as a function of normalized momentum flux ratio for different number of nozzle.

5.3 Influence of the Number of Nozzles

The difference between the maximum and the minimum local temperatures in the chamber cross-section area is defined as the parameter to evaluate the mixing pattern. Figure 5-5 shows the temperature differences at $z/D=2$ as a function of normalized momentum flux for various number of nozzles for chamber diameter of 1.0 m. The number of nozzles was also varied from 8 to 20 and the diameter of the pipe was 0.2 m. It is obvious that the optimum value for all number of nozzles which gives the lowest temperature difference was found at a value J/n^2 of about 0.4. However, it can be seen that with an increasing number of nozzles the mixing quality will be improved. An increase in the number of nozzle from 8 to 16

results in a strong improvement of the mixing quality. With an increase from 16 to 20 only a slight improvement can be achieved. It is obvious that for a number of nozzles equal to or greater than 16, the mixing quality is nearly independent for values of J/n^2 greater than 0.4. Therefore for a chamber diameter of 1.0 m, in order to attain a wide range of temperature difference for example of about 40 K, a number of nozzles equal to or greater than 16 with values of J/n^2 greater than 0.4 must be used.

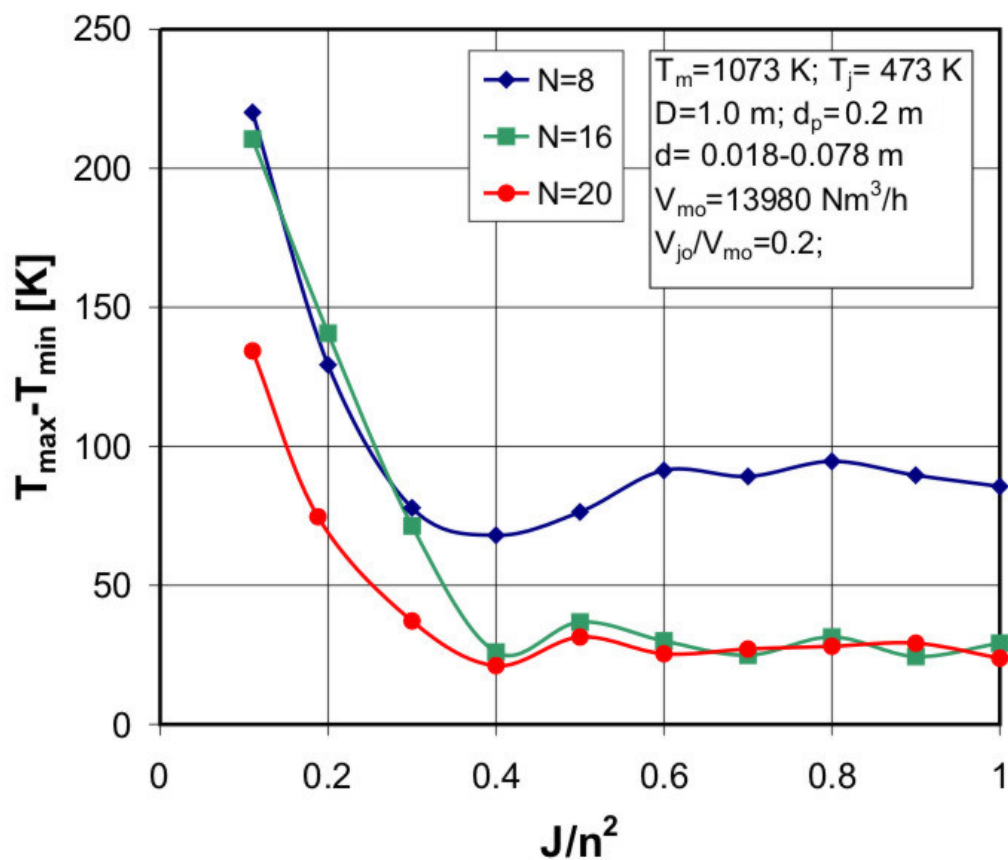


Figure 5-5: The temperature differences at $z/D=2$ as a function of normalized momentum flux for three number of nozzles

Figure 5-6 show the temperature difference for constant nozzle diameter of 0.03 m and constant $\dot{V}_{jo}/\dot{V}_{mo} = 0.2$ at $z/D=2$ as a function of normalized momentum flux. For industrial practices, changing the jet velocity by maintaining a fixed nozzle diameter is more practical than changing the nozzles. It is clear that both

shows the same tendencies and again the lowest temperature difference is found at a value J/n^2 of about 0.4

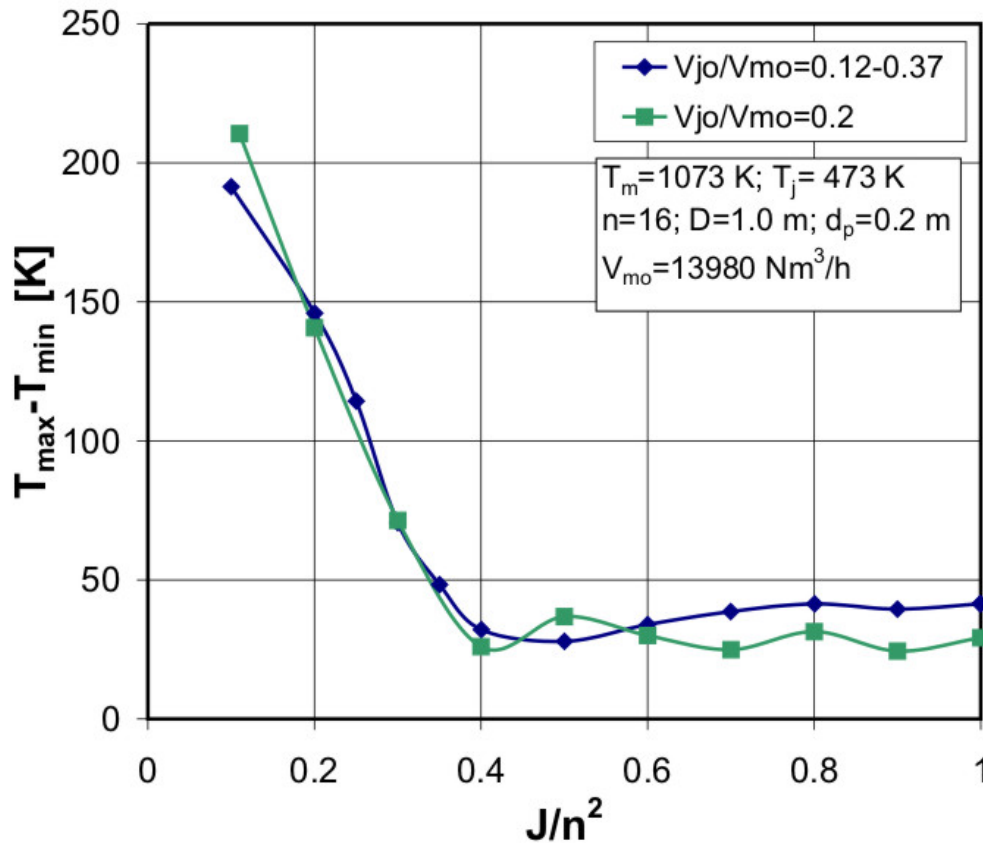


Figure 5-6: The temperature differences for constant nozzle $d=0.03$ m or constant $\dot{V}_{jo}/\dot{V}_{mo}=0.2$ at $z/D=2$ as a function of normalized momentum flux.

Figure 5-7 show the temperature difference for small chamber as a function of normalized momentum flux. The normal mainstream flow rate V_{mo} for $D=0.3$ and 0.4 m were 1000 and 1750 Nm^3/h respectively. Different than before both show the same tendencies but the highest temperature difference is found at a value J/n^2 of about 0.4.

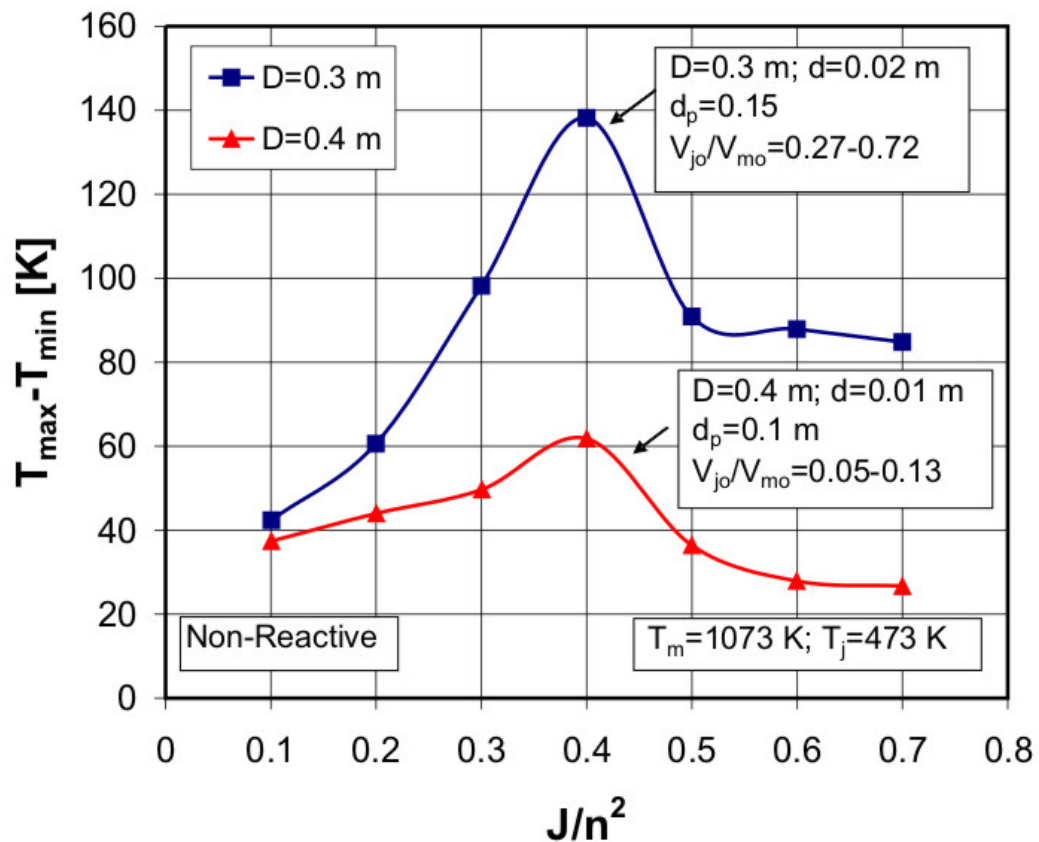


Figure 5-7: The temperature differences for small chamber diameter as a function of normalized momentum flux.

Figure 5-8 shows further the influence of this J/n^2 on penetration depth for a non-reactive flow with 12 nozzles, $D=0.3$ m and $d_p=0.15$ m. It is clear that even at $J/n^2=0.1$, the jet creates a moderate penetration and results in quite homogeneous mixing downstream. At $J/n^2=0.7$, the jets hit the chamber wall and mixed back into stream even near the jet entry point. But at $J/n^2=0.4$ it can be seen that the jets also hit the chamber wall but do not mixed back so deep into stream thus creating very bad mixing downstream. Therefore for small chamber diameter with big inner pipe diameter the desired condition which gives the optimum temperature homogenisation is somewhat as can be found at $J/n^2=0.1$ or even less which directly gives a moderate penetration depth into a cross-flow and gives better mixing downstream.

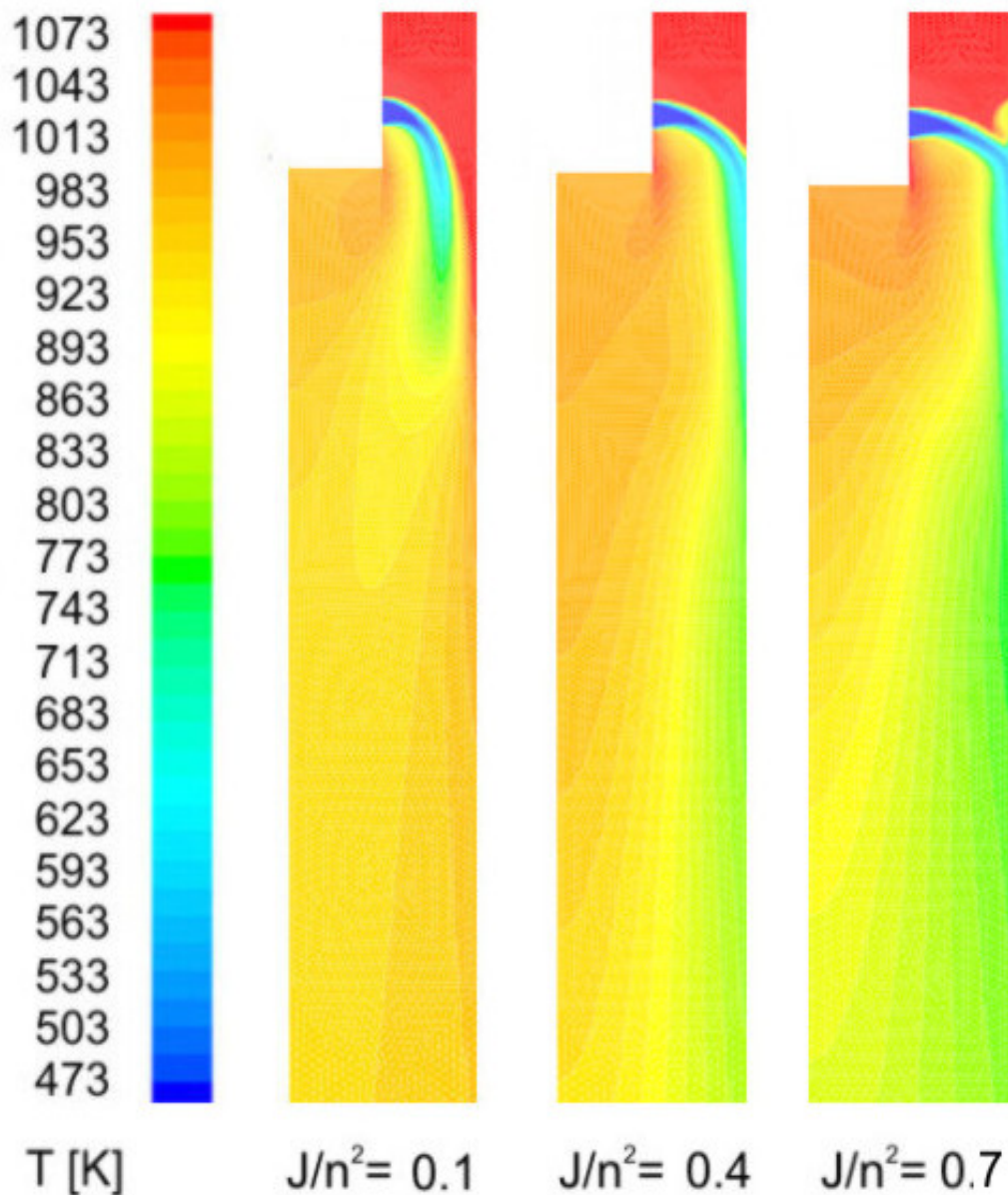


Figure 5-8: Influence of momentum flux ratio of jet to mainstream on penetration depth for small chamber diameter

A high number of nozzles and a high value of J/n^2 result in a high pressure drop caused a high jet velocity. As an example, Figure 5-8 shows the jet velocity as a function of the normalized momentum flux ratio with the number of nozzles as parameter. It can be seen that the velocity increases with J/n^2 and with the number of nozzles. Referring back to Figure 5-6, It is shown that higher volumetric flow ratio between jets to the mainstream greater than 0.2 is still

possible without deteriorating the mixing quality. But this high volumetric flow ratio between jets to the mainstream of about 0.37 is because of high jet velocity of 220 m/s. Therefore some considerations to the optimum operating condition must be made, since higher the number of nozzles means higher jet velocity also noise level, and lower number of nozzles means having a bad mixing downstream.

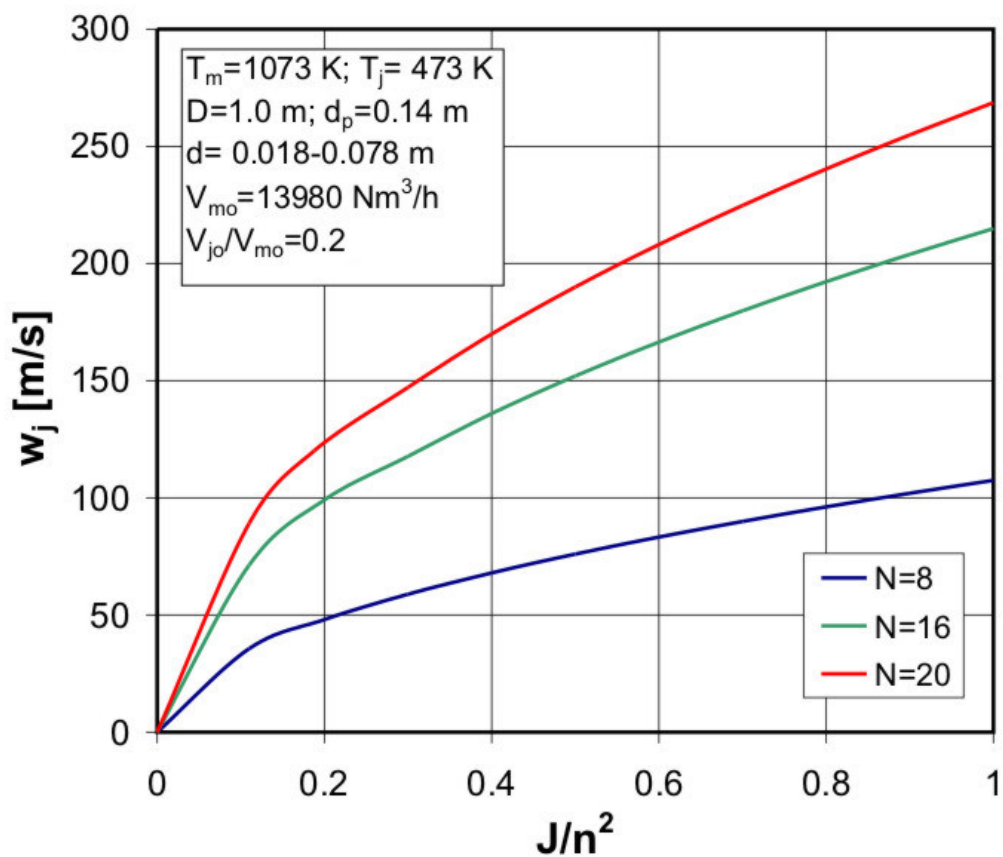


Figure 5-8: Influence of the number of nozzles on the jet velocity as a function of normalized momentum flux ratio.

C O N C L U S I O N S

Several conclusions that can be made are follows:

1. The normalised momentum flux ratio (J/n^2) of jets to mainstream significantly influences the mixing characteristics of multiple jets in cross-flow of the cylindrical chamber.
2. The penetration depth (h/R) is mainly influenced by the normalised momentum flux ratio (J/n^2).
3. A minimum difference of the maximum and minimum temperature ($T_{max}-T_{min}$) in the cross-sectional area was obtained at h/R of about 0.6.
4. The penetration depth (h/R) of about 0.6 corresponds to a normalised momentum flux ratio (J/n^2) of about 0.3, which is similar to results of the previous studies even for different applications and parameters.
5. Increasing the number of nozzle gives a better mixing.
6. For high number of nozzles the mixing quality becomes independent of the normalised momentum flux ratio (J/n^2) for values greater than 0.3. This is an important result for the chemical process industry because of the changing power and throughput, therefore a wide range of J/n^2 can be conducted.
7. The number of nozzles necessary to be independent of the normalised momentum flux ratio (J/n^2) for values greater than 0.3 depends on the chamber diameter. For a small diameter of 0.3 m 16 number of nozzles are sufficient, and for a large chamber diameter of 2 m 32 number of nozzles are required to produce similar level of temperature differences.
8. A single row of jets always gives better mixing quality in comparison with the double rows with staggered arrangement.
9. Double rows with inline arrangement will improve the mixing quality only if the injected volumetric flows produce over and under-penetrated jets for a $\dot{V}_{j01}/\dot{V}_{j02}$ ratio of 3/1 or 1/3 which correspond to volumetric flow fraction of the second rows 0.25 or 0.75.
10. Internal injection gives slightly different optimum condition than the external injection whereas here can be obtained for normalised momentum flux ratio (J/n^2) greater than 0.4

11. For a high number of nozzles, the jet velocity and therewith the pressure drop also the noise level increases.
12. The comparison of the four commercial CFD software packages: Phoenics 3.4, CFX-TASC Flow 2.11, CFX 5.5, and Fluent 6.1, gave similar computational results for the value of penetration depth.
13. The calculated velocities and temperatures using FLUENT 6.x showed an agreement in the tendencies with the measured values, especially with the scattering in the circumferential direction.

R E F E R E N C E S

Abramovich GN (1963). The Theory of Turbulent Jets. Cambridge. MIT Press.

Adler D, Baron A (1979). Prediction of a Three Dimensional Jet in Cross-flow, AIAA Journal 17-2: 168-174.

AIAA (1998). Guide for the Verification Validation of Computational Fluid Dynamics Simulations. American Institute of Aeronautics Astronautics (AIAA) G-077-1998.

Andreopoulos J, Rodi W (1984). Experimental Investigation of Jets in a Cross-flow. Journal of Fluid Mechanics. 138: 93-127.

Bain DB, Smith CE, Holdeman JD (1995). Jet Mixing Emission Characteristics of Transverse Jets in Annular Cylindrical Confined Cross-flow. NASA Technical Memorandum 106976 AIAA-95-2995. Prepared for the 31st Joint Propulsion Conference and Exhibit. San Diego, California.

Blomeyer M, Krautkremer BH, Hennecke DK (1996). Optimum mixing for a Two Sided Injection From Opposing Rows of Staggered Jets into a Confined Cross-flow. ASME paper 96-GT-486:1-6.

Chang YR, Chen KS (1994). Measurement of Opposing Heated Line Jets Discharged at an Angle to a Confined Cross-flow. International Journal of Heat and Mass Transfer. 37-18: 2935-2946.

Chang YR, Chen KS (1995). Prediction of Opposing Turbulent Line Jets Discharged Laterally into a Confined Cross-flow. International Journal of Heat and Mass Transfer. 38-9:1693-1703.

Chao YC, Ho WC (1992). Numerical Investigations of Heated and Unheated Lateral Jets Discharging into a Confined Swirling Cross-flow. Numerical Heat Transfer. Part A. 22: 343-361.

Coelho SLV, Hunt JCR (1989). The Dynamics of the Near Field of Strong Jets in Cross-flow, Journal of Fluid Mechanics. 200: 95-120.

Cox GB (1976). Multiple Jet Correlation for Gas Turbine Combustor Design. Journal for Engineering for Power. 98: 265-273.

Demuren AO (1986). Modeling Turbulent Jets in Cross flow. Encyclopedia of Fluid Mechanics - Vol 2: Dynamics of Single-Fluid Flows Mixing. Houston: Gulf Publishing.

Demuren AO (1994). Modeling Jets in Cross Flow. NASA CR-194965 ICASE Report No. 94-71. Hampton.

Doerr TH, Blomeyer M, Hennecke DK (1995). Optimization of Multiple Jets Mixing with Confined Cross-flow. ASME paper 95-GT-313: 1-9.

ERCOFTAC (2000). Quality and Trust in Industrial CFD. European Research Community on Flow, Turbulence and Combustion Best Practice Guidelines.

Fearn R, Weston, RP (1974). Vorticity Associated with a Jet in a Cross flow. AIAA Journal.12: 1666–1671.

FLUENT (2003). FLUENT User Guide, Tutorial, and Notes for FLUENT v6.1, FLUENT User Services Centre, FLUENT Inc.

Forney LJ (1986). Jet Injection for Optimum Pipeline Mixing. Encyclopedia of Fluid Mechanics - Vol 2: Dynamics of Single-Fluid Flows Mixing. Houston.:Gulf Publishing.

Forney LJ, Nafia N (1996). Optimum Jet Mixing in a Tubular reactor. AIChE Journal. 42-11: 3113-3122.

Guangbin H, Guo Y, Hsu AT (1999). The Effect of Schmidt Number on Turbulent Scalar Mixing in a Jet-in-Cross-flow. *International Journal of Heat and Mass Transfer*. 42: 3727-3738.

Hatch MS, Sowa WA, Samuelsen GS, Holdeman JD (1992). Jet Mixing into a Heated Cross Flow in a Cylindrical Duct: Influence of Geometry and Flow Variations. NASA Technical Memorandum 105390 AIAA-92-0773. Prepared for the 30th Aerospace Sciences Meeting and Exhibit. Reno, Nevada.

Hatch MS, Sowa WA, Samuelsen GS (1995). Geometry Flow Influences on Jet Mixing in a Cylindrical Duct. *Journal Propulsion Power*. 11-3: 393-402.

Hatch MS, Sowa WA, Samuelsen GS (1996). Influence of Geometry and Flow Variation on Jet Mixing and NO Formation in a Model Staged Combustor Mixer with Eight Orifices. NASA Contractor Report 194473. Prepared for Lewis Research Center.

Holdeman JD, Srinivasan R, Berenfeld A (1984). Experiments in Dilution Jet Mixing. *AIAA Journal*. 22-10: 1436-1443.

Holdeman JD, Srinivasan R (1986). Modeling Dilution Jet Flowfields. *Journal of Propulsion and Power*. 2-1: 4-10.

Holdeman JD, Srinivasan R, Coleman EB, Meyers GD, White CD (1987). Effects of Multiple Rows and Noncircular Orifices on Dilution Jet Mixing. *Journal of Propulsion and Power*. 3-3: 219-226.

Holdeman JD (1993). Mixing of Multiple Jets with a Confined Subsonic Cross-flow. *Progress in Energy and Combustion Science*. 19: 31-70.

Holdeman JD, Srinivasan R, White CD (1993). An Empirical Model of the Effects of Curvature and Convergence on Dilution Jet Mixing. AIAA-88-3180:1-18.

Holdeman JD, Liscinsky, DS, Oechsle VL, Samuelsen GS, Smith CE (1997). Mixing of Multiple Jets with a Confined Subsonic Cross-flow: Part I – Cylindrical Duct. *Journal of Engineering for Gas Turbines and Power*. 119: 852-862.

Holdeman JD, Liscinsky, DS, Bain DB (1999). Mixing of Multiple Jets with a Confined Subsonic Cross-flow: Part II – Opposed Rows of Orifices in Rectangular Ducts. *Journal of Engineering for Gas Turbines and Power*. 121: 551-562.

Howe GW, Li Z, Shih TIP, Nguyen HL (1991). Simulation of Mixing in the Quick Quench Region of a Rich Burn-Quick Quench Mix-Lean Burn Combustor, AIAA-91-0410, Prepared for 29th Aerospace Sciences Meeting, Reno, Nevada.

Isaac KM, Schetz JA (1982) Analysis of Multiple Jets in a Cross-flow, *Journal of Fluids Engineering*. 104: 489-492.

Kadotani K, Goldstein RJ (1979). On the Nature of Jets Entering a Turbulent Flow, part A -. Jet-Mainstream Interaction. *Journal of Engineering for Power*. 101: 459-465.

Kamotani Y, Greber I (1972). Experiments on a Turbulent Jet in a Cross Flow. *AIAA Journal*. 10-11: 1425-1429.

Kelso RM., Lim TT, Perry AE (1996). An Experimental Study of a Round Jet in a Cross-Flow. *Journal of Fluid Mechanics*. 306:111-144

Kroll JT, Sowa WA, Samuelsen GS, Holdeman JD (1993). Optimization of Circular Orifice jets Mixing into a Heated Cross Flow in a Cylindrical Duct. NASA Technical Memorandum 105984 AIAA-93-0249. Prepared for the 31st Aerospace Science Meeting, Nevada.

Leong MY, Samuelsen GS, Holdeman JD (1995). Jet Mixing in a Reacting Cylindrical Cross-flow. NASA Technical Memorandum 106975 AIAA-95-3109. Prepared for the 31st Joint Propulsion Conference and Exhibit. San Diego, California.

Lim TT, New TH, Luo SC (2001). On the Development of Large-Scale Structures of a Jet normal to a Cross Flow. *Physics of Fluids*. 13: 770-775.

Makihata T, Miyai Y (1983) Prediction of the Trajectory of Triple Jets in a Uniform Crossflow, *Journal of Fluids Engineering*. 105: 91-97.

Margason RJ (1993) Fifty Years of Jet in Cross-flow Research. *Computational and Experimental Assessment of Jets in Cross Flow*. AGARD-CP-534, Winchester, UK.

Mewes D, Fellhölder A (1994). Visualization of the Concentration Profiles in the Entrance section of a Fixed Bed Catalytic Reactor – Premixing of Two Gaseous Components. *Chemical Engineering Science*. 49-24B: 5243-5255.

Muppidi S (2006). Direct Numerical Simulations and Modeling of Jets in Cross-flow. Ph.D. Dissertation, University of Minnesota. USA.

Needham DJ, Riley N, Lyton CC, Smith JHB (1988). A Jet in Cross-flow, *Journal of Fluid Mechanics*. 188: 159-184.

Needham DJ, Riley N, Smith JHB (1990). A Jet in Cross-flow, Part 2, *Journal of Fluid Mechanics*. 211: 515-528.

New TH, Lim TT, Luo SC (2003). Elliptic Jets in Cross-flow. *Journal of Fluid Mechanics*. 494: 119-140

Nirmolo A, Woche H, Specht E (2003). Mixing of Combustible Gases in a Cylindrical Chamber with Radial Injection of Air. *Proceedings of Conference on Modelling Flow (CMFF 2003) - Vol 1*. Eds by Lajos T, Vad J. Budapest, Hungary: 301-307.

Nirmolo A, Woche H, Specht E, Praetor R, Skroch R (2007). Gas Mixing in Cylindrical Chambers after Radial Jets Injection. *Progress in Computational Fluid Dynamics: An International Journal*. Vol 7, Inderscience Publisher. 8:447-456.

Nirmolo A, Woche H, Specht E (2008). Mixing of Jets in Cross Flow after Double Rows of Radial Injections. *Chemical Engineering and Technology*. Vol 31. WILEY-VCH Verlag GmbH & Co. 2: 294-300.

Nirmolo A, Woche H, Specht E (2008). Temperature Homogenization of Reactive and Non-Reactive Flows after Radial Jet Injections in Confined Cross-Flow. *Engineering Applications of Computational Fluid Mechanics*. The Hong Kong Polytechnic University. Vol. 2, 1: 85–94

Nishiyama H, Ota T, Hamada M, Takahashi Y (1991). Temperature Fluctuations of Two Dimensional Slightly Heated Jet Issuing into a Cross-Flow. *Proceedings of the 2nd World Conference on Experimental Heat Transfer, Fluid Mechanics and Thermodynamics*. 436-442.

Oechsle VL, Mongia HC, Holdeman JD (1992). A Parametric Numerical Study of Mixing in a Cylindrical Duct. NASA Technical Memorandum 105695 AIAA-92-3088. Prepared for the 28th Joint Propulsion Conference and Exhibit. Nashville, Tennessee.

Oechsle VL, Mongia HC, Holdeman JD (1993). An Analytical Study of Dilution Jet Mixing in a Cylindrical Duct. NASA Technical Memorandum 106181 AIAA-93-2043. Prepared for the 29th Joint Propulsion Conference and Exhibit. Monterey, California.

Oechsle VL, Holdeman JD (1995). Numerical Mixing Calculations of Confined Reacting Jet Flows in a Cylindrical Duct. AIAA-95-0733. Prepared for the 33rd Aerospace Sciences Meeting and Exhibit. Reno, Nevada.

Pietrzyk, J.R., Bogard D.G. Bogard, Crawford M.E. (1988). Hydrodynamic Measurements of a Jets in a Cross Flow for Gas Turbine Film Cooling Applications. JJ Mechanical Engineering Department, University of Texas, Austin.

Rajaratnam (1976). *Turbulent Jets*. New York: Elsevier Scientific Publishing Company.

Reményi K (1987). *Industrial Firing*. Budapest: Akadémiai Kiadó.

Richards CD, Samuelsen GS (1992). The Role of Primary Jets in the Dome Region Aerodynamics of Model Can Combustor. *Journal of Engineering for Gas Turbines and Power*. 114: 21-26.

Schatzmann M (1979). An Integral Model of Plume Rise, *Atmospheric Environment*. 13: 721-731.

Schetz JA (1980). Injection and Mixing in Turbulent Flow. *Progress in Astronautics and Aeronautics*. 68-1-200.

Schetz JA (1986). Hydrodynamics of Jets in Cross-flow. *Encyclopedia of Fluid Mechanics - Vol 2: Dynamics of Single-Fluid Flows Mixing*. Houston: Gulf Publishing.

Smith CE, Talpallikar MV, Holdeman JD (1991). A CFD Study of Jet Mixing in Reduced Flow Areas for Lower Combustor Emissions. NASA Technical Memorandum 104411 AIAA-90-2460. Prepared for the 27th Joint Propulsion Conference. Sacramento, California.

Tao Y, Adler W, Specht E (2002). Numerical Analysis of Multiple jets Discharging into a Confined Cylindrical Cross-flow. *Proceedings of the Institution of Mechanical Engineers Part E: Journal of Process Mechanical Engineering*. 216: 173-180.

Talpallikar MV, Smith CE, Lai MC (1990) Rapid Mix Concept for Low Emissions Combustors in Gas Turbine Engines, NASA Contractor Report 185292.

Vranos A, Liscinsky DS, True B, Holdeman JD (1991). Experimental Study of Cross-stream Mixing in a Cylindrical Duct. NASA Technical Memorandum 105180 AIAA-91-2459. Prepared for the 27th Joint Propulsion Conference, Sacramento, California.

Wang E, et al., (2004). Micromachined Jets for Liquid Impingement Cooling of VLSI Chips, *Journal of Microelectromechanics System*. 13: 833-842.

Wegner B, Huai Y, Sadiki A (2004). Comparative Study of Turbulent Mixing in Jet in Cross-Flow Configurations Using LES. *International Journal of Heat and Fluid Flow*. 25: 767-775.

Wittig SLK, Elbahar OMF, Noll BE (1984). Temperature Profile Development in Turbulent Mixing of Coolant Jets with a Confined Hot Cross-Flow. *Journal of Engineering for Gas Turbines and Power*. 106: 193-197.

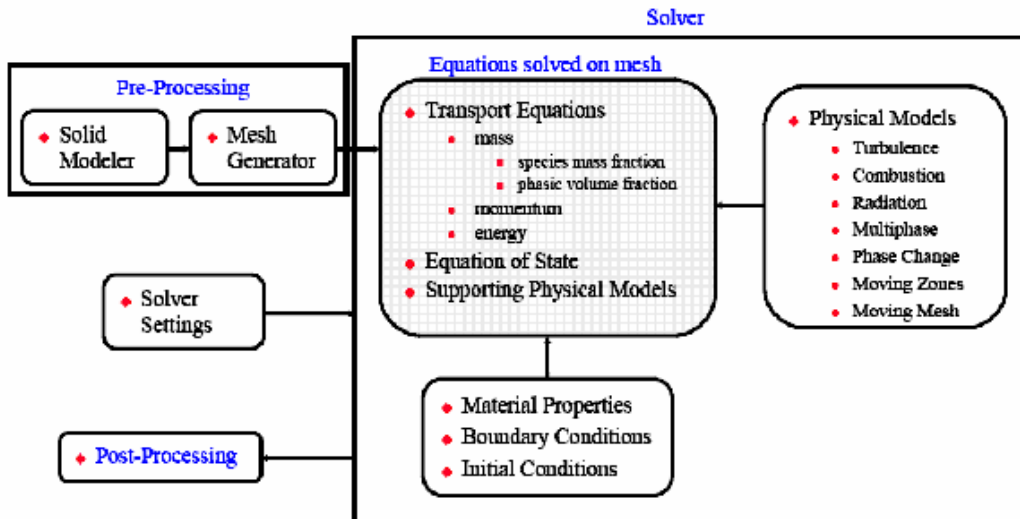
Woche H, Nirmolo A, Skroch R, Specht E (2005). Intensive Mixing of Radial Nozzle Jets with a Main Flow. *Gaswaerme International*. Vulkan-Verlag. 54-5: 301-307.

Woche H, Nirmolo A, Specht E (2006). Design of combustion chambers with radial air injection for temperature homogenization. *Gaswaerme International*. Vulkan-Verlag. 55-5: 338-341.

Yoshida T, Goldstein RJ (1984). On the Nature of Jets Issuing from a Row of Holes into a Low Reynolds Number Mainstream Flow. *Journal of Engineering for Gas Turbines and Power*. 106: 612-618.

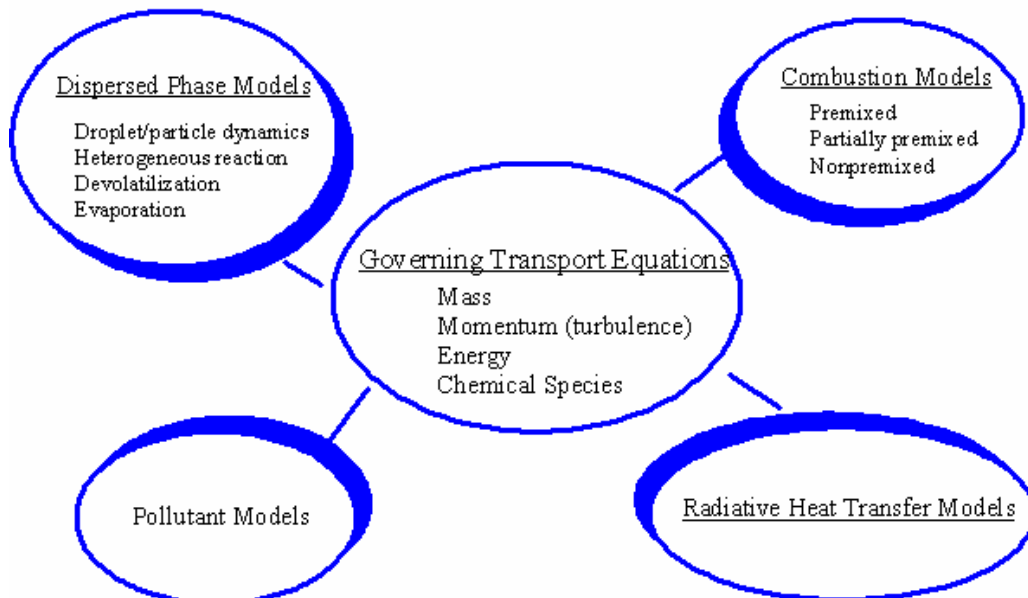
APPENDIX

A. CFD Modeling Overview [FLUENT, 2003]



B. Combustion Modeling in FLUENT

B.1 Aspects of Combustion Modeling [FLUENT, 2003]



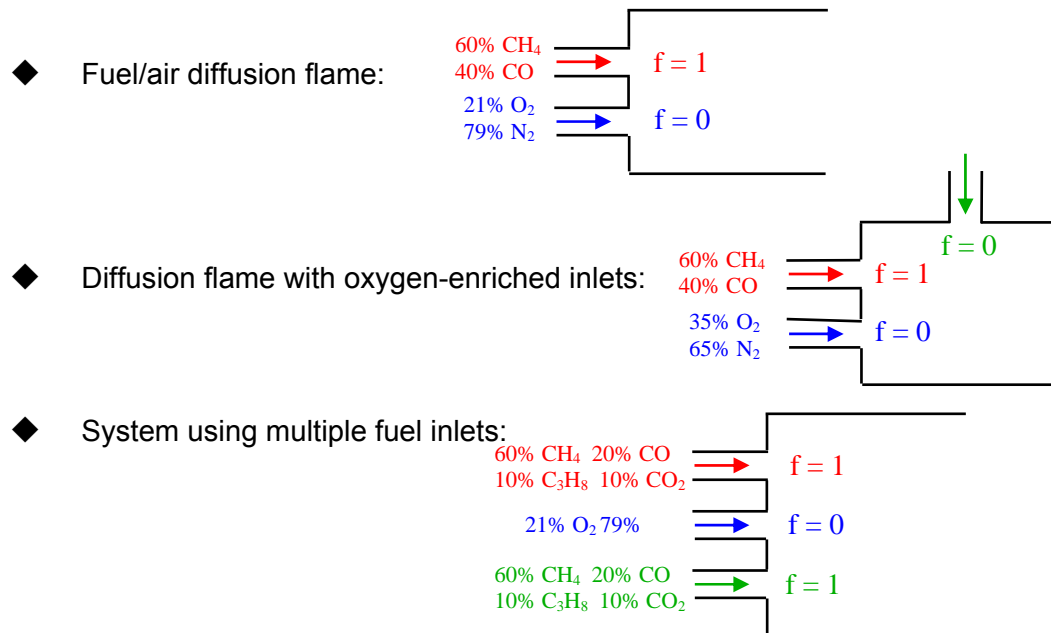
B.2 Combustion Models Available in FLUENT

- ◆ Gas phase combustion
 - Generalized finite rate formulation (Magnussen model)
 - Conserved scalar PDF model (one and two mixture fractions)
 - Laminar flamelet model (V5)
 - Zimont model (V5)
- ◆ Discrete phase model
 - Turbulent particle dispersion
 - ◆ Stochastic tracking
 - ◆ Particle cloud model (V5)
 - Pulverized coal and oil spray combustion submodels
- ◆ Radiation models: DTRM, P-1, Rosseland and Discrete Ordinates (V5)
- ◆ Turbulence models: k - ϵ , RNG k - ϵ , RSM, Realizable k - ϵ (V5) and LES (V5)
- ◆ Pollutant models: NO_x with reburn chemistry (V5) and soot

B.3 Modeling Chemical Kinetics in Combustion

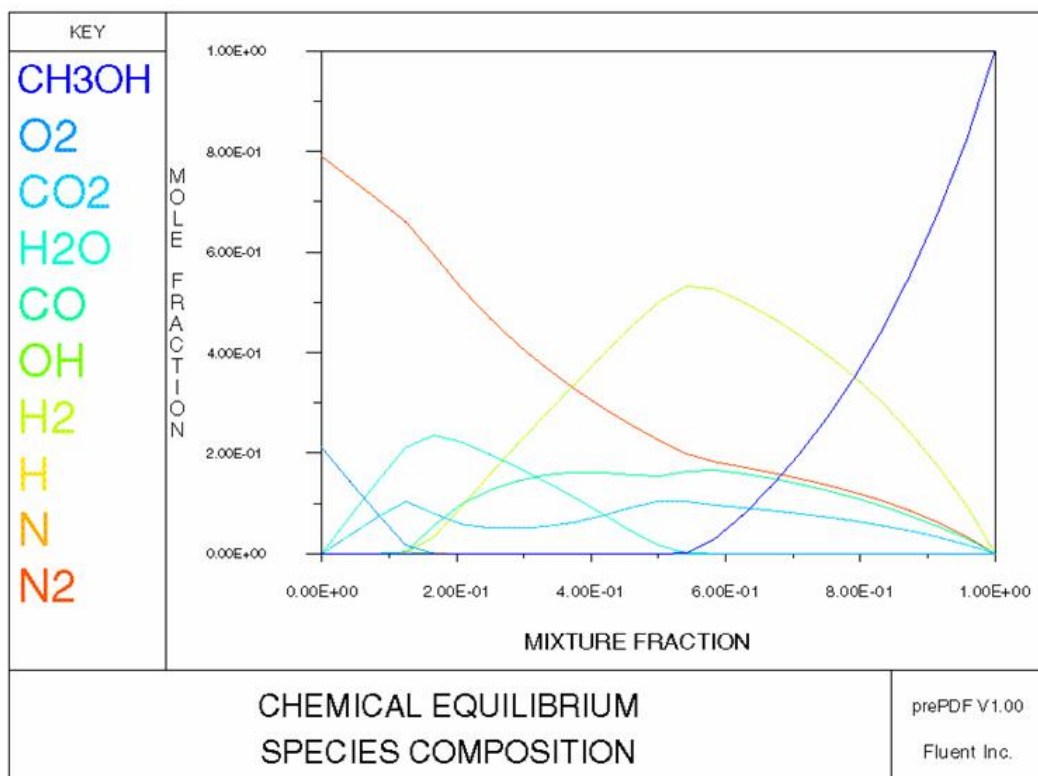
- ◆ Challenging
 - Most practical combustion processes are turbulent
 - Rate expressions are highly nonlinear; turbulence-chemistry interactions are important
 - Realistic chemical mechanisms have tens of species, hundreds of reactions and stiff kinetics (widely disparate time scales)
- ◆ Practical approaches
 - Reduced chemical mechanisms
 - Finite rate combustion model
 - Decouple reaction chemistry from turbulent flow and mixing
 - Mixture fraction approaches
 - ◆ Equilibrium chemistry PDF model
 - ◆ Laminar flamelet
 - Progress variable
 - ◆ Zimont model

B.4 Modeling Using a Single Mixture Fraction



B.5 Equilibrium Approximation of System Chemistry

- ◆ Chemistry is assumed to be fast enough to achieve equilibrium.
- ◆ Intermediate species are included.



B.6 Combustion Guidelines and Solution Strategies

◆ Start in 2D

- Determine applicability of model physics
- Mesh resolution requirements (resolve shear layers)
- Solution parameters and convergence settings

◆ Boundary conditions

- Combustion is often very sensitive to inlet boundary conditions
 - Correct velocity and scalar profiles can be critical
- Wall heat transfer is challenging to predict; if known, specify wall temperature instead of external convection/radiation BC

◆ Initial conditions

- While steady-state solution is independent of the IC, poor IC may cause divergence due to the number and nonlinearity of the transport equations
- Cold flow solution, then gas combustion, then particles, then radiation
- For strongly swirling flows, increase the swirl gradually

◆ Underrelaxation Factors

- The effect of under-relaxation is highly nonlinear
 - Decrease the diverging residual URF in increments of 0.1
 - Underrelax density when using the mixture fraction PDF model (0.5)
 - Underrelax velocity for high bouyancy flows
 - Underrelax pressure for high speed flows
- Once solution is stable, attempt to increase all URFs to as close to defaults as possible (and at least 0.9 for T , $P-1$, swirl and species (or mixture fraction statistics))

◆ Discretization

- Start with first order accuracy, then converge with second order to improve accuracy
- Second order discretization especially important for tri/tet meshes

◆ Discrete Phase Model - to increase stability,

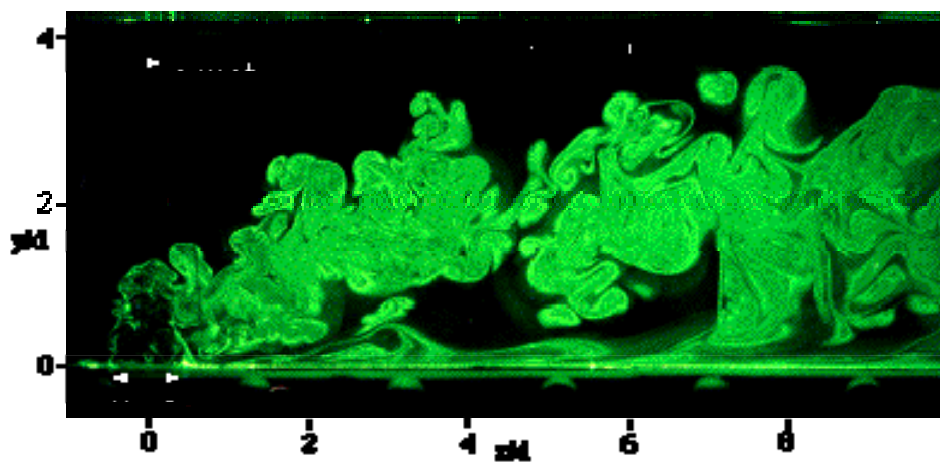
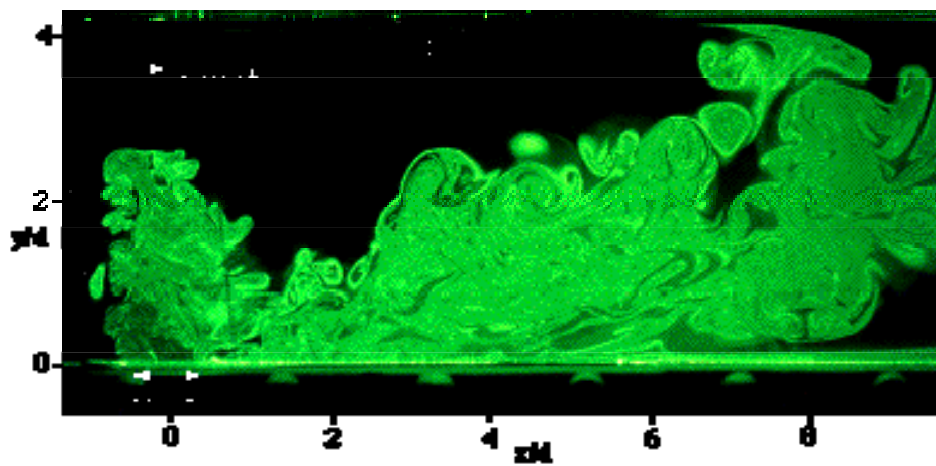
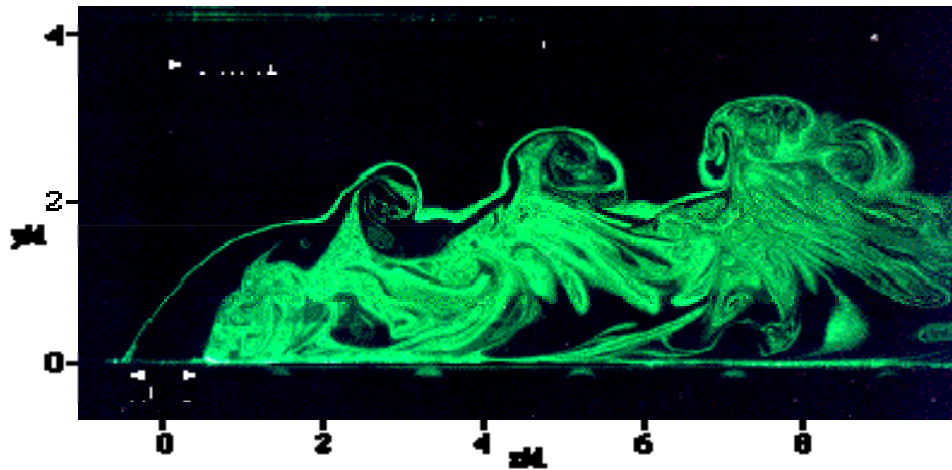
- Increase number of stochastic tracks (or use particle cloud model)
- Decrease DPM URF and increase number of gas phase iterations per DPM

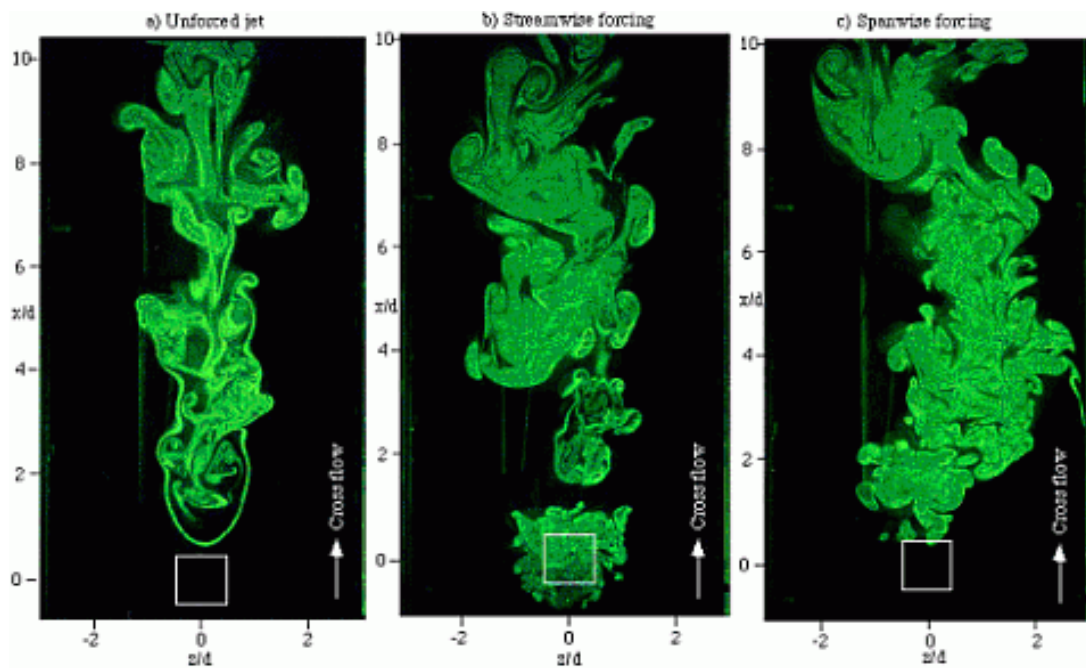
-
- ◆ **Magnussen model**
 - Defaults to finite rate/eddy-dissipation (Arrhenius/Magnussen)
 - For nonpremixed (diffusion) flames turn off finite rate
 - Premixed flames require Arrhenius term so that reactants don't burn prematurely
 - May require a high temperature initialization/patch
 - Use temperature dependent C_p 's to reduce unrealistically high temperatures
 - ◆ **Mixture fraction PDF model**
 - Model of choice if underlying assumptions are valid
 - Use adequate numbers of discrete points in look up tables to ensure accurate interpolation (no affect on run-time expense)
 - Use beta PDF shape
 - ◆ **Turbulence**
 - Start with standard $k-\varepsilon$ model
 - Switch to RNG $k-\varepsilon$, Realizable $k-\varepsilon$ or RSM to obtain better agreement with data and/or to analyze sensitivity to the turbulence model
 - ◆ **Judging Convergence**
 - Residuals should be less than 10^{-3} except for T , $P-1$ and *species*, which should be less than 10^{-6}
 - The mass and energy flux reports must balance
 - Monitor variables of interest (e.g. mean temperature at the outlet)
 - Ensure contour plots of field variables are smooth, realistic and steady

C. Jets in Crossflow Simulation Gallery

C.1 Innovative Scientific Solutions, Inc.

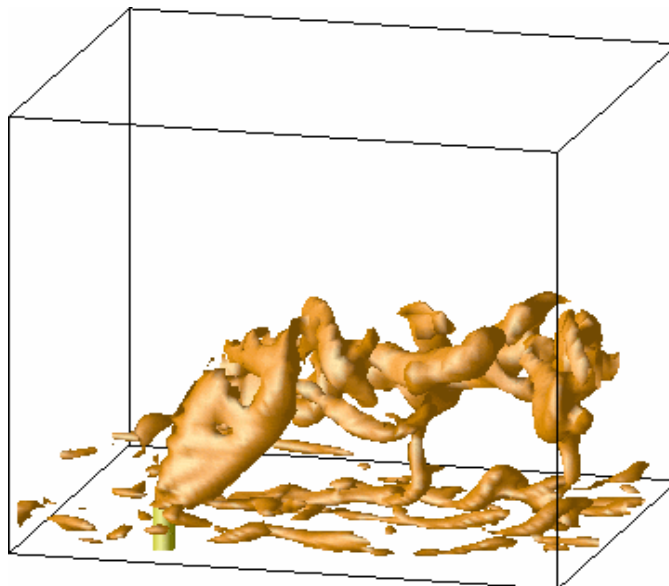
<http://www.innssi.com/rms02.htm>



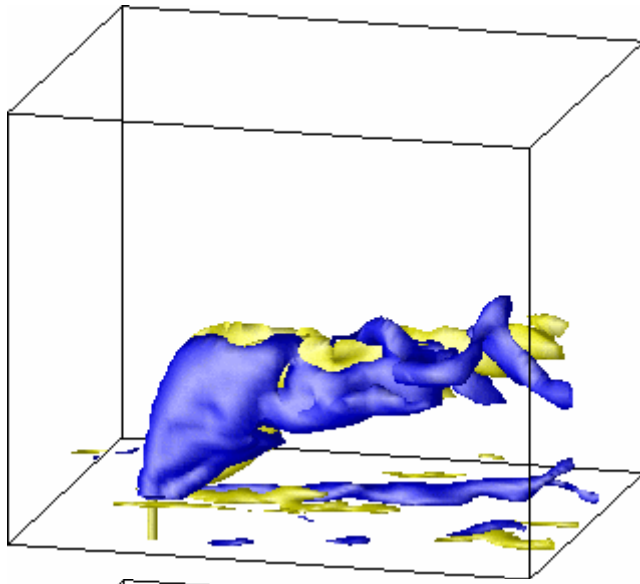


C.2 Division of Fluid Mechanics – Lund University

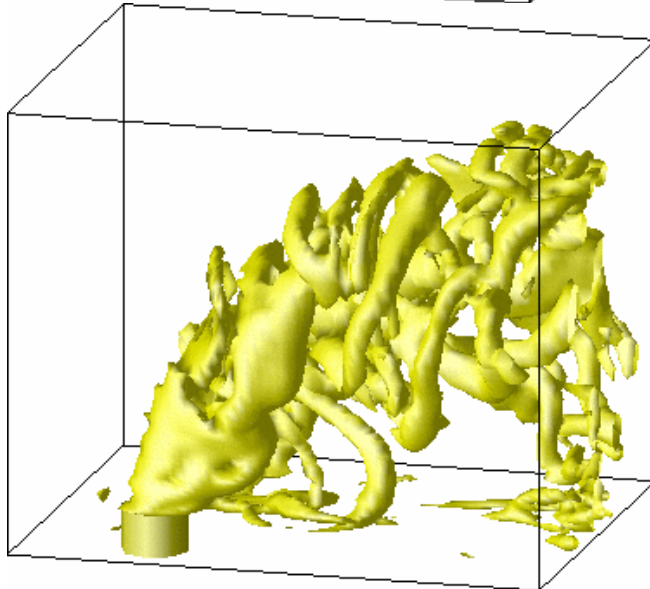
<http://www.fm.vok.lth.se/Research/Gallery/gallery.html>



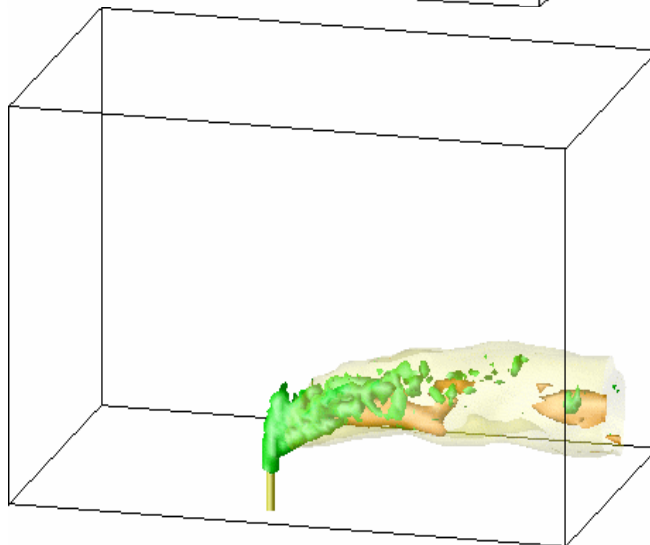
Vortex visualization with λ_2 in the flow field of a jet in crossflow: Counter-rotating vortex pair, tornado-like upright wake vortices, and horseshoe vortex



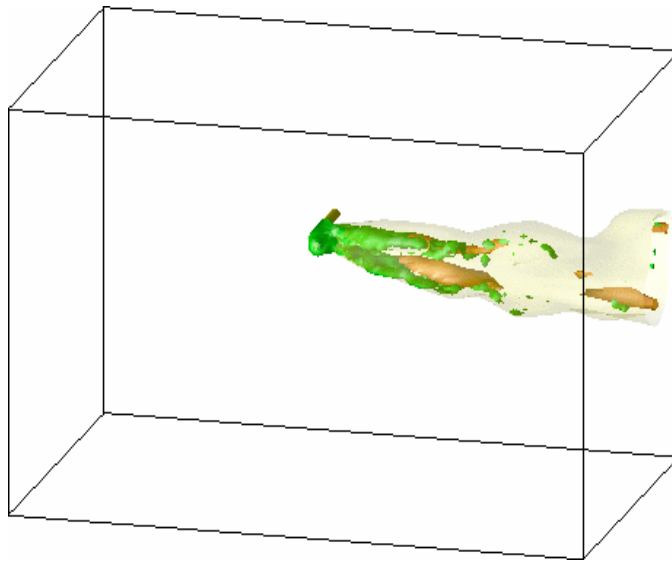
Streamwise vorticity isosurfaces in the flow field of a jet in crossflow (blue: positive, yellow: negative): Counter-rotating vortex pair and horseshoe vortex



Vortex visualization with λ_2 in the flow field of a jet in crossflow: Tornado-like upright wake vortices

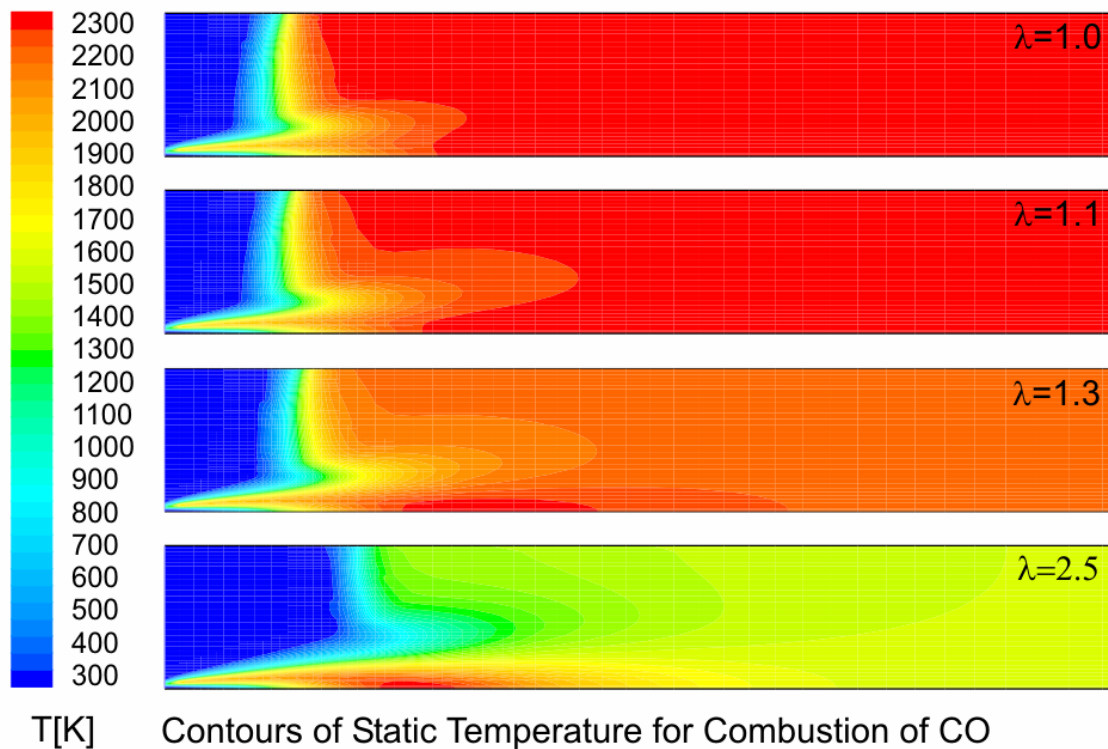


Side view of evaporating spray jet in crossflow (green: Liquid phase volume fraction isosurface; light orange: Mixture fraction isosurface, low value; dark orange: Mixture fraction isosurface, high value, fuel rich pockets)



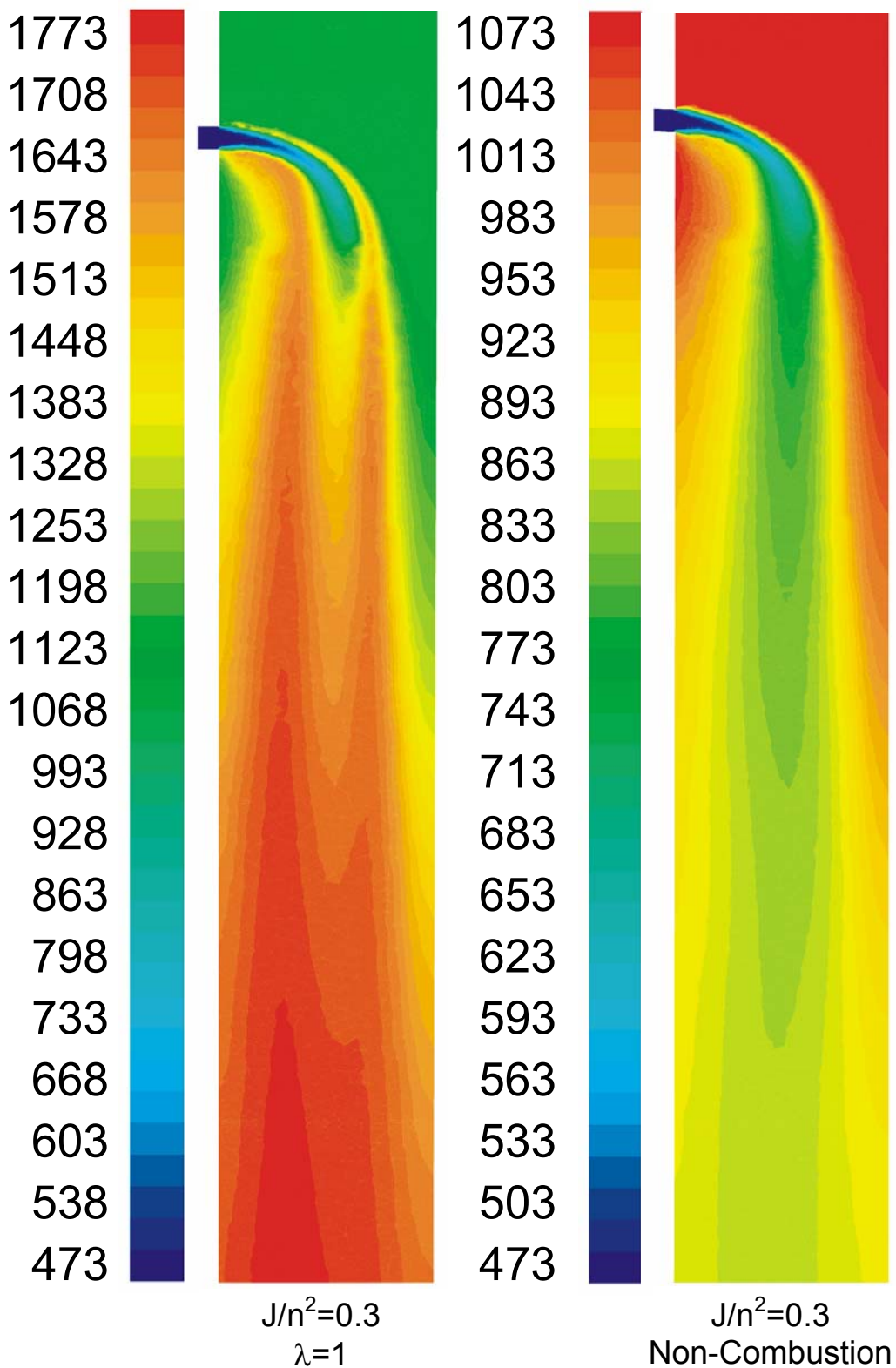
Top view of evaporating spray jet in crossflow (green: Liquid phase volume fraction isosurface; light orange: Mixture fraction isosurface, low value; dark orange: Mixture fraction isosurface, high value, fuel rich pockets)

C.3 ISUT – Otto-von-Guericke-University of Magdeburg

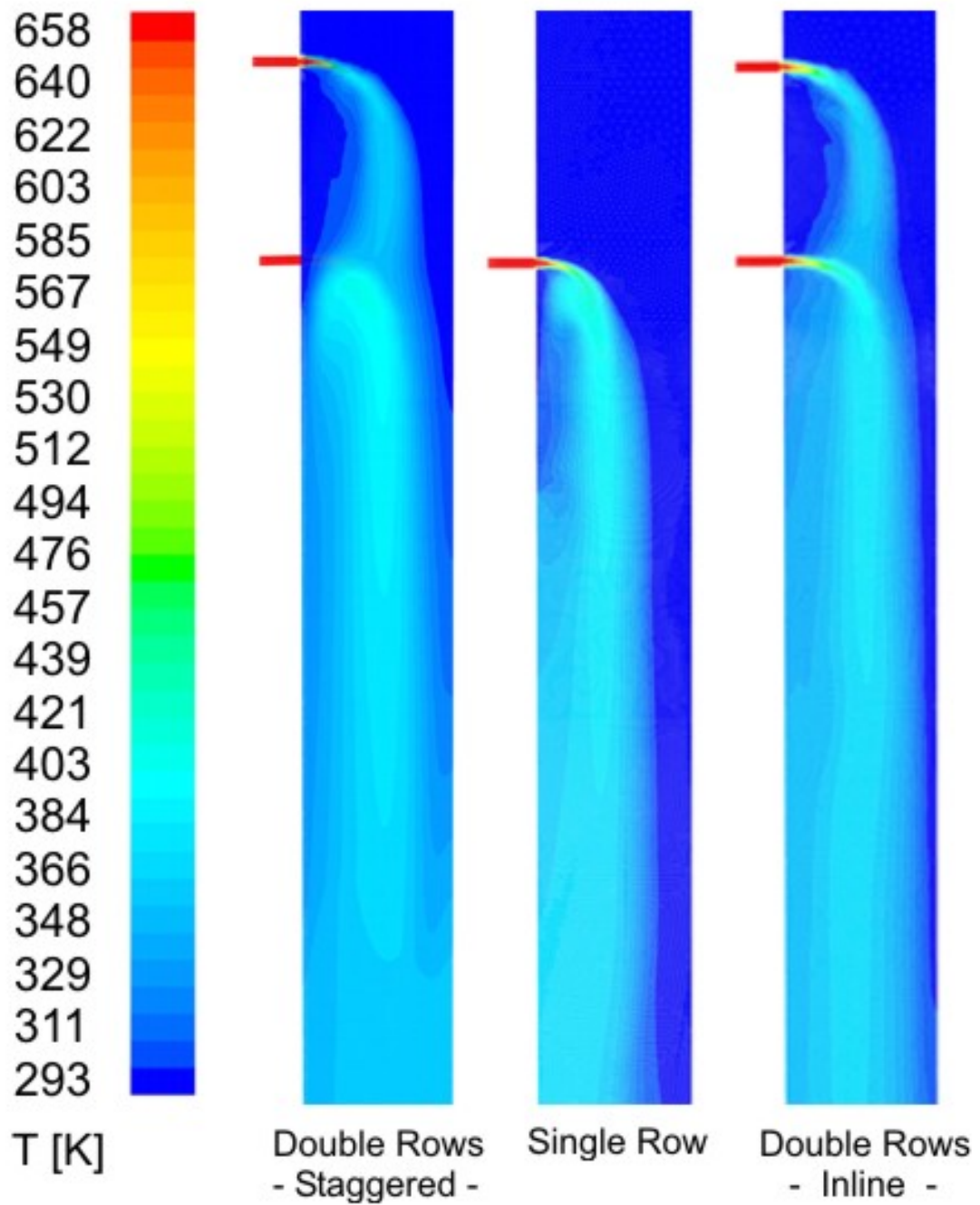


T[K]

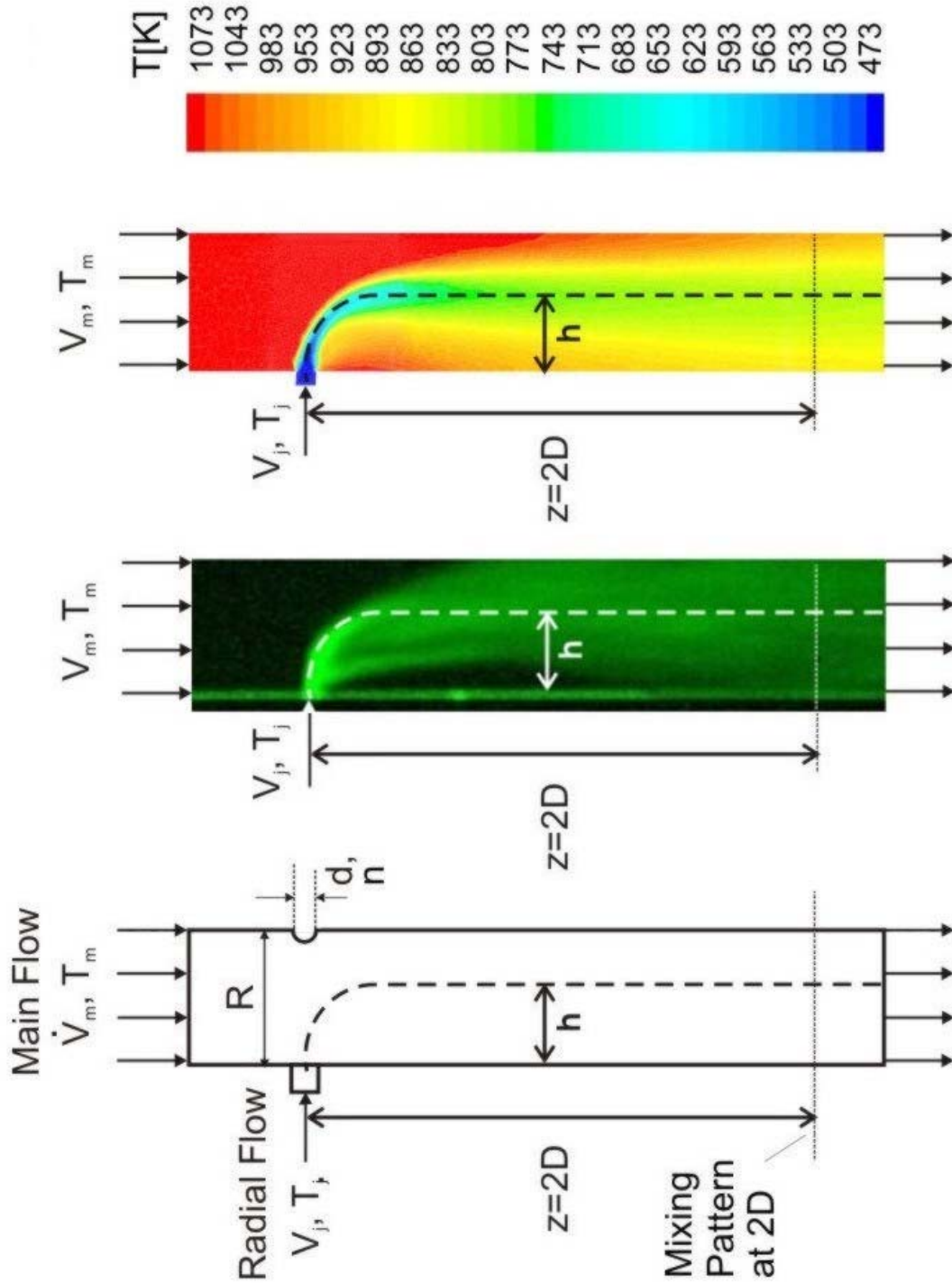
Contours of Static Temperature for Combustion of CO



Contours for $N=12$ and $D=2$ m at Optimum Condition



Contours for $N=16$ and $D=0.3$ m using Single Row and Double Rows Arrangements at Optimum Condition



**Comparison between Experiment and CFD Simulation
at Optimum Condition**

CURRICULUM VITAE

Name: **Nirmolo, Aryoso**

Date of birth: 08.08.1970

Place of birth: Yogyakarta, Indonesia

Nationality: Indonesian

Gender: Male

Education profile:

2002 – 2007: Ph.D. in Process Engineering

Institute of Fluid Dynamics and Thermodynamics at Otto-von-Guericke-University, Magdeburg, Germany

Subject: *Optimization of Radial Jets Mixing in Cross-Flow of Combustion Chambers using Computational Fluid Dynamics*

1999 – 2001: M.Sc. in Chemical Process Engineering

Joint International Master Program from Bandung Institute of Technology, Indonesia and Otto-von-Guericke-University, Magdeburg, Germany

Subject: *Characterization of Atomized Spray*

1998 – 1999: B.Sc. in Chemical Engineering

Gadjah Mada University, Indonesia

Subject: *Preliminary Plant Design of Melamine Formaldehyde from Melamine and Methanol*

1989 – 1993: Chemical Engineering

Gadjah Mada University, Indonesia

Subject: *Modeling and Simulation of a Drying Process in a Fixed-Bed Grain Dryer*

Occupation:

Process Engineer - SEZ AG

RDE – Equipment - CDS Concept

SEZ-Strasse 1

A-9500 Villach